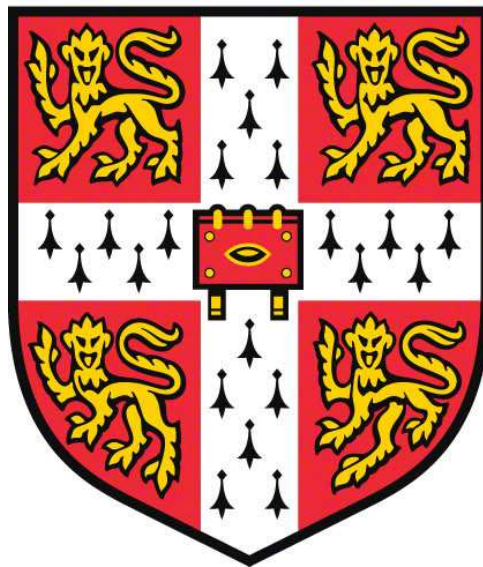


# Finding the edge: Net-shape surface sculpting during cold spray deposition



Sam Antony Brown

Trinity College

University of Cambridge

This thesis is submitted for the degree of

Doctor of Philosophy

February 2021



---

# Declaration

---

This thesis is the result of my own work and includes nothing which is the outcome of work done in collaboration except as declared in the Preface and specified in the text. I further state that no substantial part of my thesis has already been submitted, or, is being concurrently submitted for any such degree, diploma or other qualification at the University of Cambridge or any other University or similar institution except as declared in the Preface and specified in the text. It does not exceed the prescribed word limit for the relevant Degree Committee.

Sam Antony Brown

February 2021



# **Title: “Finding the edge: Net-shape surface sculpting during cold spray deposition”**

**Author: Sam Antony Brown**

---

## **Abstract**

---

This thesis provides an overview of how a successful method for structuring cold spray deposition was developed, allowing the creation of defined surfaces from a previously uncontrolled deposition profile.

When considering both additive and traditional manufacturing techniques, there remains a gap in the market for a high build rate, low-cost manufacturing system, capable of building net shape structures with good material properties from a range of difficult to work with engineering materials. A cold spray system had the potential to meet these requirements, and to provide additional benefits from being a solid-state fusion process, but the technique lacked the structural control capabilities required.

The aim of this body of work was to develop methods for controlling the shape of depositing material, allowing the creation of three-dimensional structures, and determining an approach which would allow the creation of flexible manufacturing platform. A limited number of attempts had been previously made to control the deposition shape. These methods met with limited success, did not offer real control over the shape of the deposit during operation, and presented issues of accuracy, reliability, and repeatability.

In this work, a series of concepts for shaping the deposition of the material were tested for the creation of flat vertical surfaces. Copper was used as the deposition powder as it readily deposits with cold spray under easily manageable conditions. The samples were investigated for shape conformity, surface roughness, porosity and build height, using optical microscopy and a white light interferometer. Successful shaping was delivered using masks, wide flow impeding backstops and thinner flow separating tools, provided the non-adhering powder had sufficient room to be cleared from the deposition zone. The thinner tool was further developed, as it allowed better positioning in smaller spaces for future systems.

Computational fluid dynamics models were created to assist with the understanding of some inconsistencies in deposit quality. The results of these simulations showed minimal alteration to the particle trajectory was caused by the alteration of gas dynamics from the introduction of obstacles.

The developed thin tool deposition concept was then successfully tested for robustness with deposition of further materials, and with the inclusion of laser irradiation of the substrate. It was demonstrated that the density, deposition efficiency and build heights are comparable with those expected from typical cold spray/supersonic laser deposition deposits. Following this, a range of building block structures were created, to further advance the shaping capabilities of the system, and demonstrate the freedom of deposition profile. Flat surfaces, thin walls, corners, curves, rings and overhangs were all shown to build efficiently without further complication.

It is concluded that it is both possible to control the shape of the depositing material during cold spray, and possible to do so without adversely affecting the deposit characteristics that give cold spray manufacturing its specific advantages over other manufacturing methods.

The next steps for this process are to create a more flexible system, automating the placement of the shaping tool and using a 5 or 6 axis bed and nozzle positioning setup. Further to that, precise control over the powder dosage, and the development of a known parameter space for select materials would progress the system to an additive capable platform.

---

# Acknowledgements

---

There are many thanks I need to give, to people who have supported me through this lengthy process.

My thanks:

To the small cold spray team at the IfM. Andrew, for your help and instruction over the years, and your friendship. David, for your encouragement and enthusiasm when I started generating results, it meant more than you realise. Bill and Martin for heading the group and accepting me for the PhD, and the EPSRC for funding this project.

To Chris and Jason, my partners in crime, I wouldn't have made it without you keeping me sane, or at least close to sanity, over the years. I'm glad we all got out alive.

To Payne, I am ever grateful for the 2-week stay when I had no place to live that lasted much, much longer, and for the introduction to modern board games. And for your friendship, tedious though it may be at times... And to Tony of course, for agreeing to keep me sheltered despite my occasional absence from the TCS.

To Clare, Francisco and Jack for the help, the good times, and the laughs. To Chris S and Franco for the practical help, advice, and conversation you gave from across the desk, and to Sophie and Alice for their help and patience when dealing with us mere administrative mortals.

To all the others in the Centre for Industrial Photonics, graduated and remaining, who have made the office over the last years a place of fun, thought-provoking discussion, and occasional shared misery. Good luck to those still writing!

To all my Trinity lot, the Zoo and keepers alike, the reason I wanted to come back to Cambridge was to meet further intelligent and interesting people. But I ended up settling for you lot, and couldn't have made a better choice, great times I will remember forever.

And to all the many other friends, colleagues and acquaintances who made Cambridge a special place, bureaucracy aside, you have my sincere gratitude.

I would especially like to thank my family, who encouraged me when I wasn't sure I could make it, sorry it took so long! Thanks for being (fairly) patient, I couldn't have got here without you. Now it's finally over, I might get a job again.

And finally, to Faye, for saving me from a haven of gloom I sometimes found myself in whilst writing, and helping me believe I could actually do it. All of this was worth it, just for meeting you.

---

# Contents

---

Declaration .....	i
Abstract .....	iii
Acknowledgements .....	v
Contents .....	vi
Chapter 1 - Introduction.....	1
1.1. Research motivation.....	1
1.2. Research aims.....	1
1.3. Thesis synopsis .....	2
Chapter 2 – Literature review.....	3
Chapter 3 – Experimental setup.....	3
Chapter 4 – Exploration of deposition shaping .....	3
Chapter 5 – Generation and validation of computational flow models.....	3
Chapter 6 – Progression of structural control .....	4
Chapter 7 – Conclusions and recommendations.....	4
Chapter 2 - Literature Review .....	5
2.1. Introduction.....	5
2.2. Metal additive manufacturing overview .....	5
2.2.1. Powder Bed .....	5
2.2.2. Directed energy deposition .....	9
2.2.3. Coating Techniques .....	11
2.3. Traditional manufacturing techniques .....	13
2.3.1. Forging.....	14
2.3.2. Casting .....	14
2.3.3. CNC machining.....	15
2.4. Overview of manufacturing techniques .....	16
2.5. Cold Spray.....	19

2.6.	Cold Spray discovery .....	19
2.7.	Experimental arrangement .....	19
2.7.1.	Apparatus .....	19
2.7.2.	Typical cold spray parameters.....	21
2.8.	Deposition mechanism.....	21
2.9.	Deposition shape.....	24
2.9.1.	Free-standing cold spray deposition profile.....	24
2.9.2.	Current deposition shape control capabilities .....	25
2.10.	Deposition characteristics .....	30
2.10.1.	Physical properties .....	30
2.10.2.	Material properties .....	31
2.10.3.	Process properties.....	32
2.11.	Supersonic laser deposition (Laser assisted cold spray) .....	33
2.12.	Computational fluid dynamics modelling .....	34
2.12.1.	Governing flow equations.....	34
2.12.2.	Boundary conditions .....	34
2.12.3.	Turbulence models.....	35
2.12.4.	Meshing.....	36
2.12.5.	Particle tracking.....	36
2.13.	Areas of application.....	36
2.13.1.	Wear resistance.....	37
2.13.2.	Corrosion and erosion resistance.....	37
2.13.3.	Joining.....	38
2.13.4.	Additive manufacturing and restoration.....	38
2.14.	Summary .....	40
Chapter 3 -	Experimental setup .....	41
3.1.	Introduction .....	41
3.2.	Health and Safety .....	41
3.3.	Cold Spray System .....	41

3.3.1.	Powder feeder .....	41
3.3.2.	Gas heater.....	42
3.3.3.	Nozzle .....	43
3.3.4.	Laser and pyrometer .....	45
3.3.5.	Auxiliary equipment .....	46
3.4.	Operational Control.....	46
3.4.1.	Preparation.....	46
3.4.2.	Powder handling.....	46
3.4.3.	Positioning .....	47
3.4.4.	Process control .....	48
3.4.5.	Post process.....	49
3.5.	Methods of Analysis .....	49
3.5.1.	Shape conformity .....	49
3.5.2.	Surface roughness .....	50
3.5.3.	Metallography .....	51
3.5.4.	Build height.....	52
Chapter 4 -	Exploration of deposition shaping concepts .....	53
4.1.	Introduction.....	53
4.2.	Parameters .....	53
4.3.	Masking plate .....	54
4.3.1.	Small feature section.....	55
4.3.2.	Nozzle alignment section.....	56
4.4.	Backstop .....	58
4.4.1.	Backstop deposition results.....	59
4.5.	Flow separator.....	61
4.5.1.	Flow separator deposition results.....	63
4.6.	Discussion .....	64
4.7.	Powder recycling .....	66
4.8.	Summary.....	67

Chapter 5 -	Generation and validation of computational flow models .....	69
5.1.	Introduction .....	69
5.2.	Model construction .....	69
5.2.1.	Assumptions .....	70
5.2.2.	Dimensions .....	70
5.2.3.	Geometry and meshing .....	70
5.2.4.	Solver parameter selection .....	72
5.3.	Two-dimensional modelling .....	75
5.3.1.	Model progression .....	75
5.3.2.	Initial results .....	75
5.3.3.	Two-dimensional mesh independence .....	77
5.3.4.	Two-dimensional obstacle addition .....	78
5.4.	Model validation with literature .....	79
5.5.	Three-dimensional modelling .....	82
5.5.1.	Three-dimensional mesh independence .....	83
5.5.2.	Comparison with two-dimensional model .....	83
5.6.	Three-dimensional obstacle addition .....	85
5.7.	Particle tracking results .....	87
5.8.	Confirmatory literature on particle trajectory models .....	91
5.9.	Summary .....	92
Chapter 6 -	Progression of structural control .....	95
6.1.	Introduction .....	95
6.2.	Flow separator height .....	95
6.3.	Material investigation .....	96
6.3.1.	Copper .....	97
6.3.2.	Titanium .....	101
6.3.3.	Stainless steel (316L) .....	105
6.4.	Supersonic laser deposition .....	107
6.4.1.	Titanium without laser vs with laser .....	108

6.4.2.	Controlled deposition of Stellite 21.....	110
6.5.	Effect of flow separator roughness .....	110
6.6.	Building block structures .....	111
6.6.1.	Walls .....	112
6.6.2.	Thin wall section .....	114
6.6.3.	Corners .....	115
6.6.4.	Curves .....	117
6.7.	Ring manufacture .....	118
6.7.1.	Copper ring .....	118
6.7.2.	Titanium rings and tool replacement .....	120
6.7.3.	Ring with centre.....	122
6.7.4.	Ring with flange .....	123
6.8.	Discussion .....	124
6.9.	Summary.....	126
Chapter 7 -	Conclusions and recommendations .....	127
7.1.	Introduction.....	127
7.2.	Summary and conclusions from analysis.....	127
7.3.	Future Recommendations .....	128
7.3.1.	Positional control.....	128
7.3.2.	Shape control.....	129
7.3.3.	Parameter exploration and process control.....	129
References.....		131
Appendix A .....		138

## Figures

Figure 1 -	ARCAM EBM system schematic [6] .....	7
Figure 2 -	Sandia LENS System [8] .....	9
Figure 3 -	PTA deposition torch .....	11
Figure 4 -	Sciaky electron beam additive manufacturing (EBAM) system [10] .....	11

Figure 5 - Flame spraying schematic [11].....	12
Figure 6 - Wire arc spraying [11].....	13
Figure 7 - Hot forging of titanium [13].....	14
Figure 8 – Cold spray schematic [16] .....	20
Figure 9 - Sequence of particle impact (a) 4.4 ns; (b) 13.2 ns; (c) 22.0 ns and (d) 30.8 ns. [35].....	22
Figure 10 - FIB cross section image of cold sprayed powder particle, arrow points to the jet [44] .....	23
Figure 11 – Schematic of rollups caused by interfacial instabilities [36] .....	24
Figure 12 - Single track cold spray deposition profile reaching the critical build angle (different materials to viewing).....	25
Figure 13 - Tessellation for structuring cold spray deposition.....	25
Figure 14 - Pyramidal fin arrays from cold spray through a mesh (a) as deposited (b) after cross sectioning [35].....	26
Figure 15 – Mask [53].....	26
Figure 16 - Pyramid deposit formed by masked cold spray [53] .....	27
Figure 17 - Cold spray deposition of copper particles (a) non-swirled flow (b) swirled flow [54].....	28
Figure 18 – Slotted nozzles and cold spray deposition [55].....	28
Figure 19 – Cold-sprayed construction of a component (a) on a blank to provide structure and (b) removed from blank and machined [56] .....	29
Figure 20 - Titanium sprayed with aluminium mould [50].....	30
Figure 21 - Copper and aluminium layered cold spray deposit [50] .....	32
Figure 22 – SLD setup .....	33
Figure 23 - Hermle MPA 40 hybrid cold spray and machining centre .....	38
Figure 24 - Spee3d additive cold spray system .....	39
Figure 25 - VRC Gen III manual cold spray deposition system [119].....	39
Figure 26 – Praxair TAFA Model 1264, high pressure open loop wheel powder feeder .....	42
Figure 27 – Gas heater .....	43
Figure 28 – Diagram of the tungsten carbide cold spray nozzle [DLV190] at the IfM .....	44
Figure 29 - Laser head and pyrometer positioning in the build chamber.....	45
Figure 30 – Powder feeder mounted on a load cell.....	47
Figure 31 - Aerotech control software used for nozzle positioning.....	48
Figure 32 - Cold spray process control software.....	49
Figure 33 - Veeco Wyko NT3300 used for surface roughness measurements .....	50
Figure 34 - Sample Veeco Wyko NT3300 surface roughness measurement output image .....	51
Figure 35 - Porosity measurement example of 4% porous Al cold spray deposit .....	52
Figure 36 – Mask experiment setup and mask outline (150 x 150 mm) with nozzle path of 8 mm spray track.....	55

Figure 37 – A typical failed small feature deposition pattern .....	55
Figure 38 – Side view of the deposit formed in nozzle alignment section, after mask removal .....	56
Figure 39 – Samples from the nozzle conformity section, where the nozzle’s central axis is offset from parallel with the wall by (a) +2 mm, (b) +1 mm, (c) 0 mm, (d) -1 mm, and (e) -2 mm.....	57
Figure 40 – Vertical wall build height vs central alignment of the nozzle with feature edge with 3 mm mask thickness, for one 15 mm/s layer and two 30 mm/s layers.....	58
Figure 41 – Backstop design figure, nozzle traverse direction is into the page. ....	59
Figure 42 – Example of successful copper deposition against 6 mm backstop, with decreasing traverse rates of 15, 7.5, 5, 3.75 and 3 mm/s.....	59
Figure 43 - Successful copper deposition against 10 mm backstop, at a steady declining traverse rate from 25 to 3.75 mm/s .....	60
Figure 44 – Failed copper deposition adjacent to 10 mm height backstop at 25, 15, 7.5, 5 and 3.75 mm/s .....	60
Figure 45 - Nozzle alignment shadow .....	60
Figure 46 – Stepped backstop result at heights of 2, 4, 6, 8 and 10 mm at 5 mm/s traverse rate.....	61
Figure 47 – Flow separator diagram.....	62
Figure 48 - Copper deposition cross sections [3, 3.75, 7.5, 15, 25, 50, 100 mm/s], with all parameters as described in Section 4.2. ....	63
Figure 49 - Traverse rate vs surface roughness for copper flow separator deposits.....	64
Figure 50 - Powder particles (a) before and (b) after spraying through the system.....	67
Figure 51 - Diagram showing the effects of tool wall position on tool adjacent deposit shape.....	65
Figure 52 - Geometry creation screenshot.....	71
Figure 53 – Mesh creation screenshot of early mesh model .....	72
Figure 54 – Graph depicting the gas velocity along nozzle centreline for solutions including different order upwind equation terms .....	75
Figure 55 – Simulation generated gas velocity map of the cold spray nozzle with open exhaust area, with parameters as established in Section 5.2.4.....	76
Figure 56 – 2D Simulation generated gas velocity map of cold spray nozzle and substrate at 40 mm stand-off distance.....	76
Figure 57 – Schlieren image of shock structure vs offset distance [128].....	77
Figure 58 – Centreline gas velocity comparison for 2D mesh independence demonstration .....	78
Figure 59 – Axisymmetric obstacles in nozzle exhaust .....	79
Figure 60 - Meyer and Lupoi nozzle diagram .....	80
Figure 61 – Comparative centreline gas velocity results of simulation with literature .....	80
Figure 62 - Particle velocity comparison to literature data [89] .....	81
Figure 63 – 3D nozzle with open expansion/substrate .....	82

Figure 64 – 3D mesh independence test.....	83
Figure 65 – Comparison of 3D and 2D nozzle simulations with substrate at 40 mm standoff.....	84
Figure 66 – Centreline gas velocity comparison of 2D and 3D FLUENT models .....	84
Figure 67 – Absolute percentage difference between 2D and 3D models .....	85
Figure 68 – Gas structure at the central plane of 3D model showing gas velocity magnitudes with (a) no obstacle, (b) with 19 mm backstop, and (c) with 19 mm flow separator .....	86
Figure 69 - Gas flow lines around flow separator .....	86
Figure 70 – Simulations of (a) nozzle and substrate at 40 mm stand-off distance, plus added flow separators at (b) 10 mm, (c) 19 mm and (d) 28 mm.....	87
Figure 71 - Particle velocities calculated from differing initial velocities.....	88
Figure 72 – Simulated 40-micron diameter particle trajectory past a 20 mm tall, 1 mm thick flow separator .....	89
Figure 73 – Simulated 40-micron diameter particle trajectory from the nozzle exhaust, past a 20 mm tall backstop .....	89
Figure 74 - Pressure maps for flow separator and backstop FLUENT models .....	90
Figure 75 – Mean displacement of particle from original trajectory .....	92
<i>Figure 76 – Single track, single layer deposit with variable height flow separator at 5 mm/s (Flow separator outline drawn in).....</i>	<i>96</i>
Figure 77 - Copper deposition cross sections [3, 3.75, 7.5, 15, 25, 50, 100 mm/s] .....	98
Figure 78 – Copper layer build height vs traverse rate .....	98
Figure 79 - Copper porosity vs traverse rate.....	99
Figure 80 – Microscope image showing surface and bulk density, 500 micron scale represents approximately 10-15 particle diameters.....	100
Figure 81 - Nozzle path diagram for diagonal height.....	101
Figure 82 - Copper diagonal test .....	101
Figure 83 – Build profile of titanium nozzle alignment test after sectioning at the centre.....	102
Figure 84 - Titanium deposits adjacent to flow separator at 3.75, 5, 7.5, 15 and 25 mm/s.....	103
Figure 85 – Titanium deposits surface roughness vs traverse rate.....	103
Figure 86 - Surface height vs traverse rate for Ti deposit.....	104
Figure 87 – Titanium sample porosity vs nozzle traverse rates .....	104
Figure 88 – Build profile of steel nozzle alignment test.....	105
Figure 89 - Steel deposits, cross sectioned to display surface profile, at 3.75, 7.5, 15 and 25 mm/s	106
Figure 90 – Steel surface finish vs traverse rate .....	106
Figure 91 – Steel layer height vs traverse rate.....	107
Figure 92 - Steel samples porosity vs traverse rate .....	107

Figure 93 – Supersonic laser deposition of titanium shaped with flow separator, sectioned to show shape .....	108
Figure 94 – Comparison of Ti and Ti + laser assistance for porosity, average build height and surface roughness .....	109
Figure 95 – Supersonic laser deposition of Stellite 21 shaped with flow separator at 25, 15, 7.5 and 3.75 mm/s, at 500 °C with additional 1.5 kW laser power.....	110
Figure 96 – Graph of initial tool face roughness vs deposit surface roughness (Ra) .....	111
Figure 97 – Diagram of setup for flow separator to be positioned over the substrate .....	112
Figure 98 – Separator positioning sample.....	113
Figure 99 - Flow separator setup for thin wall features.....	114
Figure 100 – 8 mm copper wall section.....	115
Figure 101 – Nozzle spray pattern for corner deposition .....	116
Figure 102 - Rounded corner deposit (a) prior to and (b) post sectioning.....	116
Figure 103 - Square corner deposit formed using flow separator after sectioning .....	117
Figure 104 – Curved copper surface.....	117
Figure 105 – Ring manufacture setup diagram .....	118
Figure 106 – Copper ring (a) as deposited and (b) after sectioning .....	119
Figure 107 - Thicker copper ring.....	120
Figure 108 - Titanium ring after first stage of construction .....	121
Figure 109 – Deposited titanium tube, 55 mm height, 89 mm diameter .....	121
Figure 110 - Titanium ring creation with defined inner and outer surfaces, using flow separator tube and centre cup.....	122
Figure 111 – Sectioned titanium ring with inner and outer face sculpted.....	123
Figure 112 - System setup diagram for flange creation .....	124
Figure 113 - Titanium ring with protruding flange .....	124
Figure 114 – Flow separator-nozzle alignment angle.....	130

---

# Chapter 1 - Introduction

---

## 1.1. Research motivation

Metallic additive manufacturing is a rapidly growing field, having piqued the interest of both the public and private sectors, leading to investment across a range of fields including aerospace, motorsport and medical implants. One of the greatest limiting factors in the development of metallic additive manufacturing technologies has been the achievable build rate. Powder bed machines are limited by a maximum layer depth, melt pool scan speed and powder distribution rate, while blown powder systems that melt the material must limit their deposition rate or face large residual stresses in their components. They are also limited in material choices and often require post process machining and heat treatment.

Conversely, cold spray and supersonic laser deposition are capable of depositing a range of metals in bulk, with high densities and compressive loading. Cold spray also offers other unique benefits in the creation of metal components that cannot be replicated in processes involving melting, owing to the solid-state nature of the deposition. It is capable of retaining the microstructure of the powder during deposition, and is capable of depositing a variety of materials as well as mixtures of metals. It is also capable of handling temperature sensitive materials without damaging their unique material properties. However, there is limited control over the shaping of the deposit, and this is a significant problem that needs to be overcome to reduce the waste, time and cost of a cold spray additive system.

## 1.2. Research aims

It is expected that this research will demonstrate that a viable method for creating defined surfaces using a cold spray system with a view of creating 3D structures is desirable, allowing the development of a system to fill a competitive niche for cold spray in the metal additive manufacturing space. This research aims to investigate potential methods of shape control, attempt to characterise their effectiveness, and provide some understanding of the phenomena which govern the success or failure of the different methods. With the level of control expected it is likely that this will be for large, low complexity components, with high fidelity surfaces made in small to medium quantities.

The research will aim to create building block structures, such as flat walls, corners and curves which could be extrapolated into more complicated shapes. The research will aim to demonstrate that the created concept will be viable for a range of engineering materials, and also capable of functioning with laser assisted heating without further complicating factors. The positioning and control of the

accepted solution required to build more complex shapes will be outside of the scope of this work, as is the parameter space exploration to determine the optimal deposition conditions and limits of the achievable structures.

The scope and aims of this research led to the following questions and objectives being established at the beginning of the research, to investigate the feasibility, limitations and potential of utilising the cold spray system for 3D structuring:

- Where are the areas of opportunity in the additive manufacturing landscape, and how might cold spray find a competitive advantage in this space?
  - Determine the capabilities of current metal additive manufacturing systems, and identify the shortcomings of the processes and components
  - Evaluate the current cold spray deposition mechanism and structure
  - Examine the current applications of cold spray technology and determine the need for, and requirements of, an additive cold spray system
  - Investigate the principle applications for an additive cold spray system, and how this will affect the system to be designed
- Can cold spray deposits be controlled to directly produce net shape objects?
  - Conceptualise and test a series of solutions for defining the edges of the deposition profile
  - Determine the best approach for creation of high-fidelity surfaces and bulk near net-shape structures, focussing on surface finish and deposition shape above other parameters
  - Examine viability of different materials and the effect of laser heating
  - Create building block structures using the cold spray system that could be extrapolated into more complex shapes
- Can simulation and visualisation of the gas structure around obstacles inform the development of concepts, and indicate limitations of certain methods?
  - Construct fluid dynamics models of the gas jet from the cold spray nozzle
  - Incorporate particle tracking methods into the simulations in order to model standard particle trajectory and velocity from inlet to substrate
  - Extend simulation to cover flow obstructions, in order to understand the effects on shockwave structure and how this alters particle trajectory
  - Use simulation data to explain and predict deposition outcomes when utilising the developed profile shaping methods

### **1.3. Thesis synopsis**

This section contains a brief overview of each remaining chapter in this thesis, detailing the content and structure of the work presented within.

## **Chapter 2 – Literature review**

This chapter details the current metallic additive manufacturing landscape which, alongside traditional manufacturing methodology, is examined for an area of opportunity for cold spray in which capability is lacking. Each manufacturing method is assessed for its competences and limitations. A brief overview of the cold spray process from its discovery, through to its most recent applications in industry, is then provided. The cold spray deposition mechanism is then discussed, with the two most prominent theories presented and analysed, before an examination of the benefits and limitations of cold spray deposition, to assess whether cold spray has the capability to fill this competitive niche. The current deposition control capabilities of cold spray are explored, and the approaches to modelling cold spray are examined, to inform the initial concepts investigated in this thesis.

## **Chapter 3 – Experimental setup**

The experimental equipment which makes up the cold spray system at the Institute for Manufacturing, used for all trials in this report, is introduced. This chapter presents the standard operating procedures of the system, and goes on to detail the analytical equipment and methods used for the examination of the deposits in the subsequent chapters.

## **Chapter 4 – Exploration of deposition shaping**

Chapter 4 shows the progression of concepts for deposition shaping to create a cold spray deposit with a vertical, flat wall, using copper powder for these proof of concept trials. The effect of traverse rate on the resulting depositions is investigated, along with the effects of the nozzle alignment in relation to the edge of the forming tool. The structures are inspected to assess shape, and the experiments reviewed for ease of development into a fully three-dimensional manufacturing platform.

## **Chapter 5 – Generation and validation of computational flow models**

This chapter details the procedure for creating computational fluid dynamics (CFD) models of the cold spray nozzle and exhaust region above the substrate, first in a two-dimensional axi-symmetrical model, then developed in three dimensions to allow the addition of non-symmetric obstacles. In order to validate the accuracy of the simulations, the same method was used to model a nozzle from a published paper, and the results compared to those in the paper. Particle tracking and the chosen deposit shaping tools were subsequently added to the model to determine how the addition of obstacles affected gas flow and particle trajectory.

## **Chapter 6 – Progression of structural control**

In this chapter further material options are attempted using the shaping method developed, including materials requiring the addition of a laser for deposition, to determine how the structuring capabilities seen in Chapter 4 are affected. The effect of backstop roughness on the deposit, and the positioning of the backstop in relation to the substrate are examined. This chapter then presents the attempts to build further shapes once the method for manufacture had been established, namely corners, curves and overhangs, which by extrapolation can be used to create more complex shapes. The manufacture of several demonstration rings with defined surfaces was then completed in titanium.

## **Chapter 7 – Conclusions and recommendations**

The final chapter summarises the progress made from the experimental and simulated work, laying out the progression from concepts through to the final construction capabilities at the time of writing of this thesis. It also introduces a plan for the extension of this work, examining the possibility of converting the advancements made into a functioning additive manufacturing system.

---

# Chapter 2 - Literature Review

---

## **2.1. Introduction**

This chapter contains an overview of current metal manufacturing techniques, both traditional and additive, against which an additive cold spray system would be competing, in order to assess whether there is a competitive niche for an additive cold spray system. Each technique is examined for its process characteristics and manufacturing uses, before the market as a whole is discussed.

Following this examination, an introduction to the cold spray process is presented, comprising the discovery of the phenomenon, typical experimental arrangement, gas flow and deposition mechanism, to provide an overview of the current state of the field. Understanding the gas structure and practicalities of deposition are vital in understanding how to manipulate the deposition shape. Following this is an examination of cold spray characteristics, along with current cold spray deposition control capabilities and its applications, including any research into additive manufacturing.

## **2.2. Metal additive manufacturing overview**

Metal additive manufacturing has of late been receiving attention for both industrial and academic purposes. Much of the focus has been on the geometric freedom offered by powder bed systems, with a range of engineering materials that can be difficult form using traditional manufacturing processes. This has been particularly of interest in aerospace and medical component manufacture for complex component generation[1], for part number and assembly reduction [2], [3], and in the construction of low volume custom components [4], [5].

For the establishment of a cold spray process that is capable of creating net shape structures, it is important to consider how this technology would compete with existing manufacturing routes. Once the strengths and weaknesses of these methods have been analysed, the specific advantages of cold spray over other systems can be investigated, and a net shape cold spray system designed to exploit them. Presented in this section is the state of the art in research and industry for additive manufacturing techniques.

### **2.2.1. Powder Bed**

Powder bed fusion processes involve the targeted consolidation of individual layers of powdered material by providing energy to localised regions of a build area, creating the component in the build chamber from the bottom up. After each layer has been completed, the build platform on which the

components are created will be incrementally lowered, and fresh powder will then be distributed and levelled across the build area.

All powder bed technologies share some common advantages and disadvantages, with the layer by layer approach to component consolidation allowing for intricate and internal feature to be created, while also meaning long lead times as each layer is processed in sequence.

#### **2.2.1.1. Electron beam melting**

In electron beam melting (EBM) systems, the consolidation energy is provided by an electron beam, generated within the machine. This beam is then split and controlled via three pairs of electromagnetic coils, for positioning, focus and astigmatism, allowing fast scan rates as the beam position can be rapidly changed. The layout of a typical system can be seen in Figure 1, depicting the layout of an Arcam A2X machine [6]. This allows the system to maintain several melt pools concurrently, multiplying the rate at which the build can be consolidated. In order to allow the electron beam to reach the powder bed, the build chamber must be kept under a high level of vacuum for the duration of the build. The chamber is evacuated to approximately  $4 \times 10^{-3}$  mbar, having been evacuated further and allowed partial pressurisation with helium. When the electron beam hits the powder particles in the bed, the kinetic energy of the electrons is converted into thermal energy, creating a melt pool that is moved across the surface of the powder bed to consolidate the layer.

The beam power provided from the tungsten filament is 3 kW, with an absorption efficiency of approximately 70% due to backscatter from the powder, and a minimum beam diameter of 180  $\mu\text{m}$  focused at the powder bed. Lanthanum boride crystals are replacing the tungsten alloy filaments in the newer EBM systems, allowing for a smaller spot diameter and therefore finer control of the melt pool, though these are not yet in common use.

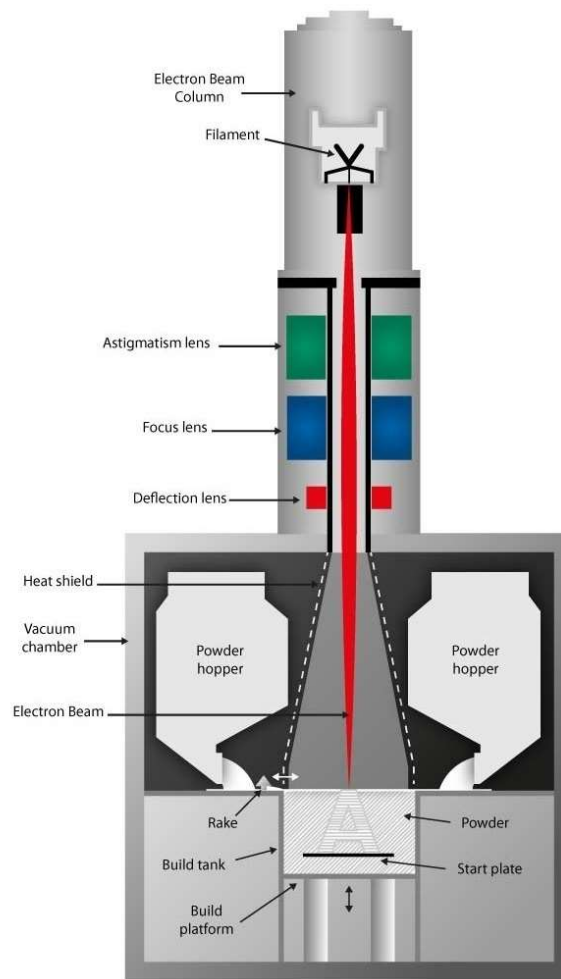


*Figure 1 - ARCAM EBM system schematic [6]*

Materials currently used in EBM machines include titanium alloys, aluminium alloys, steels, Inconel and nickel alloys. Powder sizes used in EBM machines vary from 40 – 70  $\mu\text{m}$ . EBM manufacturing is currently the fastest of the powder bed fusion processes, capable of producing up to 1kg of material per hour in a build volume of 500 x 280 x 320 mm.

EBM machines are capable of building components that are up to 99.9% dense, with a minimum feature size of approximately 0.1 mm. The typical stated machine accuracy is +/- 0.1 mm. Components for engineering applications typically require post processing to improve the surface finish, with surface roughness values of  $R_a \sim 30 \mu\text{m}$  in currently available commercial machines, though the Arcam Q20 has demonstrated a higher quality surface finish than any previous commercial machine.

The machines are also expensive, costing in excess of £1m per machine, and, for relatively new systems, this is a high capital expenditure for companies when the machine cannot be guaranteed to work as per their requirements. It also means that there is a much higher cost to change for companies with a legacy process, and so presents higher risk.

### **2.2.1.2. Laser powder bed fusion**

As with other powder bed processes, the construction of components using laser-powder bed fusion (LPBF) machines – also known as Selective Laser Melting (SLM), Direct Metal Laser Sintering (DMLS) and Laser Cusing – follows the procedure of consolidating the powdered feed material on a given layer, lowering the build platform and recoating the surface with a level surface of powder for consolidation into the next layer. In LPBF machines, the consolidation energy is provided by a laser beam, which is guided by galvanometers to melt the pattern required for that layer in the powder bed. To avoid oxidation of the powder as it is melted, the build chamber is converted to an inert environment, typically Argon or Nitrogen depending on the material.

Typical deposition rates of LPBF machines range from tens of grams to a maximum of 1kg an hour. The build area on LPBF machines has been steadily increasing, with the largest being approximately 800 x 400 x 500 mm. LPBF produces high density components, over 99%, with a typical surface finish  $R_a \sim 4 - 10 \mu\text{m}$ . The minimum feature size varies between 0.04 - 0.2 mm depending on the laser spot size, with an accuracy of 0.02 – 0.05 mm.

As the powder is melted during consolidation and the build chamber is not heated, it is difficult to control the microstructure of the component. The rapid cooling of the layers after creation due to the lack of a heated bed leads to large residual stresses in the component [7]. The component must therefore be fastened to the build plate by supports, and the entire build heat-treated before being removed from the base plate to avoid warping.

LPBF machines are currently typically being used for prototyping of components, especially in aerospace, for manufacturing of medical implants and injection mould tools, as conformal cooling channels can be made directly below the surface.

### **2.2.1.3. Selective laser sintering**

Similarly to selective laser melting, laser sintering works by selectively heating regions of the available build area by irradiation with the laser spot. The difference is that in laser sintering, the powder is heated by the beam to just below its melting point rather than above, allowing coalescence at the contact points without melting the bulk of the powder.

The lack of melting does create a rougher surface finish than LPBF components, and a higher porosity than other forms of metal powder bed fusion. There are methods around this, such as the diffusion of other metals throughout the material or isostatic pressing, which in some cases can be beneficial.

## 2.2.2. Directed energy deposition

Processes that fall into the directed energy deposition (DED) category involve the deposition of material to build a geometry by feeding the material as required into a melt pool generated by a focussed source of thermal energy. These systems are typically mounted on a multi-axis robotic arm above a fixed bed, or occasionally are fixed in position over a multi-axis bed.

### 2.2.2.1. Blown powder laser deposition

The first type of DED systems are those being developed from laser cladding systems used to coat existing geometries, to allow the freeform fabrication of components. In blown powder laser deposition techniques [also known as laser engineered net shaping (LENS) or laser consolidation], a melt pool is created and maintained using a high-power laser system, typically between 0.5 – 3 kW, focussed onto the substrate or previous layer. The materials to be deposited, typically metallic powders, are then fed into the melt pool via powder feeders. The melt pool is moved along the surface to create a layer of deposited material, and the component is typically built up layer by layer on a 3-axis bed, up to a maximum size of 400 x 400 [8]. Some systems involve a 5-axis bed, with the greater geometric freedom allowing for the creation of more complex components without requiring large support structures. These systems offer a rate of deposition that is typically between 1-2 kg/hr [9].

Laser powder fusion systems are capable of working with a range of metals including steels, titanium and its alloys, and aluminium. These systems also have the possibility to offer multi-material and functionally graded components, including in-process alloying using side jets, with careful attention required to the material melting points.

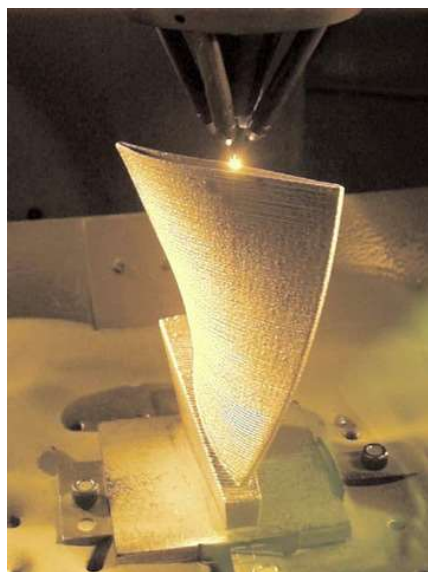


*Figure 2 - Sandia LENS System [8]*

Components manufactured by laser engineered net shaping show densities upwards of 95 – 99 %, depending on the material and cladding parameters, and exhibit decent metallurgical properties, with hardness values similar to those of the bulk material. Laser powder fusion systems provide poor feature resolution in comparison to powder bed systems, as the typical melt pool size is in the order of a few millimetres. These processes still have some beneficial applications, where the production of near net shape components requiring a small degree of finishing is a vast improvement on machining the entire component from a larger block, in terms of waste, time and cost reduction.

The required melting of the powder also introduces further disadvantages of this method of manufacturing. The large amount of thermal energy creates high residual stresses in the completed components and means that the microstructure cannot be easily controlled during deposition, both of which would require heat treatment following manufacture. It also means that the atmosphere needs to be carefully controlled in order to avoid oxidation of the part as it is being created. If being used for component repair or feature addition, the deposition will also create a large heat affected zone in the substrate component, creating thermal stresses and affecting the microstructure too, though this could potentially be corrected with post heat treatment.

Current applications of laser engineered net shaping techniques include the repair of high value components, particularly those with difficult to work materials such as injection moulding tools and non-critical aerospace parts, and the manufacture of parts for medical implants and aerospace.

Companies often offer these applications as services, as the machines can be costly and require specialist knowledge to use correctly. These companies are developing worldwide, such as IREPA laser and BeAM in France, Accusfusion in Canada, Optomec in the USA.

#### **2.2.2.2. Wire fed power systems**

Power welding systems create and maintain a melt pool with a large-scale plasma-welding torch or electron source, as shown in Figure 3, where material is fed through a powder stream or spooled from a wire for a more controlled material input rate. These systems are capable of depositing bulk material at rates of between 1-20 kg/hr, over a large area for the creation of large-scale components.

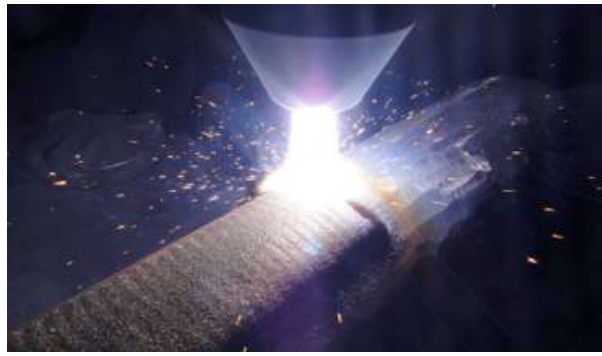


*Figure 3 - PTA deposition torch*

The required temperature and high deposition rate when using PTA machines can cause a range of issues similar to those faced by blown powder methods. The created geometries have very large residual stresses, and induce large heat affected zones into any substrate. It is not possible to accurately control the microstructure of the deposition, as the thermal gradients will vary and the process is not temperature controlled. Upon cooling, there is the possibility of creating voids and cracks, and the gas shrouding required in some processes can lead to air bubbles being captured at higher deposition speeds. The density of components produced by wire fed power systems is often >99%.

These capabilities are also often provided as a service, from companies such as Norsk Titanium, though commercial machines are available from Sciaky in addition to the service option that they provide.

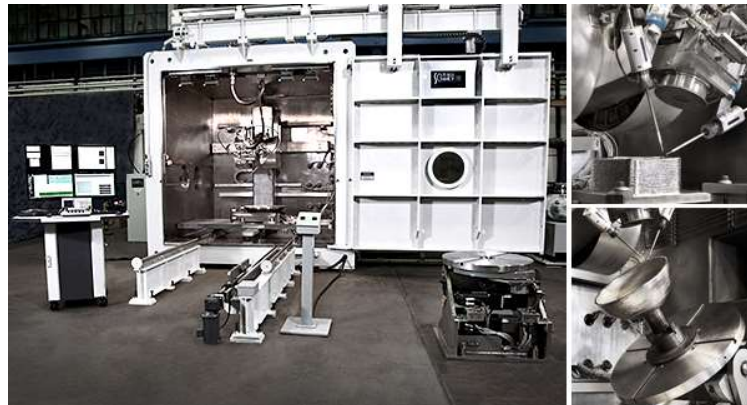


*Figure 4 - Sciaky electron beam additive manufacturing (EBAM) system [10]*

### **2.2.3. Coating Techniques**

Coating techniques are often used in the remanufacture of components in order to reclaim the value of damaged components. Plasma spraying has already been mentioned as a method for 3D geometry creation, and is also used for coating creation, and several of the other techniques are being investigated for development into 3D structuring systems. However, all of the processes noted in this

section face similar issues due to the temperature at which the material is deposited, typically 1000° - 3000° Celsius depending on the material, which will cause heat affected zones in the substrate, potential porosity and residual stresses in the substrate and deposit.

### 2.2.3.1. Flame Spraying

When coating by flame spraying, the material to be clad is fed into the flame of an oxyacetylene torch, in wire or powder form, where it melts and forms droplets of approximately 50 µm in diameter. The droplets are pushed by the oxyacetylene gas stream towards the substrate at relatively low speeds of 50 - 100 m/s, where they spread upon impact and bond as they solidify.

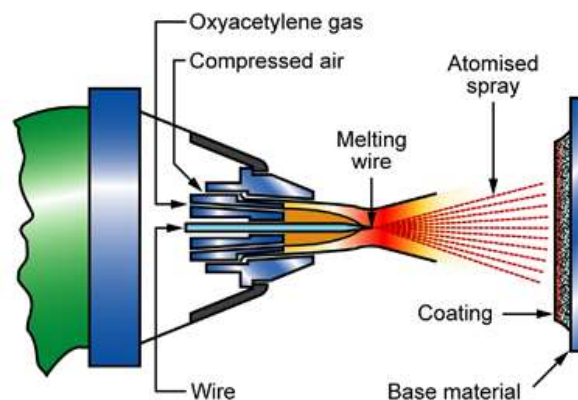


Figure 5 - Flame spraying schematic [11]

Wire fed systems often produce higher quality coatings as the material feed rate can be more carefully controlled, and the material must be molten before it will leave through the nozzle, unlike with powder feedstock which is not guaranteed to be molten.

Flame spray deposits have a surface roughness (Ra) of 30 – 50 µm, which would require post-process machining. This is due to the particle size of the feedstock powder and the droplets formed by the wire melting. Capable of achieving deposition rates of up to 15 kg/hr, flame spraying is one of the fastest processes available, but deposits can have porosity of 10 - 15%, depending on the material. This is typically caused by the entrapment of the accelerating gas in the molten deposit before solidification.

### 2.2.3.2. High velocity oxygen fuel deposition

HVOF is essentially the same process as flame spraying, except that the fuel system has been modified to give much higher spray velocity, which can often exceed 1000 m/s. In HVOF spraying, a high-pressure gas stream is generated by the continuous combustion of a fuel, gas or liquid based, with oxygen in a combustion vessel. This gas stream is directed through a converging-diverging nozzle, similarly to that in a cold spray system, in order to accelerate the flow to supersonic speeds. Powder

is then injected into the stream, where it melts due to the high gas temperatures before impacting the substrate and solidifying.

The porosity of HVOF coatings is typically lower than 1% though can contain impurities from the combustion gases and oxidation of the depositing material, with build rates of up to 9 kg/hr [12, p. 89].

### 2.2.3.3. Wire Arc Spraying

In wire arc spraying, the molten feedstock is provided by the feeding of wire into an atomising gas, whereby the electrical discharge between the two wires causes them to melt. These molten droplets are then accelerated by the gas towards the substrate, where they solidify upon impact. Coating materials are restricted to metals available as wire, and occasionally ceramics, glass or carbon that can be sourced as wire.

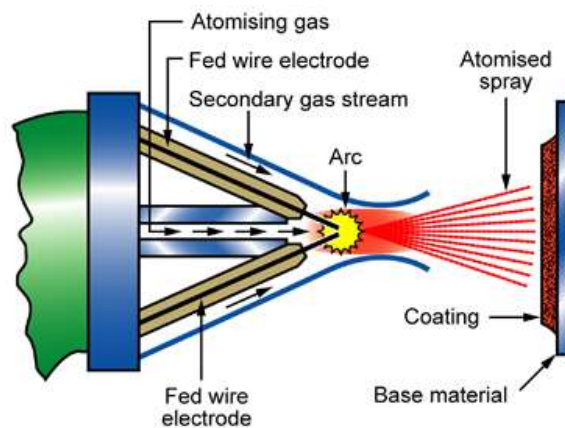


Figure 6 - Wire arc spraying [11]

This method is capable of depositing material at rates of up to 20 kg/hr, but can be up to 20% porous depending on the materials.

## 2.3. Traditional manufacturing techniques

In addition to competing with other metal additive systems, all additive manufacturing systems are faced with the challenge of outperforming the more traditional, established manufacturing techniques. They compete for advantage in areas ranging from cost, time or energy savings to waste reduction, wider material choices or microstructure control. This section contains a brief outline of the strengths and weaknesses of each method, and how they compare to standard additive techniques, as well as a potential cold spray system.

### 2.3.1. Forging

Forging processes shape metal using compressive forces, pressing, pounding or squeezing, to work the original billet into the desired shape with hammers, presses or dies, as shown in Figure 7. Forging may be done across a range of temperatures, usually classified by comparison to a material's recrystallization temperature. Cold forging of metal components can cause work hardening of the metal, as it is strengthened by the dislocation movement during plastic deformation. In hot forging, the temperature is high enough to allow the metal to recrystallize, avoiding the work hardening effects. There is also warm forging, whereby the material is heated to increase ductility and reduce tool or press loading, but not sufficiently to allow recrystallization.



*Figure 7 - Hot forging of titanium [13]*

Forging methods are capable of producing a vast range of size of component, from small objects of a few hundred grams, to equipment for heavy industry at over 200 tonnes. The parts produced have excellent structural integrity, with the method of formation ensuring that they are almost 100% dense, without the possibility of gas pockets or cracks when cooled appropriately.

The high repeatability of the process and good mechanical strength of the components are also major advantages of forging, particularly when safety critical components are required. Forged components exhibit good mechanical strength, and are dimensionally accurate, with Ra values of 2 – 20  $\mu\text{m}$ .

However forging has certain limitations when it comes to production. Expensive and sizeable equipment is required for each new component to be built, requiring large manufacturing batches to become cost-effective. There is also limited shape potential, as moulds cannot be overlapping or contain internal features such as threading, and there is difficulty in post machining processes.

### 2.3.2. Casting

Metal casting involves the pouring of molten metal into moulds where it solidifies to take the shape of the mould. There are several types of casting, and choosing which type to use depends on factors such as production volume, material, cost and dimensional accuracy required. As all of the casting methods

are molten processes, all will have problems with solidification shrinkage, the potential for gas pockets and porosity.

Sand casting consists of moulds that have been shaped into a mould cavity using natural or synthetic sand, by pressing around a wooden or metal pattern of the required part. After the pouring of the molten metal, the part is cooled and the sand broken away to reveal the final shape. Typically used in the manufacture of large parts with high production volumes, the surface finish of these parts is rough,  $R_a \sim 10 - 50 \mu\text{m}$ , so extra stock is added for post-process machining.

In die-casting, the molten material is injected under high pressure into a reusable metal mould, helping to ensure the production of repeatable objects. The high-pressure aids in ensuring the entirety of the mould is filled, and care is taken during design to ensure that material solidification will not occur and block the filling of the mould. These moulds provide a very smooth surface finish,  $R_a \sim 0.5 - 2 \mu\text{m}$ , and so require minimal post processing.

There are limitations to casting, as there are limitations to the materials that can practically be poured while molten and that have moulds that can withstand repeated use at these temperatures, as well as the costs associated with this problem. The initial costs can be expensive, so this process is not practical for small volume production. The complexity of design is also limited by the ability to create a separable mould to remove the component.

Due to the different types of casting, applications range from making small components, such as small toys, to large steam turbine blades.

### **2.3.3. CNC machining**

CNC machining involves the subtractive machining of components from a larger starting billet. These machines are typically flexible systems, capable of making many different components on the same machine with only a change of program required. This is aided by the fact that there is effective CAD integration, so a part can be designed and quickly made machine ready. The process can be very precise, with machines able to cope with tolerances of 0.01 mm, and with excellent surface finishing capabilities, from 0.2 – 5  $\mu\text{m}$ . The process is also highly reliable, producing identical components over large production runs, which can be operated continuously until maintenance is required.

However, machining large volumes of components is costly and time consuming, and can generate large quantities of machining waste. Certain materials will also be extremely difficult to machine, for example those used in hard-facing or wear resistant applications.

## 2.4. Overview of manufacturing techniques

Table 1 – Metal manufacturing methods properties overview - 2018 (\*maximum build area for commercial system, not theoretical maximum)

<u>System</u>	<u>Surface roughness</u> Ra (µm)	<u>Density</u> (% of fully dense)	<u>Deposition rate</u> (kg/hr)	<u>Accuracy</u> (± mm)	<u>Near net shape</u> capability level	<u>Maximum build area*</u> (mm)	<u>Materials</u>	<u>Relative Cost</u>	<u>Common Applications</u>	<u>Key Advantages</u>
<b>EBM</b>	25 - 130	Up to 99.9	0.1 - 1	0.2	High	500 x 280 x 320	Ferrous and non-ferrous metals and alloys, commonly steels, bronze, Al, Ti and Ni	High	Prototyping, rapid tooling, aero components, medical devices/prosthetics	Complex and internal features and good microstructure
<b>LBPF</b>	5 - 40	Up to 99.9	0.1 - 0.5	0.05	High	800 x 400 x 500		High		High accuracy allows for small and complex features, and good surface finish
<b>DED - Laser</b>	4 - 10	90 +	3	0.1	Medium	2000 x 1500 x 750	Ferrous and non-ferrous metals and alloys, commonly steels, Al, Ti, Co, Ni and bronze	Medium	Aerospace components, tool repair, large structural components	Large components, high accuracy, good for repair
<b>DED - E-beam</b>	8 - 15	99 +	10	0.25	Medium	2000 x 1500 x 750		Medium		Large components, high deposition rate with high density
<b>Wire Arc AM</b>	10 - 30	99 +	0.5 - 20	2+	Medium	3000 x 3000 x 10000		Medium		Highest achievable deposition rates, large material options
<b>Forging</b>	2 - 20	Up to 100	Variable	Mould accuracy down to 0.01	High	5000 x 3000 x 1000	Most metals	Medium	Automotive, agricultural, oil and gas, heavy industry	Well established process, high quality surface finish, high accuracy

<b>Casting</b>	0.5 - 50	90 - 98	Variable	Mould accuracy down to 0.01	High	Large scale variation	Al, Mg, Cu, Zr and other low-cost metals	Low in volume	<i>Transport, machine tools, heavy industry, household</i>	<i>Well established process, can create very large components, cheapest option</i>
<b>CNC Machining</b>	0.2 - 5	Up to 100	Variable	0.01	Very High	2000 x 3500 X 10000	Most metals	High	<i>Aerospace, household, automotive</i>	<i>Best achievable surface finish</i>
<b>Flame Spraying</b>	30 - 50	85 - 99	1 - 15	0.5 - 1	Low	2000 x 1500 x 750	Al, Cu, Ni, Sn, Zr, steels	Low	<i>Corrosion protection, component repair, surface coating</i>	<i>Low cost and simple</i>
<b>HVOF</b>	50 - 100	99 +	1 - 9	0.5 - 1	Low	2000 x 1000 x 750	Tungsten carbide, Chromium carbide, Aluminium bronze	Low	<i>Oil and gas, power, mining, aerospace</i>	<i>High density, low cost approach</i>

As can be seen from Table 1, the systems capable of rapid build rate are typically those that suffer from a lack of accuracy. They also tend to have secondary problems, lacking variety in material options or creating residual stresses in the components from the high operating temperatures.

Alternatively, those systems with high accuracy and high-fidelity surfaces are those with comparatively much slower build rates, to allow for a greater level of complexity in the components. Whilst this increases the variety of manufacturable components, it also creates much longer lead times and manufacturing times per machine, usually also at a significant increase in cost and the manufacturing development required.

There is clearly an opportunity space for the potential development of a system that approaches the ideal of a high build rate, high accuracy, high fidelity system that creates the required material and mechanical properties without being prohibitively expensive or creating secondary complications such as residual thermal stresses or porosity.

When investigating potential techniques for filling this space, the relatively high achievable build rate and controllable material properties of cold spray coatings suggested that it was a practical prospect for development, prompting further investigation of the current state of the art in cold spray, detailed in the subsequent sections.

## 2.5. Cold Spray

As can be seen from the overview of additive manufacturing techniques, there is a gap in the market for a high build rate, high density, near net capable system to compete with components that are usually cast, or require materials that prove difficult for other manufacturing methods.

In order to determine the viability of creating an additive capable system from cold spray to fill this niche, the mechanisms and capabilities of the coating system must first be understood. In the subsections that follow, the cold spray method is introduced, along with the deposition method and deposit characteristics. These areas are scrutinised to determine whether the cold spray system is suitable for adaptation to an additive platform.

## 2.6. Cold Spray discovery

Cold gas-dynamic spraying was discovered at the Institute of Theoretical and Applied Mechanics of the Siberian Branch of the Russian Academy of Sciences (ITAM SB RAS) by Professor Anatolii Papyrin and colleagues, during a study into the flow field around an obstacle in a two-phase flow, of gas and powder particles, in a wind tunnel [14],[15]. Particles of aluminium travelling at velocity of approximately 400 – 450 m/s were found to adhere to the surface of the cylindrical obstacle at 280 K, causing a thick coating to be built up, whilst Plexiglass particles did not adhere, and bronze particles were found to cause erosion under the same conditions.

*“The microphotographs of the sprayed layer showed that the coating consists of strongly deformed and densely packed particles uniformly covering the surface. The coating has a scaly structure with dense packing without noticeable pores and voids.”*

- Professor Anatolii Papyrin [15]

This phenomenon was noted by the team, published and further investigated at the academy, leading to the development of the cold spray systems in use today.

## 2.7. Experimental arrangement

Though the cold spray systems vary between institutions as they are adapted for specific purposes or research requirements, for example the addition of a laser as explained in Section 2.11, the underlying fundamental system is common to all.

### 2.7.1. Apparatus

High-pressure gas is required for the process, and is provided to the system before being split into two streams. This gas is often heated in order to increase the local speed of sound, and its positive drag

force on particles, allowing the highest possible gas velocity, and therefore powder velocity, for a given temperature. The powder to be deposited is then entrained within the jet of carrier gas by means of a high-pressure powder feeder, before recombining with the other gas stream at the nozzle entrance. The nozzles used in cold spray are converging-diverging (de Laval) nozzles, explored in more detail in Section 2.9. The carrier gas is accelerated through the nozzle as the pressure drops to atmospheric pressure, accelerating the powder to velocities typically between 500 – 800 m/s. This powder stream is then directed towards the substrate, whereupon it forms a coating during impact.

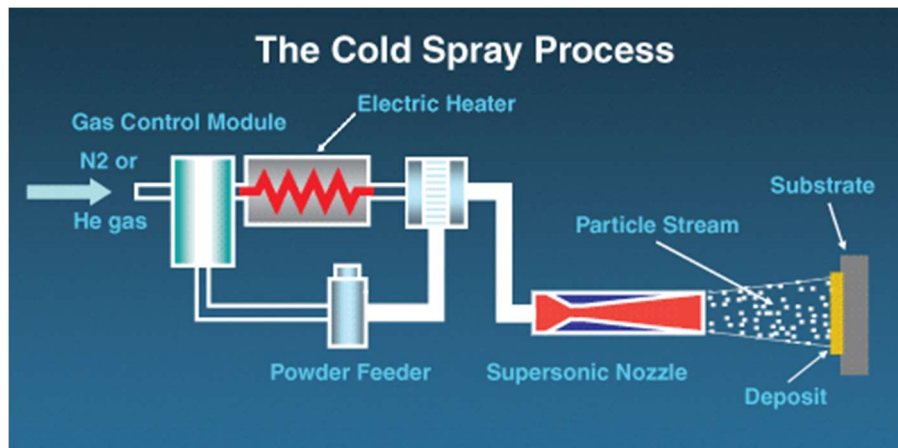


Figure 8 – Cold spray schematic [16]

Less commonly, a low-pressure gas supply is used to pick up powder from the powder feeder, and the powder is fed into the supersonic nozzle, usually radially instead of coaxially, downstream of the throat. This is more typical of portable cold spray systems, as smaller, lower-pressure powder feeders can then be used.

Most systems will also employ ancillary equipment for control and safety purposes, such as positioning stages, rotary stages, articulated robots and environmental control chambers. There is no reason why either the nozzle or the bed couldn't be mounted upon a 6-axis platform, allowing for complete dimensional freedom of the substrate relative to the nozzle.

## 2.7.2. Typical cold spray parameters

Table 2 – Typical cold spray parameters

Parameters	Typical Values
Gas Type	Helium, nitrogen, air, water vapour
Gas Pressure	0.5 – 5 MPa
Gas Temperature	0 – 1100 °C
Powder Material	Various metals and alloys, (commonly Cu, Al, Fe, Ni, Ti, W), composites
Powder Particle Size	1 – 100 µm
Gas Flow Rate	500 – 4000 litres/min
Powder Feed Rate	Up to 20 kg/hr (material dependent)
Standoff Distance	10 – 40 mm
Impact Angle	Perpendicular ± 60 ° (material dependent)
Substrate Material	Metals, glass, polymers, ceramics
Traverse Rate	Flat: 0 – 100 mm/s
	Rotational: 0 – 500 mm/s

## 2.8. Deposition mechanism

It is important that the deposition mechanism is understood, as developed concepts should not adversely affect the deposition capability, whilst attempting to avoid issues with adherence to any shaping mechanism.

The velocity of the powder particles is the key variable in providing enough energy to promote deposit-substrate bonding. A series of experiments were conducted to determine at what velocity the mechanism moved from one of erosion at low velocities, noted to have been previously demonstrated by Preece [17] at particle velocities of 10 – 100 m/s, to one of adhesion and subsequent cohesion. This velocity was termed the “critical velocity”, and changes depending on particle size, material and properties. Critical velocities have been widely studied in order to provide specific values for given powder-substrate combinations, with a range of experiments [18]–[22] and numerical simulations [23]–[25] conducted. Similar investigations regarding critical velocities have been carried out for larger powder particles, for a process called “kinetic spraying” [26]–[29] involving the same principles. The

critical velocity has been shown to be dependent on the diameter of the particles, with the smaller particles having a higher critical velocity [30], [31].

Similar to the critical velocity, there is a critical angle of impact with the substrate beyond which the powder particle will not adhere. Deposition efficiency – the proportion of impinging powder that adheres to the surface – is reduced as the incident angle is reduced from normal to the substrate towards this critical angle. This was demonstrated with the deposition of titanium at 20 bar and 240°C, showing little change between 90° and 70°, but a rapid fall to 10% when decreased from 70° to 50° [32], [33], and has been noted in many papers since. This phenomenon is also noted as powder is deposited from a stationary nozzle, as the deposit builds forms a conical peak that stops expanding when the angle of the sides of the cone become the critical angle, explained further in Section 2.9.1.

The bonding mechanism between powder particles and the substrate has been extensively researched by a range of authors over the last fifteen years, and is widely accepted to be in majority due to intermetallic bonding between the powder particles and the substrate all occurring in the solid state [23], [34]. The impact of the powder particle causes the oxide layers on the particle and the substrate to rupture and be pushed to the sides of the impact zone, which exposes “clean” metal faces of the substrate and particle to each other under high contact pressure, allowing for intimate metallic bonding, as shown in the simulation in Figure 9.

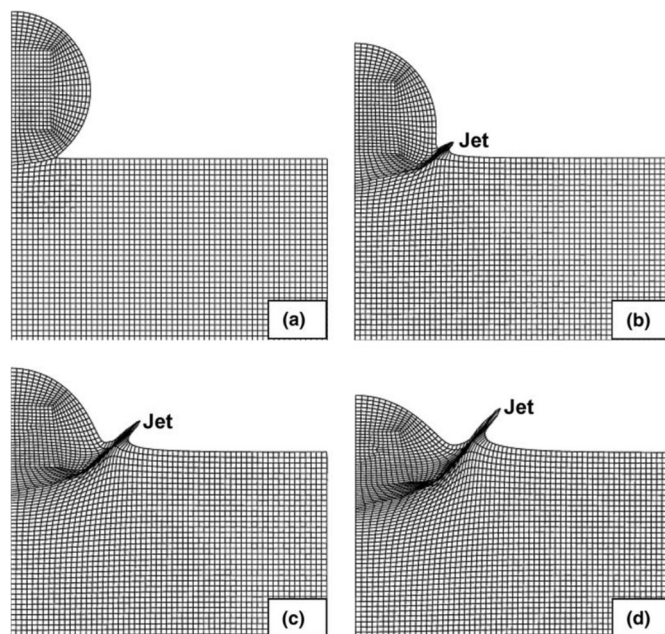
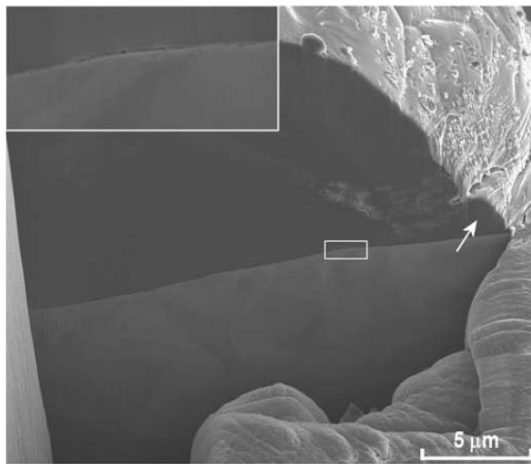


Figure 9 - Sequence of particle impact (a) 4.4 ns; (b) 13.2 ns; (c) 22.0 ns and (d) 30.8 ns. [35]

The mechanism that facilitates this exposure of clean surfaces is thought to be the adiabatic shear, as the powder particles impact into the substrate material, causing local plastic deformation, and the “jets” that can be seen when cross-sectioned, as shown in Figure 10 [35]–[41]. Normally the strain is

distributed evenly across the material, however in adiabatic shear situations the energy transfer is too rapid, meaning that a narrow layer, or “band”, of intense shearing occurs. This causes localised raises in temperature which are not diffused quickly enough into the bulk material, causing high material softening and allowing for the plastic deformation that can be observed. A few papers have indicated that in these areas there may be evidence of localised melting at the interfaces, but this is not widely accepted [42].

More recently, papers have begun to examine whether there can be alternative explanations for the jetting of the powder particles, mainly that there is a pressure release at the particle boundary [43]. The formation of the jets from the particle is not disputed, solely the mechanism by which they are formed.



*Figure 10 - FIB cross section image of cold sprayed powder particle, arrow points to the jet [44]*

It is also believed that there is some mechanical interlocking of the powder and substrate providing an extra bond strength to the deposits, or even the majority of the deposition strength in less ductile particles. Simple topological bonding is suggested whereby the powder particle is encapsulated by the substrate after impact and the subsequent impacts, causing a mechanical linkage. There is also the suggestion that the two surfaces flowing over each other as the particle shears on impact may cause vortices or rollup of material on a smaller length scale [36], as shown in Figure 11.

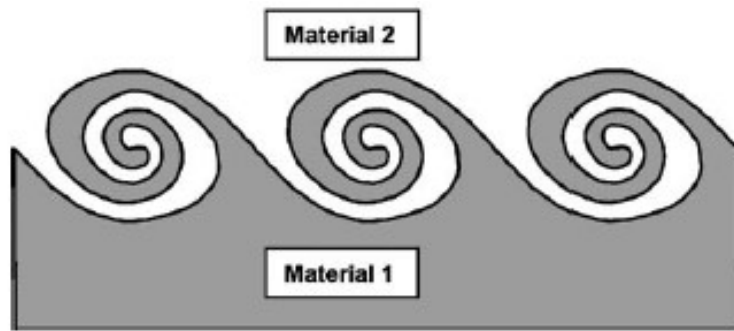


*Figure 11 – Schematic of rollups caused by interfacial instabilities [36]*

These theories are both contested as individually they do not provide sufficient bond strength to account for that which is measured [34]. Most recently, theories presenting a combination of these bonding mechanisms have emerged, though whether the majority of the noted bond strength can be attributed to metallurgical or mechanical bonding is still not agreed upon [45].

Given the recently demonstrated ability of cold spray to deposit metal coatings onto non-metallic substrates [46], [47], and the ability to deposit plastic, glass and ceramic particles, there must be a level of mechanical interlocking at least between the first layer of impacting particles and the substrates. It is therefore extremely likely that there is also a level of mechanical interlocking between the subsequent layers also, strengthened by the metallurgical bonding mentioned previously.

## **2.9. Deposition shape**

The largest challenge facing the development of an additive cold spray system is altering the structure of the deposit as it is formed. A method is required to control the shape of the deposition, without negatively impacting the properties of the deposit, or losing the advantages that cold spray provides.

### **2.9.1. Free-standing cold spray deposition profile**

As powder is accelerated through the cold spray nozzle from the powder needle, the diverging nature of the gas causes the powder stream to diverge also. This causes a Gaussian distribution of particles around the centreline of the nozzle, and therefore a Gaussian deposit is formed. As subsequent layers are deposited, these Gaussians will stack upon each other until the critical angle is reached, mentioned in Section 2.8, whereby no further powder will adhere, leaving the triangular profile to finish, shown in Figure 12a. To counter this, the most typical approach is to deposit evenly spaced tracks with low heights and then pass back over the spaces in between, attempting to even the surface before the critical angle is approached.

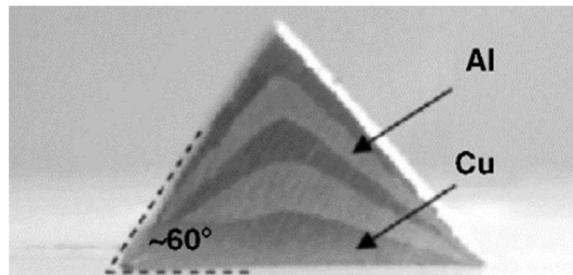


Figure 12 - Single track cold spray deposition profile reaching the critical build angle (different materials to viewing)

## 2.9.2. Current deposition shape control capabilities

The use of cold spray as a potential mechanism for freeform fabrication or direct part manufacture is mentioned on several occasions, most often in review papers, which suggest potential for the technology in this area [48]–[50]. However, there has been little published on altering the profile of cold spray deposits, with most research in this area seeming to focus on flattening the profile of each layer by increasing the traverse rate, allowing easier deposition of even coatings when adjacent tracks are overlapped. The little that has been published is detailed in this subsection.

### 2.9.2.1. Angling

Several attempts have been made to create shapes approximating a final shape by depositing subsequent tracks at an angle to the first, in order to build out layers in different directions. As can be seen from Figure 13, it is possible to approximate a vertical surface using this angling and subsequent deposition technique [50]. However, to do this the layers must be built tall enough to start with to become the deposition substrate for the next tessellated deposition, reducing deposition efficiency as the deposit is built steeper. The available shapes are also limited by the ability to position the nozzle appropriately for deposition, and by the fact that there will always be an angled surface at the sides of the deposit.

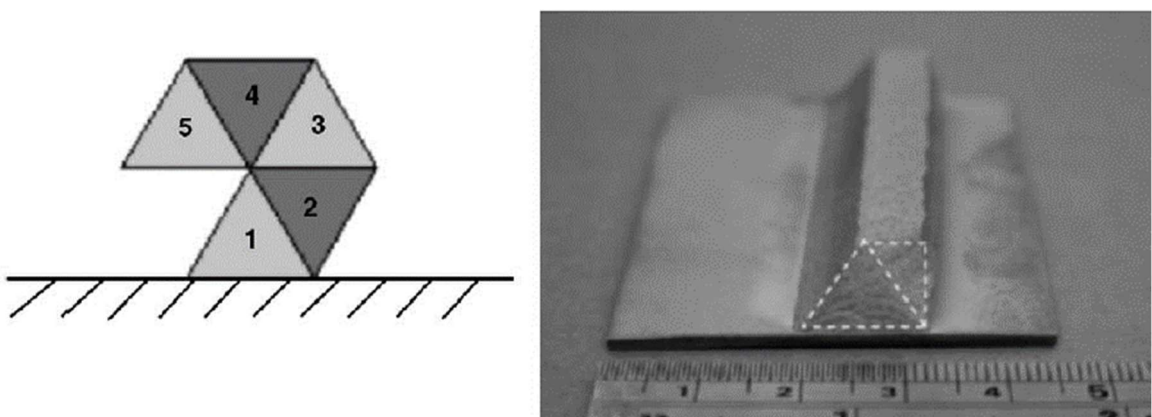


Figure 13 - Tessellation for structuring cold spray deposition

### 2.9.2.2. Masking

The largest alteration to the deposition profile of as deposited powder was an investigation conducted on the use of masks to create near net shape pyramidal fins for a heat exchanger [51], as seen in Figure 14. A steel wire mesh was placed 25 mm in front of the nozzle, at a set, 2 mm offset distance from the substrate, and aluminium sprayed through [51], [52]. The material used was AL A5001, sprayed at 30 bar and 300 °C. The effect of this was to create pyramidal deposits on the substrate, while it was noted that the top of the wire mesh also becomes fouled with depositing aluminium. As can be seen below, the formed deposits were 5 % porous and the surfaces of the pyramids were rough .

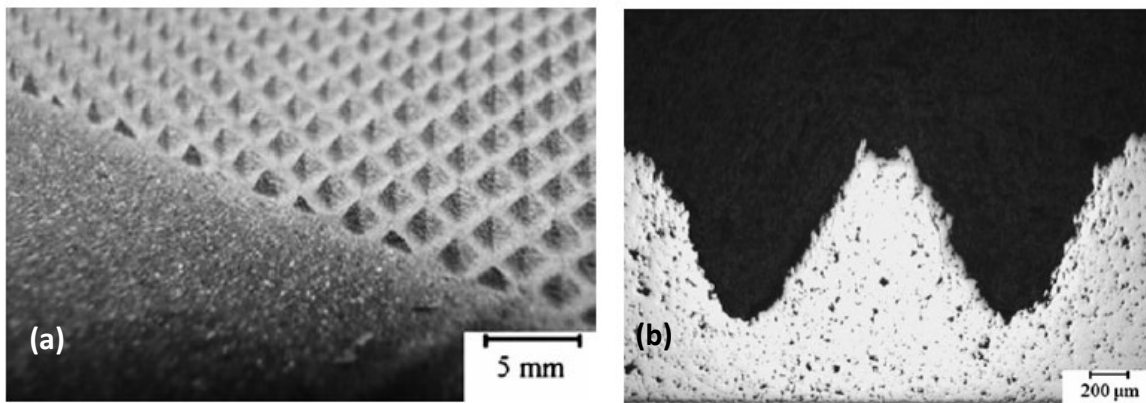


Figure 14 - Pyramidal fin arrays from cold spray through a mesh (a) as deposited (b) after cross sectioning [35]

A similar study was conducted to determine the effects of placing a mask consisting of a plate with a circular aperture in the gas stream [53], as shown in Figure 15. A substrate was placed at variable distances behind the mask, with similar results. A polymer washer was added to the powder facing side of the mask in an effort to create a smaller replaceable surface, minimising the problems caused by fouling of the mask. While this would potentially reduce the turnover rate of masks, it would likely not stop the fouling of the surface which may affect the deposition, and may introduce contaminating polymer particles into the deposition zone if any is eroded from the washer.

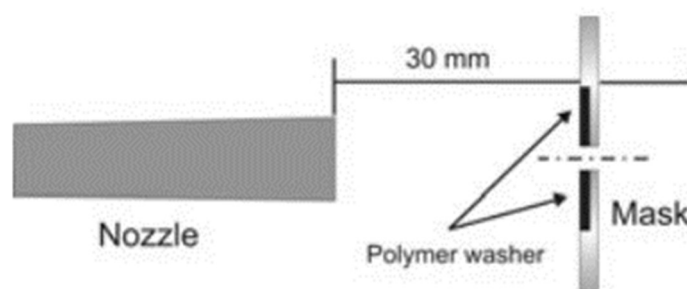


Figure 15 – Mask [53]

The depositions formed during this study, seen in Figure 16, appear similar in nature to those formed from the typical cold spray process, with perhaps a wider scattering of particles onto the substrate, as the gas flow diverges under the mask causing smaller particles to be dragged further from the centreline.



*Figure 16 - Pyramid deposit formed by masked cold spray [53]*

The deposits formed in both of these cases are still defined by the critical build angle of the depositing powder. While the deposition has been altered from the typically form, it has been achieved by placing further reductions and restrictions on the deposit structure, which doesn't suggest great potential for future applications.

No further control has been demonstrated over the shape of the depositing powder using masks, other than to limit it to pyramids, however this masking approach has clearly altered the deposition, and so further investigation into the use of masks would be a sensible starting point to the research in this thesis.

### **2.9.2.3. Flow Swirling**

Another method of altering the deposition profile was attempted by the addition of a "flow swirler" upstream of the De Laval nozzle to alter the flow of the gas [54]. Kiselev et al. managed to alter the deposition structure from a conical profile to a ring shape with this method, as shown in Figure 17. The potential of finding a compromise between the two deposits and providing an even deposition profile would allow a more easily controlled build-up of cold spray deposited layers, but would require a significant amount of effort as the results would vary depending on powder size and density, gas velocity, and pressures.

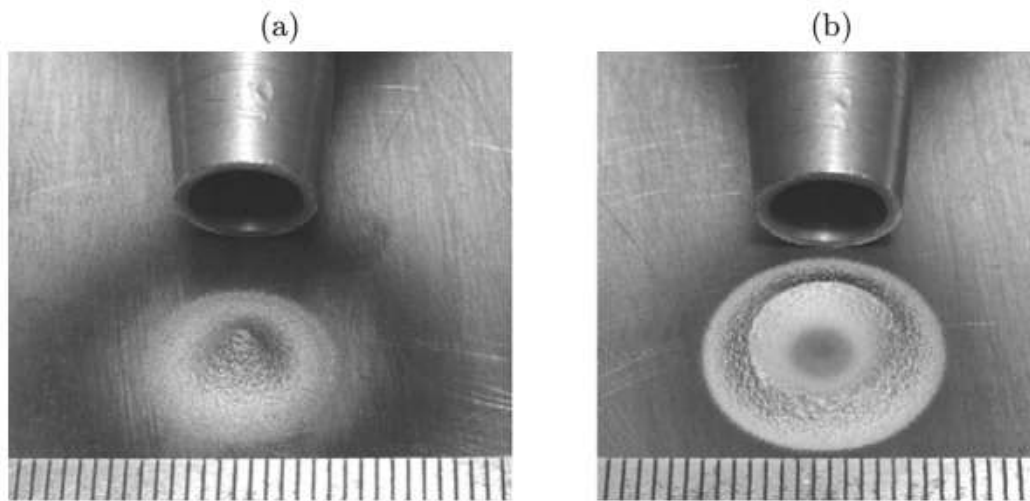


Figure 17 - Cold spray deposition of copper particles (a) non-swirled flow (b) swirled flow [54]

#### 2.9.2.4. Nozzle Slotting

In a study of unconventional nozzle designs for use in cold spray, deposition was attempted with a series of standard De Laval nozzles with the addition of 2, 3 and 4 slots, as shown in Figure 18. The deposition profiles that were generated were broadly similar to traditional cold spray, having a peak at the centre, with more powder having been deposited in line with the slots in the nozzle, as gas and powder has escaped laterally from these openings.

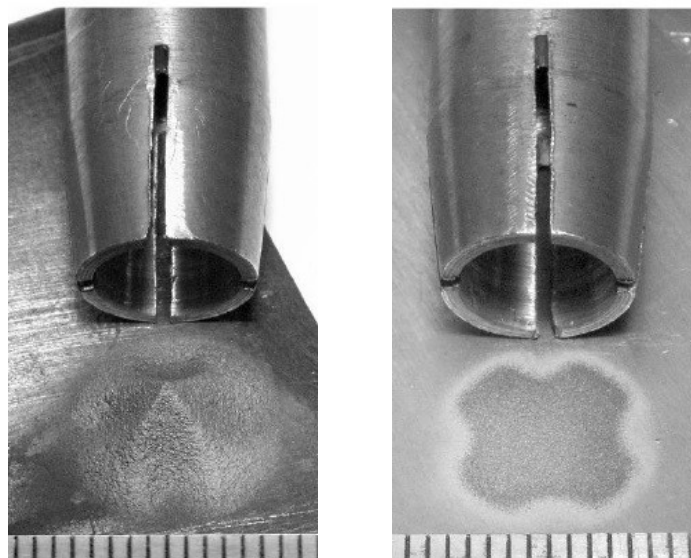


Figure 18 – Slotted nozzles and cold spray deposition [55]

Similarly to the attempt at changing the deposition profile via gas swirling, no explanation is given as to the purpose of these alterations, other than to create unusual deposition patterns. It is unlikely that this work will prove useful in the creation of an additive cold spray system without significant further development.

### 2.9.2.5. Moulds and machining

The most common method of producing a defined geometry with cold spray is machining of the deposit, both after the construction has been completed or in process, typically in a layer by layer fashion. However, this not only generates more waste material but also takes longer, using more gas, and is not suitable for difficult to machine materials, which runs directly counter to one of the main benefits of using cold spray. Examples of systems that already utilise machining can be seen in 2.13.4.

The most advanced process noted so far demonstrates a part sprayed over a blank insert or mandrel, which is then removed and finished with machining, as shown in Figure 19. It is not mentioned how the mandrel is removed, but it is likely machined away or sliced free by EDM, likely damaging the mandrel so that it cannot be reused. Even if it were reusable, component manufacture would be limited by having the correct shape of mandrel to start with, a similar problem to requiring dies and moulds for casting and forging, which only allows for a limited range of shapes. This method would also still require the machining of the outer surface once completed, so is primarily relying on final material properties alone to compete with existing manufacturing methods.

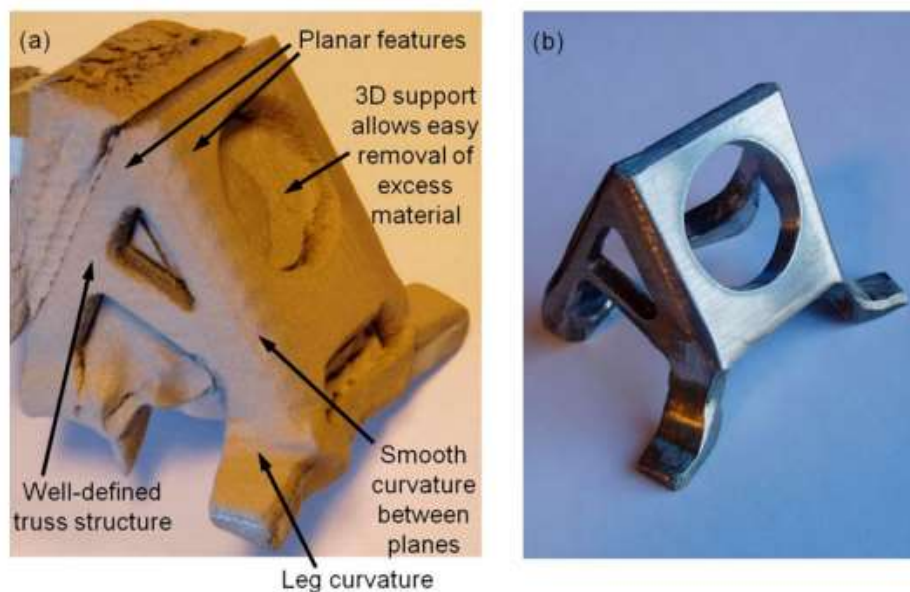


*Figure 19 – Cold-sprayed construction of a component (a) on a blank to provide structure and (b) removed from blank and machined [56]*

Some shape control has also been demonstrated from spraying titanium into an aluminium mould, as shown in Figure 20. This allows for very limited geometry control and often requires the destruction of the mould afterwards to reveal the part for more complicated features [50].



*Figure 20 - Titanium sprayed with aluminium mould [50]*

#### **2.9.2.6. Shape control summary**

It has previously been demonstrated that cold spray deposition shape can be affected both by altering the particle-gas dynamics of the process, either directly upon input (gas swirling) or near substrate (wire mesh interference), and by physical processes, such as nozzle tilting, spray moulds and post-machining. None of these methods provide well-defined free form control of the deposition, and are very limited in their application. This research proposes to investigate other potential methods for providing a greater level of control of the deposit through the placement of flow distorting objects into the gas flow, downstream of the nozzle exhaust.

### **2.10. Deposition characteristics**

Like all manufacturing processes, cold spray deposition has advantages and disadvantages in associated with both its process and the components produced. Many of the unique advantages of cold spray deposits come from the fact that deposition occurs as a solid-state process, avoiding the issues faced by competing high temperature manufacturing methods.

#### **2.10.1. Physical properties**

Depending on the process condition and materials, the porosity of the deposits formed by cold spray can be varied from 20 – 0.1 % [57]–[61]. It is noted that porosity can be lowered by increasing the particle speed, usually by increasing the gas temperature, or by increasing the substrate or particle temperature. Any loosely bound particles are either knocked free or further compacted by subsequent impacts from particles in the powder stream.

The powder particles are not heated sufficiently to cause phase changes during deposition, avoiding thermal cracking upon cooling caused by the contraction of the deposit. There is also insufficient energy for the recrystallization of the powder grains in the bulk of the particle, leaving the

microstructure in the bulk of the deposit the same as the microstructure of the original powder particles, allowing careful control of the grain size by control of the powder feedstock. This also allows for dense deposits of nano-crystalline materials, such as Ni-20Cr, WC-Co or aluminium alloys, which are capable of retaining their nanometre scale grain sizes after deposition [62]–[66].

Deposition of oxygen sensitive materials does not pose an additional challenge for cold spray systems, as the powder is not heated to high enough temperatures to accelerate oxidation [67], [68]. In addition, the accelerating gas is most commonly helium or nitrogen, which provide shielding at the deposition site. On some occasions, the oxygen content of the deposit has been noted to be lower than the average of the starting material, due in part to the likely loss of the smaller powder particles which will have a higher percentage oxygen content, and in part to the shattering of the oxide skin upon impact which may be subsequently swept away by the gas flow [69].

The low temperatures required for material deposition means that there is also little heat input into the substrate itself. This lack of thermal input to the substrate means that there is no heat-affected zone, and so no recrystallization, cracking, oxidation or induced thermal stresses arise in the substrate from this process. This allows a wide range of materials to be used for substrates that would otherwise be affected by higher temperature options.

### **2.10.2. Material properties**

Material deposited by cold spray deposition has also been demonstrated to have high hardness when compared to bulk values, sometimes even higher than the hardness of the powder particles. This is thought to be due to the effective cold working of the powder particles upon their impact and the subsequent impacts upon them by the next layer [70].

Cold spray deposits are formed by the rapid plastic deformation of particles, from the high velocity impact, in the solid state. This causes the coating to be compressive in nature [71, p. 66], as the subsequent particle impacts are effectively shot peening the previous layer of deposition [72]–[74]. Requiring only low processing temperatures, there is little difference between the temperature of the substrate and the depositing material, avoiding quenching stress prevalent in other coating techniques.

Due to the inter-particulate bonding and high density of the coatings created by cold spray, the conductivity values demonstrated are typically in excess of 92% of the bulk values, compared with approximately 50% for other thermal spray processes [69].

### 2.10.3. Process properties

Certain inherent aspects of the cold spray process provide specific benefits that are either superior or unavailable to other manufacturing processes. The cold spray process is capable of depositing material at rates of up to approximately 12 kg/hr, depending on the material [75, p. 94]. As the cold spray system is robust enough to be mounted to a robotic arm, or held above a CNC stage, and does not require a controlled environment as other systems do, the only limit to the size of the constructs that could be created is the available build platform of the machining system that it is incorporated into.

Due to the suspected bonding mechanisms and the relatively low temperatures involved in cold spray deposition, materials with highly different coefficients of thermal expansion can be bonded without the associated problems that arise due to cooling from molten processes. This allows for the exploitation of different characteristics of the combined materials. As an example, the bulk of a component could be made lightweight by being made from aluminium, with a corrosion resistant coating made from a titanium alloy to protect it from the environment.

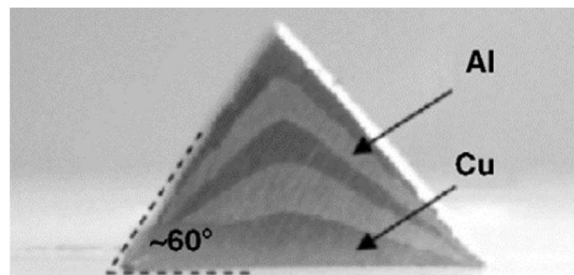


*Figure 21 - Copper and aluminium layered cold spray deposit [50]*

By altering the mixture of the powder in the cold spray jet, the composition of the deposit could be carefully controlled. The absence of melting means that powders with different melting temperatures can easily be used together, and will not affect the microstructure of the powder once deposited. This mixture could potentially be altered throughout the build, allowing for the creation of functionally graded components. Components that are manufactured with functionally graded materials have a gradual shift in composition and structure through the part, which allows equivalent changes to the properties of the material through the part. This would become of use in situations requiring different material properties in different areas of the component, for example; a bearing which is strong and lightweight, with a wear resistant but self-lubricating outer surface, a rocket nose cone graded from a strong and lightweight interior to temperature resistant exterior to avoid the problems of different thermal expansivities or a component that requires a corrosion resistant channel.

## 2.11. Supersonic laser deposition (Laser assisted cold spray)

Certain materials prove difficult to deposit when using a standard cold spray system, such as stellite or nickel super alloys, as the material hardness and yield strength means that the required velocity for deposition is too high to be practically achieved, even when using helium as the carrier gas, and may cause erosion of the substrate when approaching these velocities.

The application of a laser spot to the targeted deposition area, commonly known as supersonic laser deposition (SLD) or laser assisted cold spray (LACS), heats the substrate, reducing the critical velocity required for adhesion, and may allow the replacement of helium with nitrogen as the carrier gas, significantly reducing the cost of the process [76]. It is not known whether the heating of the substrate contributes towards the metallurgical bonding, by softening the oxide layer and allowing exposure of the metal at lower particle velocities, contributes to the mechanical interlocking, by allowing greater plastic deformation of the substrate upon impact, or raises the temperature of the material to allow a thin molten area to form more easily during impact.

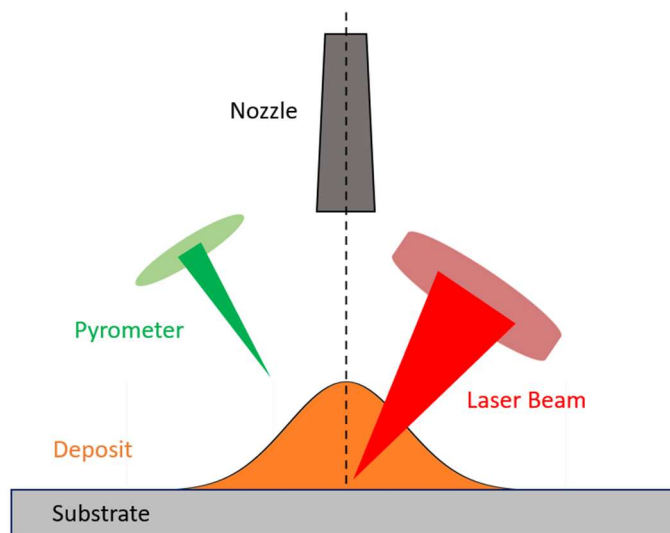


Figure 22 – SLD setup

This advancement has allowed for the deposition of a range of previously unfeasible materials, including those that are also difficult to manufacture with other processes, such as tungsten carbide, Stellite and titanium alloys. SLD has also been proven to increase the density of deposits formed at a given temperature in comparison to cold spray, and increases the deposition efficiency, for faster build rates [76]–[78].

It will be important that any developed concept does not prevent the addition of laser irradiation of the substrate so that these materials can also be shaped. It is equally important that the laser irradiation does not detrimentally affect the capabilities of the shaping method.

## 2.12. Computational fluid dynamics modelling

Experimental investigation of the supersonic gas flow and particle traverse rate in cold spray is limited by the difficulty in measurement and relatively high processing costs which would be required for each new nozzle, powder material or morphology. This has led to the development of analytical and numerical models for the investigation of the gas structure and particle velocity, most recently using computational fluid dynamics (CFD) models. This section details the most recently utilised methods for modelling of the cold spray system, and investigates the accuracy of such models.

### 2.12.1. Governing flow equations

Modern computational methods for fluid dynamics involve the solving of the Navier-Stokes equations for describing the motion of viscous fluids, consisting of the continuity equation for conservation of mass (Eq 1), an equation per dimension for the conservation of momentum (Eq 2), and the conservation of energy (Eq 3).

$$\frac{\delta \rho}{\delta t} + \frac{\delta}{\delta x_j} (\rho u_j) = 0 \quad (1)$$

$$\frac{\delta}{\delta t} (\rho u_i) + \frac{\delta}{\delta x_j} (\rho u_i u_j) = \frac{\delta}{\delta x_j} \left[ -p \delta_{ij} + \mu \left( \frac{\delta u_i}{\delta x_j} + \frac{\delta u_j}{\delta x_i} \right) \right] + S_M \quad (2)$$

$$\frac{\delta}{\delta t} (\rho C_p T) + \frac{\delta}{\delta x_j} (\rho u_j C_p T) = \frac{\delta}{\delta x_j} \left( \lambda \frac{\delta T}{\delta x_j} \right) + S_T \quad (3)$$

The flow throughout the cold spray system was regarded as steady state by all but a few models, and the ideal gas law was used as the equation of state for compressible flow.

### 2.12.2. Boundary conditions

The boundary conditions, including pressure, gas velocity, and temperature, of the model must be specified to reflect the real world situation, and very commonly are the same when modelling the cold spray system, as displayed in Table 3.

Table 3 – Most commonly used boundary conditions in cold spray gas flow simulation for pressure ( $P$ ), velocity ( $v$ ), and temperature ( $T$ ) or their derivatives representing the differential gradients at this point [79]

Model Location	Pressure	Velocity	Temperature
Nozzle/injector inlet	Specified	$\frac{\partial v}{\partial n} = 0$	Specified
Surrounding atmosphere	Specified	$\frac{\partial v}{\partial n} = 0$	$\frac{\partial T}{\partial n} = 0$
Nozzle walls	$\frac{\partial P}{\partial n} = 0$	0	$\frac{\partial T}{\partial n} = 0$
Substrate	$\frac{\partial P}{\partial n} = 0$	0	$\frac{\partial T}{\partial n} = 0$
Symmetrical axis (for 2D axisymmetric model)	$\frac{\partial P}{\partial r} = 0$	$\frac{\partial v}{\partial r} = 0$	$\frac{\partial T}{\partial r} = 0$

### 2.12.3. Turbulence models

Several different turbulence models have been used to close the Navier-Stokes equation set when modelling the cold spray gas flow. This factor has arguably the largest effect on the model accuracy. The most common model is the standard k- $\epsilon$  model, as it converges easily, requiring less computational power than other models, and is easily implementable for a variety of flow situations [80]–[88]. This model does fail to capture the smaller resolution effects, regardless of the mesh size, and has a tendency to smooth the shock waves generated by the cold spray nozzle [79].

The RNG k- $\epsilon$  model is also used commonly for cold spray and other supersonic nozzle flows [89]–[97]. The RNG model uses an extra term in the epsilon equation which improves accuracy in strained flows and low Reynolds number flows, at the expense of processing time and more complex pre-requisites when establishing the near-wall region [98].

Realizable k- $\epsilon$  methods utilise a different model for calculating the dissipation rate, epsilon, that is more suitable for calculating the mean flow of complex structures as we see in cold spray, and provides better predictions of the jet spreading effects once the flow has left the nozzle [99]–[102].

The k- $\omega$  is not commonly used for cold spray simulations, due to the difficulty in creating a converging model. Whilst the model produces more accurate near wall simulations, this is not particular concern for cold spray nozzles, though could be useful for resolving surfaces around objects which interrupt the flow downstream of a nozzle [103], [104]. The k- $\omega$  model is noted for over-predicting the shear stress within boundary layers with adverse pressure gradients, and commonly used in simulations of swirling flows and vortices, neither of which are common in cold spray.

#### **2.12.4. Meshing**

The 2D models were most commonly divided into zones of structured meshes of varying size, as this produces faster converging models. When modelled in 3D, unstructured meshing was used when the models required more complex geometry [81], [95], [101].

#### **2.12.5. Particle tracking**

There are two methods for solving computational particle-gas flow, Euler-Lagrangian discrete phase model or Euler-Euler mixtures. In all types of Euler-Euler models, the secondary phase cannot occupy the same physical space as the first phase, and the mesh interaction between the two phases must be calculated with each iteration, with the gas modelled as a continuum with a suspended secondary phase. This puts a heavy computational requirement on the solver but can provide a more accurate representation of the combined flow, particularly in particle heavy mixtures.

Lagrangian discrete phase modelling calculates the flow of the primary phase as if it were the only phase in the simulation in the Eulerian frame gas model. This method is well suited to particle-fluid flows where the volume fraction of particles is less than 10% [101]. This is the case in cold spray, where the volume fraction is typically less than 1%, with local maxima occurring around the centreline measured to be approaching 2.8% in a typical cold spray system [89].

The effects of the particles on the gas stream are typically ignored in cold spray simulation, the model is only one way coupled [22], [83], [86], [88], [102], [105]–[107]. In one way coupled models, the model is calculated to convergence, after which it calculates the force balance that this established flow regime would apply to the secondary phase via drag and turbulence with each iteration of the particle along its defined step length.

At increased powder feed rates, it has been reported that the gas-particle interaction is sufficient to cause a reduction in gas momentum, weakening the shock structures that form after the nozzle's exhaust. This can be accounted for by phase coupling the powder and gas flow using the source terms in the Navier-Stokes equations, but this situation is rare and will not be encountered in this thesis as the powder feed rate is significantly lower than that which is required [81], [82], [102], [108]–[110].

### **2.13. Areas of application**

Cold spray finds applications across a range of industrial sectors, usually determined by the specific properties of the available materials. Table 4 shows the range of functional properties that cold spray capable materials have and their typical applications.

Table 4 - Typical applications of cold spray, listed by material and functional property [111]

Functional properties of CGDS deposits	Investigated materials for CGDS deposits														Typical application fields		
	Metals and alloys	Metal/Polymer	MMCs : M/Ceramic	MMCs : M/M	Intermetallics (IMCs)	Oxides	Ceramics	WC cermets	MMCs/Cermets	MAICer	MGAIV	Stellites	Carbides	Polymers		Thermities	Nanomaterials
Corrosion resistant	<input type="checkbox"/>	<input type="checkbox"/>	<input type="checkbox"/>	<input type="checkbox"/>	<input type="checkbox"/>	<input type="checkbox"/>	<input type="checkbox"/>	<input type="checkbox"/>	<input type="checkbox"/>	<input type="checkbox"/>	<input type="checkbox"/>	<input type="checkbox"/>	<input type="checkbox"/>	<input type="checkbox"/>	<input type="checkbox"/>	<input type="checkbox"/>	Aerospace, automobile, electronics, defense, petrochemical, oil industry, energy
Oxydation resistant	<input type="checkbox"/>	<input type="checkbox"/>	<input type="checkbox"/>	<input type="checkbox"/>	<input type="checkbox"/>	<input type="checkbox"/>	<input type="checkbox"/>	<input type="checkbox"/>	<input type="checkbox"/>	<input type="checkbox"/>	<input type="checkbox"/>	<input type="checkbox"/>	<input type="checkbox"/>	<input type="checkbox"/>	<input type="checkbox"/>	<input type="checkbox"/>	Aerospace, naval, electric contact applications
Erosion (electric, by cavitation,) resistant	<input type="checkbox"/>	<input type="checkbox"/>	<input type="checkbox"/>	<input type="checkbox"/>	<input type="checkbox"/>	<input type="checkbox"/>	<input type="checkbox"/>	<input type="checkbox"/>	<input type="checkbox"/>	<input type="checkbox"/>	<input type="checkbox"/>	<input type="checkbox"/>	<input type="checkbox"/>	<input type="checkbox"/>	<input type="checkbox"/>	<input type="checkbox"/>	Variety of industrial sectors
High specific strength	<input type="checkbox"/>	<input type="checkbox"/>	<input type="checkbox"/>	<input type="checkbox"/>	<input type="checkbox"/>	<input type="checkbox"/>	<input type="checkbox"/>	<input type="checkbox"/>	<input type="checkbox"/>	<input type="checkbox"/>	<input type="checkbox"/>	<input type="checkbox"/>	<input type="checkbox"/>	<input type="checkbox"/>	<input type="checkbox"/>	<input type="checkbox"/>	Automobile, aerospace, machining, decoration
Wear resistant	<input type="checkbox"/>	<input type="checkbox"/>	<input type="checkbox"/>	<input type="checkbox"/>	<input type="checkbox"/>	<input type="checkbox"/>	<input type="checkbox"/>	<input type="checkbox"/>	<input type="checkbox"/>	<input type="checkbox"/>	<input type="checkbox"/>	<input type="checkbox"/>	<input type="checkbox"/>	<input type="checkbox"/>	<input type="checkbox"/>	<input type="checkbox"/>	Variety of industrial sectors
Abrasive	<input type="checkbox"/>	<input type="checkbox"/>	<input type="checkbox"/>	<input type="checkbox"/>	<input type="checkbox"/>	<input type="checkbox"/>	<input type="checkbox"/>	<input type="checkbox"/>	<input type="checkbox"/>	<input type="checkbox"/>	<input type="checkbox"/>	<input type="checkbox"/>	<input type="checkbox"/>	<input type="checkbox"/>	<input type="checkbox"/>	<input type="checkbox"/>	Automobile, aerospace, naval, civil engineering
Anti-friction (sliding components)	<input type="checkbox"/>	<input type="checkbox"/>	<input type="checkbox"/>	<input type="checkbox"/>	<input type="checkbox"/>	<input type="checkbox"/>	<input type="checkbox"/>	<input type="checkbox"/>	<input type="checkbox"/>	<input type="checkbox"/>	<input type="checkbox"/>	<input type="checkbox"/>	<input type="checkbox"/>	<input type="checkbox"/>	<input type="checkbox"/>	<input type="checkbox"/>	Variety of industrial sectors
Specific bonding layer	<input type="checkbox"/>	<input type="checkbox"/>	<input type="checkbox"/>	<input type="checkbox"/>	<input type="checkbox"/>	<input type="checkbox"/>	<input type="checkbox"/>	<input type="checkbox"/>	<input type="checkbox"/>	<input type="checkbox"/>	<input type="checkbox"/>	<input type="checkbox"/>	<input type="checkbox"/>	<input type="checkbox"/>	<input type="checkbox"/>	<input type="checkbox"/>	Aerospace, defense, petrochemical
Restoration	<input type="checkbox"/>	<input type="checkbox"/>	<input type="checkbox"/>	<input type="checkbox"/>	<input type="checkbox"/>	<input type="checkbox"/>	<input type="checkbox"/>	<input type="checkbox"/>	<input type="checkbox"/>	<input type="checkbox"/>	<input type="checkbox"/>	<input type="checkbox"/>	<input type="checkbox"/>	<input type="checkbox"/>	<input type="checkbox"/>	<input type="checkbox"/>	Variety of industrial sectors
Bulk material	<input type="checkbox"/>	<input type="checkbox"/>	<input type="checkbox"/>	<input type="checkbox"/>	<input type="checkbox"/>	<input type="checkbox"/>	<input type="checkbox"/>	<input type="checkbox"/>	<input type="checkbox"/>	<input type="checkbox"/>	<input type="checkbox"/>	<input type="checkbox"/>	<input type="checkbox"/>	<input type="checkbox"/>	<input type="checkbox"/>	<input type="checkbox"/>	Biomedical (dental and orthopedic implants)
Biocompatibility	<input type="checkbox"/>	<input type="checkbox"/>	<input type="checkbox"/>	<input type="checkbox"/>	<input type="checkbox"/>	<input type="checkbox"/>	<input type="checkbox"/>	<input type="checkbox"/>	<input type="checkbox"/>	<input type="checkbox"/>	<input type="checkbox"/>	<input type="checkbox"/>	<input type="checkbox"/>	<input type="checkbox"/>	<input type="checkbox"/>	<input type="checkbox"/>	Biomedical
Anti-bacterial	<input type="checkbox"/>	<input type="checkbox"/>	<input type="checkbox"/>	<input type="checkbox"/>	<input type="checkbox"/>	<input type="checkbox"/>	<input type="checkbox"/>	<input type="checkbox"/>	<input type="checkbox"/>	<input type="checkbox"/>	<input type="checkbox"/>	<input type="checkbox"/>	<input type="checkbox"/>	<input type="checkbox"/>	<input type="checkbox"/>	<input type="checkbox"/>	Electronic, aerospace, energetic, electric contact
Conductive/Insulation (electrical, thermal)	<input type="checkbox"/>	<input type="checkbox"/>	<input type="checkbox"/>	<input type="checkbox"/>	<input type="checkbox"/>	<input type="checkbox"/>	<input type="checkbox"/>	<input type="checkbox"/>	<input type="checkbox"/>	<input type="checkbox"/>	<input type="checkbox"/>	<input type="checkbox"/>	<input type="checkbox"/>	<input type="checkbox"/>	<input type="checkbox"/>	<input type="checkbox"/>	Energy generation industry
Photovoltaic performance	<input type="checkbox"/>	<input type="checkbox"/>	<input type="checkbox"/>	<input type="checkbox"/>	<input type="checkbox"/>	<input type="checkbox"/>	<input type="checkbox"/>	<input type="checkbox"/>	<input type="checkbox"/>	<input type="checkbox"/>	<input type="checkbox"/>	<input type="checkbox"/>	<input type="checkbox"/>	<input type="checkbox"/>	<input type="checkbox"/>	<input type="checkbox"/>	Energy generation industry
Photocatalytic performance	<input type="checkbox"/>	<input type="checkbox"/>	<input type="checkbox"/>	<input type="checkbox"/>	<input type="checkbox"/>	<input type="checkbox"/>	<input type="checkbox"/>	<input type="checkbox"/>	<input type="checkbox"/>	<input type="checkbox"/>	<input type="checkbox"/>	<input type="checkbox"/>	<input type="checkbox"/>	<input type="checkbox"/>	<input type="checkbox"/>	<input type="checkbox"/>	Energy generation industry, energetic

### 2.13.1. Wear resistance

Wear resistant coatings are required situations with high levels of abrasion, erosion, fatigue, fretting or cavitation erosion, in order to minimise the amount of damage caused by these interactions and prolong the life of the component. Common areas of interest include cutting inserts, cutting tools, pipe walls in pump shafts and bearings.

To function optimally, these coatings should be made from materials with high intrinsic hardness and contain minimal pores or cracks. Typical materials used for the creation of wear resistant coatings by cold spray include titanium carbide, tungsten carbide and chromium carbide.

Cold spray is still in the research stages of investigating these opportunities [112]–[115]. These materials are so hard that deposition may require mixing with a softer “binder” material, and require higher velocities to exceed the critical velocity. With the cold spray process, it is possible to produce highly dense coatings using materials that are usually difficult to handle, without damaging the component to be protected.

### 2.13.2. Corrosion and erosion resistance

Surfaces that will suffer from degradation due to their interaction with the environment also require protection, typically being coated in layers of nickel, chromium or titanium alloys. Common areas of interest include pipes, pumps and other surfaces in chemical, petrochemical or oil handling equipment, and power plants.

The use of these alloys on just the surface of the component offers significant cost reductions when compared with the cost of making a full component, but does not lessen the performance. Cold spray

is capable of providing these dense coatings evenly across the surface of components, with a lower level of oxidation than competing processes, allowing for a greater volume fraction of reactive, sacrificial material in the coating [116].

### **2.13.3. Joining**

Cold spray has also been used as a method to combine two components together, in a similar process to welding. The two components are aligned at the joining sections, and a cold spray deposit is used to create a bond between the two across the seam [117]. It has been demonstrated that the fractures are more likely to occur in the freeform section of the weld than at the interface, meaning that the maximum strength will be that of the deposited material [118].

### **2.13.4. Additive manufacturing and restoration**

Over the last five years, several companies have announced the development of new manufacturing platforms utilising cold spray deposition as part of hybrid part creation methods. Little information is currently available on these processes, however it is important to monitor these processes to note the industry interest, their target markets and their shaping capabilities.

The Hermle Metal Powder Application (MPA) technique uses superheated steam, instead of nitrogen or helium, as the accelerating gas in order to propel the powder particles through the supersonic nozzle. The resulting deposit is then machined in a layer by layer approach after deposition in order to create the desired shape, by the CNC machine in which the cold spray system has been mounted, as shown in Figure 23.

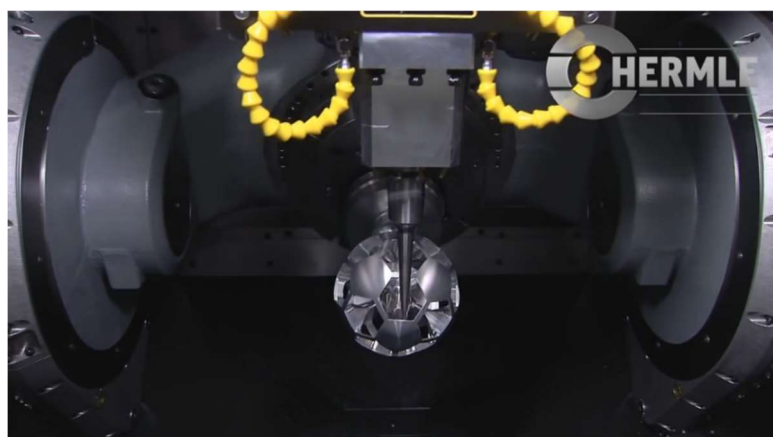


*Figure 23 - Hermle MPA 40 hybrid cold spray and machining centre*

Hermle are targeting injection moulding and die casting tools, particularly focussing on their capability to add features to pre-existing blanks, and the formation of conformal cooling channels with a water soluble filler material.

A newly established Australian company named Spee3D have a 6 axis bed for near net shape cold spray deposition, controlled by angling of the bed as mentioned in Section 2.9.2.1, and then machined post deposition, rather than layer by layer. Spee3d are targeting low cost, medium volume production components in aluminium or copper, as a direct competitor for casting.



Figure 24 - Spee3d additive cold spray system

The US Army Research Lab (ARL) has developed a manually operated cold spray system for repair of components, as shown in Figure 25, with VRC Metal Systems. Component with defects are built back up by using the handheld cold spray nozzle before taking the part for machining. It is not currently clear what the target applications will be for this system, but it is likely to be initially focused on the repair of military aircraft components. As this system is a manually driven process, the accuracy and repeatability are likely to be of a lower standard than competitive machines.



Figure 25 - VRC Gen III manual cold spray deposition system [119]

General Electric was noted to be investigating the potential of freeform fabrication using cold spray in 2013 [120], but have published little progress since the announcement of their investigation and initial trials.

In addition to the commercial endeavours, a research team in the Department for Mechanical and Manufacturing Engineering in Trinity College Dublin, headed by Dr Rocco Lupoi, has been awarded a €500,000 grant from the European Space Agency for the “Development of Cold Spray towards the next generation of Additive Manufacturing” [121]. All papers produced by this group to date have been review papers or focussed on a two-dimensional simulation of the cold spray process.

As with some conventional and additive systems, the creation of net shape structures using hybrid systems will still be limited by the capability of machining the materials, leading to limited materials choices or expensive finishing processes. The extra machining steps leads to unnecessary time, cost and material waste when compared to a potential direct net shape cold spray system.

## **2.14. Summary**

Sector analysis shows there is a space in the metallic manufacturing sector for a high speed, low cost, large scale, net-shape capable system with above standard surface finish. Cold spray has the potential to effectively fill this space, if it can overcome the current lack of structural control over the shape of its deposition, whilst maintaining the beneficial properties of the process described in Section 2.10. The benefits it provides with increased build rate, cost/energy savings and broader material choices would give it a unique placement within the manufacturing space.

Literature has demonstrated some methods exist for altering the shape of the deposit, via upstream gas interference before it enters the nozzle, and by altering the substrate conditions at the deposition zone. The best approach for developing a controllable structuring system is likely to be a downstream interruption of the combined gas and powder jet, as the particles will be travelling at a higher velocity and so the process more applicable to powders of varying size and density. It is sensible to start with a further investigation of substrate masking developed from the work noted in the literature. If successful, this can be progressed into more flexible solutions to allow for the creation of more complex geometries.

---

# Chapter 3 - Experimental setup

---

## **3.1. Introduction**

During this study, the same cold spray system, located at the University of Cambridge's Institute for Manufacturing, was used for all experiments. This chapter briefly details the apparatus combined to make the cold spray system. The operation of the cold spray system is described from the first stages of introducing the gas to the system to the recovery of the substrate and deposit. In addition, the analytical methods for acquiring the data from the deposits that will be used throughout this thesis are defined.

## **3.2. Health and Safety**

Due to the equipment and materials involved in these experiments, risk assessments were required to ensure the safety of those present. Use of metallic powders necessitates the use of filtered masks, after face-fit tests to determine the suitability, and gloves when handling containers and during machine setup. Lab coats should be worn when entering the lab, and taken off when leaving to stop the spread of powder outside of the room. Safety glasses are also required to protect the eyes from powder plumes when filling the powder hopper and operating the system. When the system is in operation, ear defenders are required upon entering the lab.

## **3.3. Cold Spray System**

### **3.3.1. Powder feeder**

A Praxair Tafa Model 1264 is used to supply the powder at high pressure to the cold spray system, an open loop wheel fed setup shown in Figure 26. The powder is contained in a sealed, pressurised powder hopper, with a heating blanket to prevent the absorption of moisture into the powder, maintaining reliable flow through the powder wheel. The powder wheel has a series of holes around its outer diameter, which fill with powder as the wheel turns. When these holes align with the outlet, the powder is fed through the piping to the injection needle in the converging section of the De Laval nozzle.

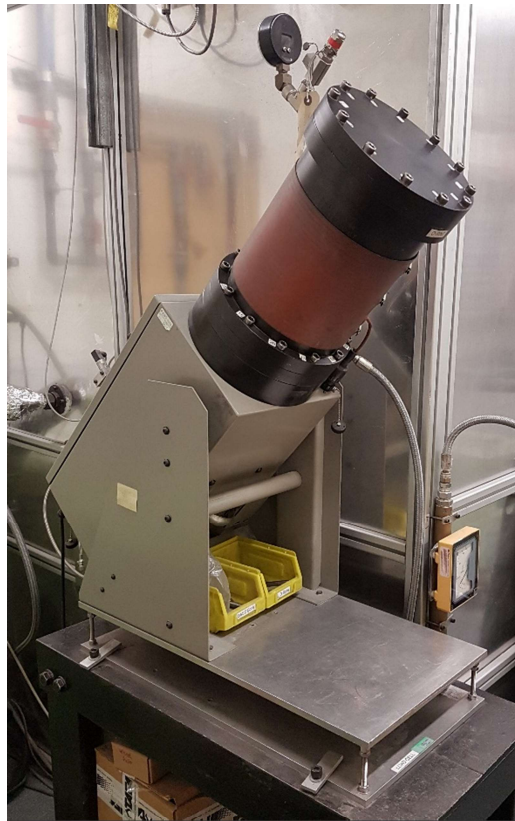


*Figure 26 – Praxair TAFE Model 1264, high pressure open loop wheel powder feeder*

The powder wheel rotates at a constant rate that can be programmed by the operator, enabling the steady supply of a specific volume of powder. The entire feeder is located on a load cell that monitors and logs the mass of the powder feeder during the experiments, with a resolution of  $\pm 0.5$  g, to calculate mass flow rates and deposition efficiency.

### **3.3.2. Gas heater**

The gas is heated using a Cold Gas Technology K2000 gas heater, capable of safely reaching nitrogen temperatures of up to 500 °C. The bulk of the gas is directed from here to the nozzle, where it recombines with the mixed powder and gas stream from the powder feeder in the converging section of the nozzle.



*Figure 27 – Gas heater*

### **3.3.3. Nozzle**

The nozzle used for all experiments within this report is a converging-diverging De Laval nozzle, with dimensions as shown in Figure 28. The gauge pressure at the inlet is 30 bar, regulated from a 200 bar nitrogen manifold cylinder pallet (MCP). The powder injection needle is directed concentrically into the converging section of the nozzle, with the tip falling 15 mm short of the 2.72 mm diameter throat. The nozzle is positioned over the substrate at a 40 mm offset, as the particles reach their maximum velocity between 20-40 mm from the nozzle exhaust, which is 7.8 mm in diameter.

At the 30 bar maximum operating pressure of this system, the nozzle is over-expanded for nitrogen, allowing the gas to expand to below atmospheric pressure, and therefore accelerate to higher velocities, allowing for greater particle velocities to be achieved at the nozzle exhaust.

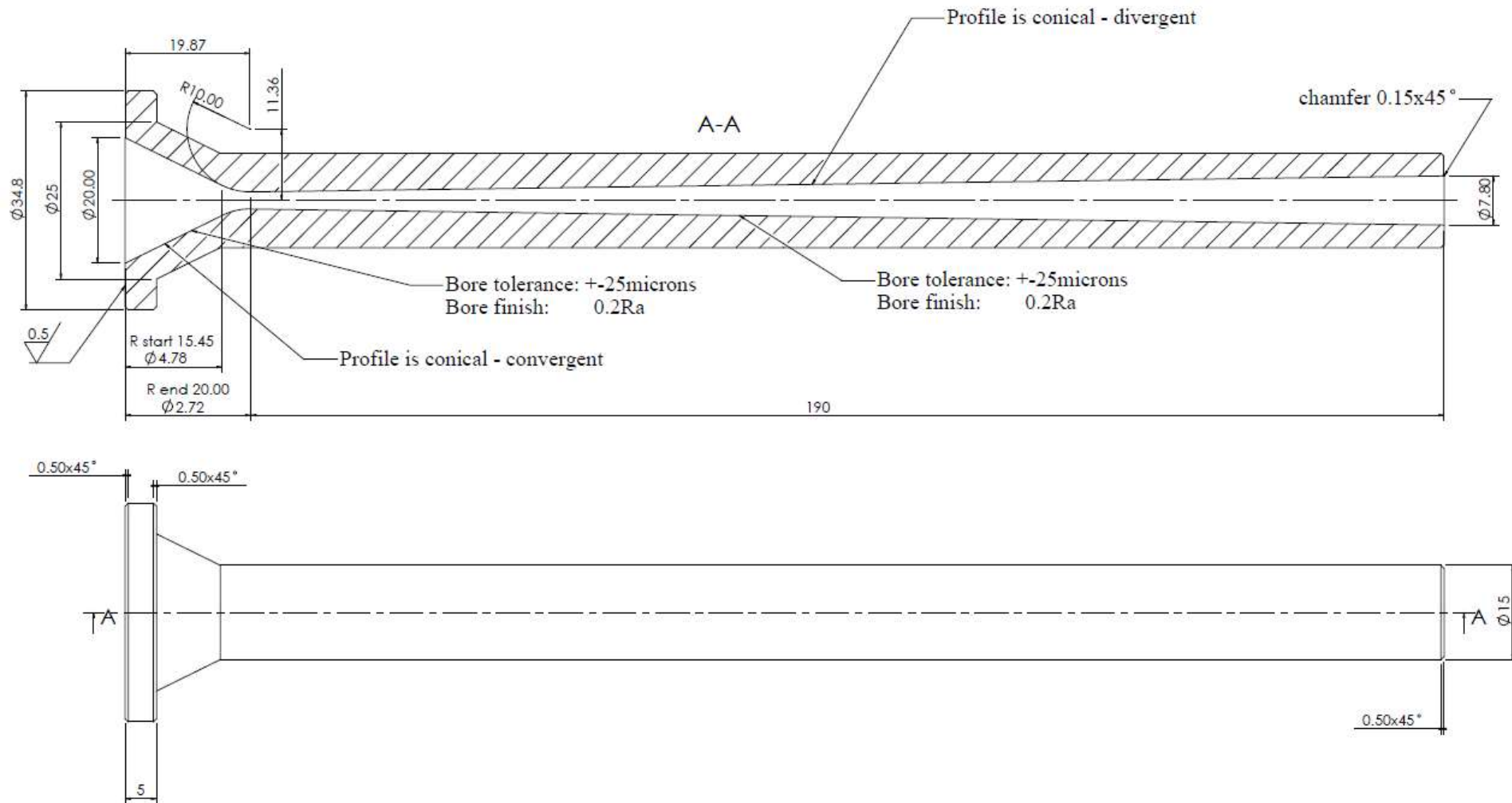


Figure 28 – Diagram of the tungsten carbide cold spray nozzle [DLV190] at the IfM

### 3.3.4. Laser and pyrometer

The laser is a 4 KW Ytterbium laser, the YLS 4000 from IPG, with a spot size of 0.06 mm at focus. As the cold spray system requires a less localised heating affect, the substrate is not positioned at the laser focus, but rather at 40 mm from the focus, to increase the spot diameter to 5.88 mm and heat an area of the substrate similar to that covered by the powder. The maximum achievable average spot intensity at this distance is  $1.5 \times 10^4 \text{ W/cm}^2$ , below the melting regime for the metals used in this thesis. The laser is controlled via an output in the Aerotech control software, and so its activation can be timed to integrate with the positioning of the stage. It is capable of providing requested power at any level up to the maximum 4 KW. The laser alignment can be seen in Figure 29, coming in through the thick black cable on the left, with the pyrometer positioned front right.



*Figure 29 - Laser head and pyrometer positioning in the build chamber*

The requested and output laser power is recorded with the operational data from the gas and powder feeds, to allow analysis and repeatability at a later date. The pyrometer will record the temperature data of the substrate under the nozzle during deposition, but does not record for the rest of the substrate.

Alternatively a specific temperature can be requested for the area under the nozzle, which will be monitored by the pyrometer as the laser power is actively altered to maintain this temperature in the substrate.

### **3.3.5. Auxiliary equipment**

Other minor equipment is used in the course of experimentation:

- The system comprises of 3 Cartesian Aerotech stages and one optional rotary stage that can be orientated as required.
- The entire system is contained within an environmental chamber, where a filtered extraction system maintains a slight negative pressure. The chamber is also light-tight, with interlocked doors to avoid human exposure to the laser.

## **3.4. Operational Control**

This subsection details the generic operating procedures that were central to each trial conducted with the cold spray apparatus. Operations that are experiment specific, for example pertaining to the positioning of masks, are detailed within the corresponding results section of this thesis.

### **3.4.1. Preparation**

Before processing begins, nitrogen stores must be checked to ensure that there is a sufficient supply to safely complete the planned experiments. A continual flow is vital for temperature control of the gas heater. The extraction system must also be turned on to maintain a safe level of nitrogen in the room, and the oxygen meter checked to be operational. It is highly advisable to conduct a dry run of the proposed experiment at a lower speed to check for nozzle collisions or other issues that would create complications during deposition. All required PPE is donned before progressing any further.

All substrates are initially cleaned with acetone in an effort to present a clean surface to aid in coating formation, before being mounted on the platform.

### **3.4.2. Powder handling**

Powders are kept dry throughout the spraying process to avoid causing problems with flow through the various narrow pipes of the powder feeder and injection needle. When preparing to spray, powder is transferred from airtight containers kept in a temperature-controlled cupboard, to the powder feeder surrounded with a heated blanket, shown in Figure 30, which is then sealed.



*Figure 30 – Powder feeder mounted on a load cell*

Once transfer is complete, the load cell is unlocked to monitor the mass of the powder in the system. This powder feeder is connected to the same PC as the control software, allowing for real-time recording of the mass, and monitoring of the powder feed rate.

### **3.4.3. Positioning**

The substrates are clamped onto a fixed platform using a series of positional levered arms. This platform can then be positioned by 3 Aerotech stages to translate the nozzle across the substrate surface and maintain the desired nozzle-substrate offset. The stages can be controlled manually, or automatically by a program written in G-Code via the Aerotech controller software, shown in Figure 31, loaded onto the same PC as the laser control and the gas and powder feeder control, with traverse rates of up to 100 mm/s.

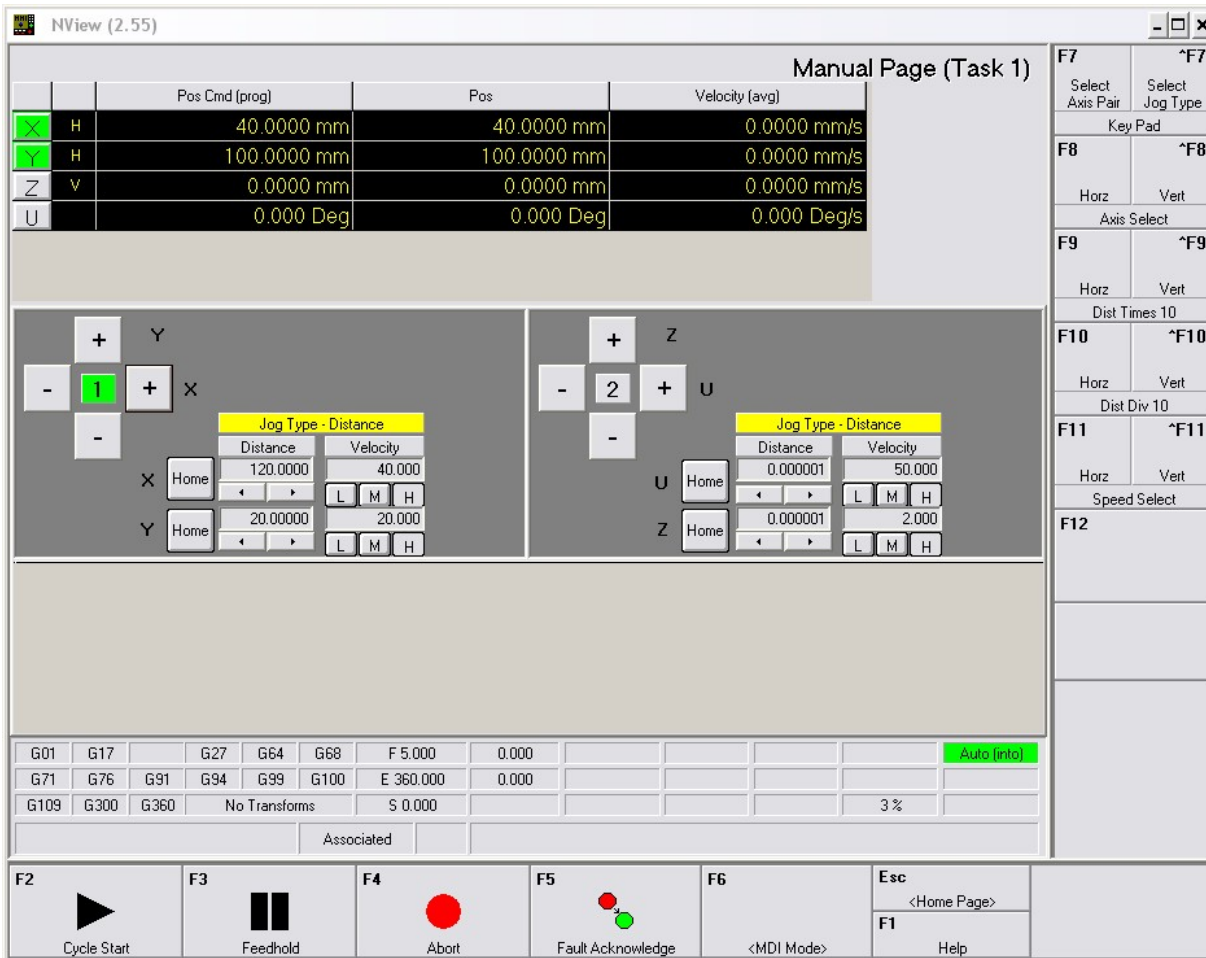


Figure 31 - Aerotech control software used for nozzle positioning

A rotary stage can also be affixed to the platform vertically or horizontally to provide a 4<sup>th</sup> axis for the system. This stage is capable of rotating small diameter cylinders to provide surface speeds in excess of 5000 mm/s.

There is no reason why different positioning equipment could not be used with greater movement range or traverse rate, as the particles are moving in excess of 500 m/s in the direction normal to the substrate. In order for the stage speed to negatively affect the particle impact angle and change the deposition, the stage would need to move at speeds of a similar order of magnitude, which is an unfeasible prospect.

Indeed, a significant upgrade to this positional capability would be required to make a cold spray system competitive with other additive manufacturing techniques. A 6-axis system would allow for much greater versatility in shape and spray angle.

### 3.4.4. Process control

The process is controlled from a software suite which monitors gas and temperature levels, and allows control of the gas and powder flow, as show in Figure 32.



Figure 32 - Cold spray process control software

Gas pressure and temperature must be monitored throughout the deposition cycle, along with powder feed rates, to ensure the reliability and repeatability of the trials. All of this data is logged with each experiment, and can be examined at a later date, along with data of requested and supplied laser power.

### 3.4.5. Post process

Upon completion of the deposition phase of the experiment, the equipment must be left to cool with the gas running to aid the cooling of the heating element, before samples are removed for analysis.

## 3.5. Methods of Analysis

The following methods will be used to determine the success of the deposits formed during experimentation.

### 3.5.1. Shape conformity

The main method of analysing the deposits made will be the conformity to the intended shape, as this is the primary success criteria for the project. This is a qualitative visual inspection rather than quantitative measure, whereby the deposits are inspected upon removal from the cold spray system to examine whether they have deposited flush to the forming tool. If a flat surface is presented with lower surface roughness than standard cold spray, the deposition will be deemed to be successful.

To confirm this visual inspection for a few of the samples, a quantitative measure of the flatness of the deposit's surface will be analysed using a Veeco Wyko NT3300 white light interferometer, shown in Figure 33. The data is presented as a scatter plot, with the stability of the gradient of the points indicating the flatness of the sample.



*Figure 33 - Veeco Wyko NT3300 used for surface roughness measurements*

### **3.5.2. Surface roughness**

The mean surface roughness of the samples was also measured using the Veeco Wyko NT3300 white light interferometer mentioned in Section 3.5.1, capable of measuring to  $\pm 0.01$  nm [122]. The 10X objective was used to scan across a 50  $\mu$ m range, 25  $\mu$ m either side of the surface in focus, using the automated stages to move independently and ensure repeatability of measurement.

Measurements are presented as a heat map, as can be seen in Figure 34. Black areas in the measurement zone occur when the surface is not reflective enough to be measured. Settings can be adjusted to interpolate from the surrounding data, though this is often not used. As long as more than 80% of the measured area is returned, the measurement will be accepted as valid.

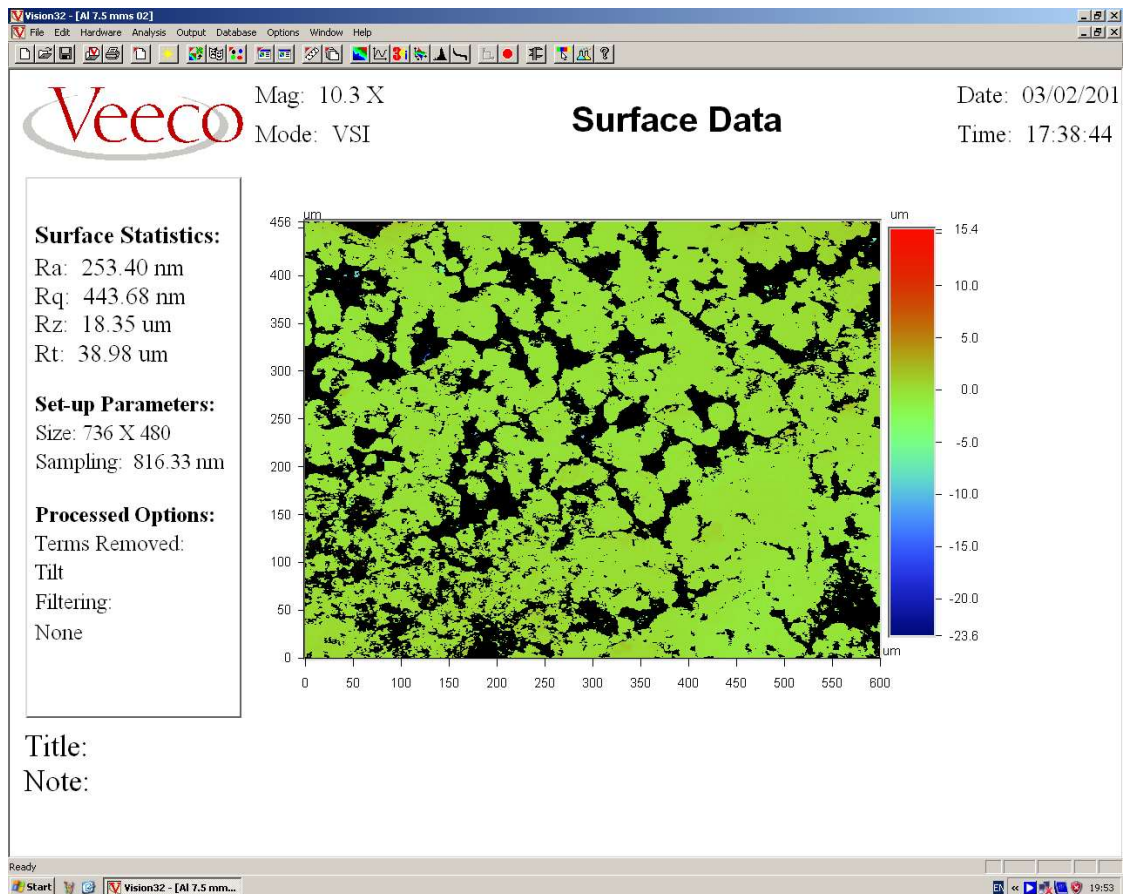


Figure 34 - Sample Veeco Wyko NT3300 surface roughness measurement output image

### 3.5.3. Metallography

Porosity measurements of the samples were collected to compare to free standing cold spray deposits. These porosity values are determined by analysing optical micrographs of cross-sections of the deposits.

The samples were sectioned using a Struers Sectom 10, mounted in resin and polished before being examined under an Olympus BX51 research microscope with a 20x lens and a JENOPTIK Laser ProgRes C10<sup>Plus</sup> camera, capable of providing real-time imaging. Image analysis software from A4i was used to record images, measure samples and record images, calculates porosity in the image by counting the number of pixels in a user defined greyscale range, and displays the result as a percentage of the total number of pixels in the area selected, as can be seen in Figure 35.

In an attempt to approximate the best porosity value for each sample, three sectioning cuts will be made in each deposit, and the porosity measured at each cut in three locations, before averaging.

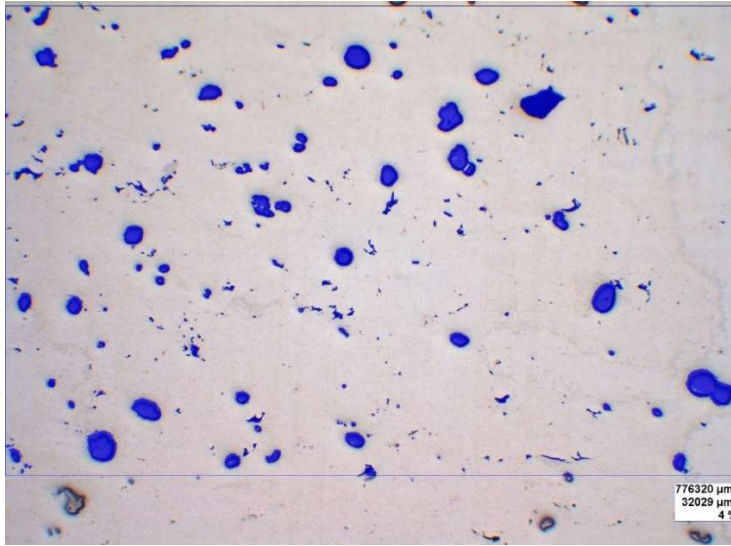


*Figure 35 - Porosity measurement example of 4% porous Al cold spray deposit*

#### **3.5.4. Build height**

Average build height per layer will also be measured using the optical microscopy suite mentioned in Section 3.5.3. There will be significant uncertainty in this measurement, as misalignment between the nozzle, substrate, and axis would cause variation in the height, as demonstrated in the diagonal alignment tests in Section 6.3. That being said, all depositions within a material type were conducted with the same alignment, allowing for comparison within that data set, and the formulation of general trends.

---

# Chapter 4 - Exploration of deposition shaping concepts

---

## 4.1. Introduction

Pursuant to the research aim, this chapter of work was conducted with two main objectives: to demonstrate the viability of creating definable surfaces, and to consider the most effective approach for creating definable surfaces of free-form shapes.

As mentioned in Section 2.8, the factor determining whether powder is successfully deposited is the particle velocity at impact being above the critical velocity threshold, normal to the substrate. The following concepts involving the alteration of the downstream deposition zone were developed ahead of other methods in an attempt to reduce any effects on the majority of the gas velocity and consequently the powder velocity and trajectory from inlet to substrate.

The experiments would be deemed successful if the samples achieved shape conformity upon visual inspection, which would be confirmed by a high surface finish, exceeding that expected from standard cold spray, caused by proximity to the deposit shaping tool. The analysis and optimisation of the developed concepts will be considered further in later chapters.

## 4.2. Parameters

In order to minimise unnecessary variation in parameters between trials, a set of parameters were fixed for all experimental trials within this chapter, summarised below in Table 5. Copper was chosen as the powder material, as it readily and densely deposits without the use of the laser, eliminating a further unnecessary variable. Copper also has a steep critical deposition angle of 60° [32], allowing for a tall single track build up. The temperature was limited to 300 °C to prevent any fouling of the nozzle, and the gauge pressure set to 30 bar, the maximum operating pressure for the system. Unless otherwise detailed, all copper experiments within this thesis used these parameters for deposition.

Table 5 - Fixed parameters

Variable	Setting
Powder	Copper – Nominal size - 38 + 15 $\mu\text{m}$
Powder feed rate	20 $\text{cm}^3/\text{min}$
Substrate	Aluminium 12 mm plate
Temperature	300 $^{\circ}\text{C}$
Gauge pressure	30 bar
Traverse Rates	3, 3.75, 5, 7.5, 15 mm/s (plus 50 & 100 mm/s for flow separator experiments)
Spray spot diameter	8 mm

### 4.3. Masking plate

A masking plate was positioned to obscure parts of the substrate, and the nozzle programmed to pass over the pattern in the mask. This would provide minimal interference with the majority of the gas flow, and was intended to have little impact on the particle trajectory and speed. It also seemed a logical extension of the work done by Cormier et al and Dupois et al [123], [124] in using a wire mesh to interrupt the gas flow and structure the deposition to pyramidal fins, though this was lacking in any real level of control, being limited only by mesh size and the critical deposition angle.

The masking plates were made at thicknesses of 1, 2 and 3 mm from steel plate using a water jet cutter. The masking plates were clamped to a 1 mm thick aluminium substrate and fixed to the machine bed, with the nozzle positioned orthogonally to the substrate and mask surface. The masking plates were divided into sections, shown in Figure 36, to investigate how different feature sizes, traverse rates, number of layers and alignment of the nozzle centreline with the face of the feature would affect the deposition of material.

In the first section of the plates, the nozzle was directed to traverse over a series of features of 1, 2, 3 and 4 mm in size, similar in scale to the wire mesh used by Cormier et al, and allows full coverage by the 8 mm spray track. This was to allow investigation of the creation small structures with fully defined side surfaces, and was conducted with traverse rates of 15, 30 and 45 mm/s for both a single layer pass and a double layer deposit.

In the second section, the effects of nozzle alignment with the features edge as it traversed parallel to the masking feature was tested. It was expected that moving parallel to the edge of the mask feature would cause less disruption to the gas flow than moving perpendicularly over the side of a feature. The nozzle was traversed along the feature at 15 mm/s for a single layer, and 30 mm/s for 2 layers, which allowed the testing of the central alignment, and with offsets of  $\pm 1$  and  $\pm 2$  mm.

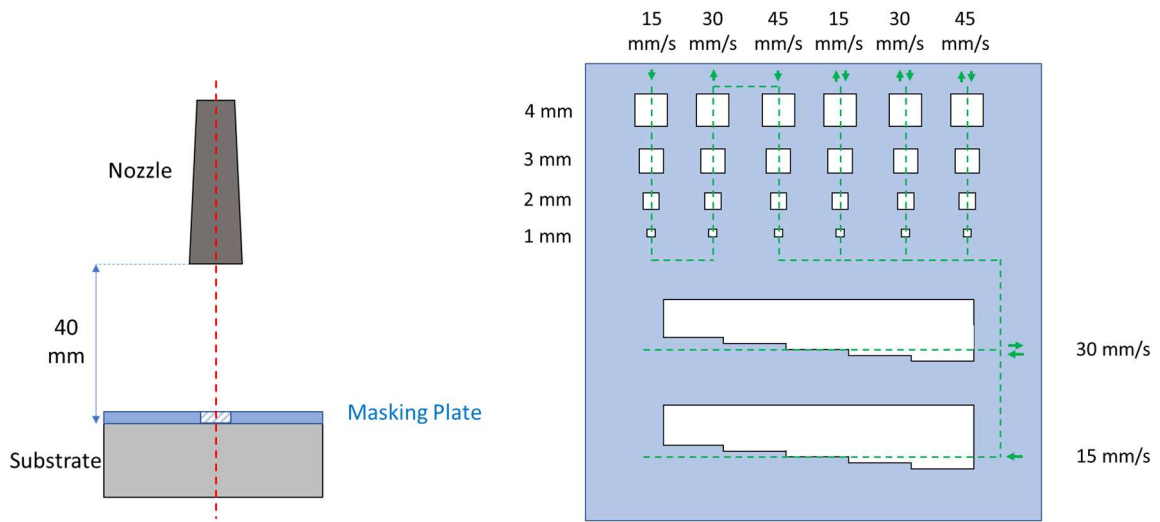


Figure 36 – Mask experiment setup and mask outline (150 x 150 mm) with nozzle path of 8 mm spray track

### 4.3.1. Small feature section

Deposition into the small feature zones of the mask was limited, being highest in the centre of the zones, and minimal at the faces of the mask, as can be seen in Figure 37. The deposition across all traverse rates was no more than 100 microns in thickness for single or double layers, compared to the expected 2 to 4 mm heights for free-standing tracks using the same parameters. The deposition failed to build any vertical surfaces adjacent to the mask on any face of the square unmasked zones, at any thickness of mask.



Figure 37 – A typical failed small feature deposition pattern

One possible cause of this could be an effect of the deposition efficiency of the process, as a significant proportion of the powder does not adhere to the substrate. In this zone, the gas jet will not be sweeping along the substrate surface, but will travel horizontally along the top face of the mask, meaning any undeposited powder may not have been blown away from within the smaller features of the masking plate, especially at the sides and corners, hindering the deposition of the subsequent incoming powder. It is even possible that powder had already collected in these sections during the trial as the powder feeder is active before the nozzle is placed over the mask. This is to ensure a continuous powder flow through the nozzle, but in a better controlled system it would be worth

examining whether powder fed only once the nozzle was in place over the mask would achieve more successful deposition into smaller features.

#### 4.3.2. Nozzle alignment section

Deposition in the nozzle alignment test section proved successful for all mask thicknesses, though deposition of the copper powder was also noted on the top surface of the masking tool. Though this did not appear to interfere with the deposition in these single- and double-layer trials, it could potentially cause problems for deposition in longer spray trials, or when considering the reusability of the masks.

In each experiment the deposit built flush to the vertical face of the mask, seen in Figure 38, with the surface created showing differing deposit build heights for each nozzle-wall offset. There was no observed bonding of the deposit to the side walls of the masking plate, with the masking plate easily removed by hand after spraying was completed.

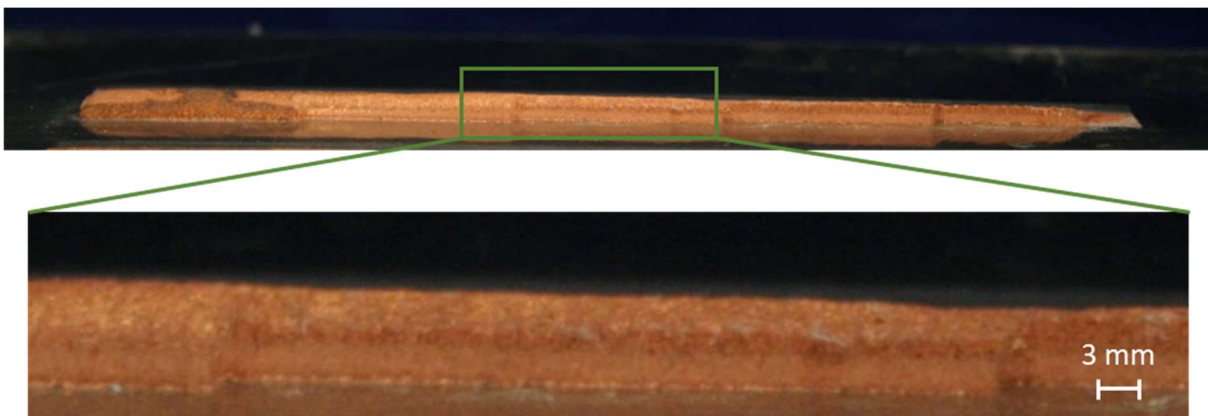


*Figure 38 – Side view of the deposit formed in nozzle alignment section, after mask removal*

The deposited surfaces were flat, and tilted from the substrate to the same degree as mask walls were from the water jet cutting, as shown in Figure 39.

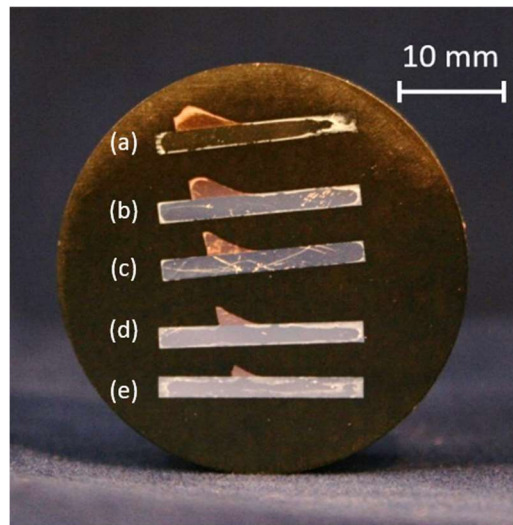


*Figure 39 – Samples from the nozzle conformity section, where the nozzle’s central axis is offset from parallel with the wall by (a) +2 mm, (b) +1 mm, (c) 0 mm, (d) -1 mm, and (e) -2 mm*

The thickness of the mask caused negligible variation in the maximum height of the deposited tracks, the minor variations seen in Figure 40 are likely to be caused by alignment discrepancies between the experiments. Multiple layers appear to work without issue, and proved a point about total build height - that the same build time will give the same cumulative build height regardless of the traverse rate.

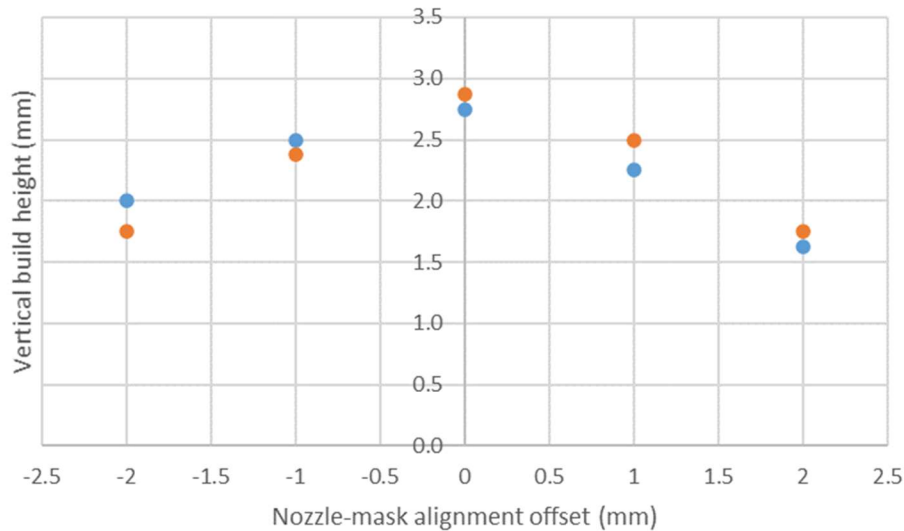


*Figure 40 – Vertical wall build height vs central alignment of the nozzle with feature edge with 3 mm mask thickness, for one 15 mm/s layer and two 30 mm/s layers*

The tallest deposited mask adjacent surface constructed when the nozzle was centrally aligned with the mask for all mask thicknesses. This was expected from the centrally peaked shape of deposition observed during standard cold spray deposition, and it is clear that the mask has not changed the local distribution of particles that have impacted, but rather prevented a portion from reaching the substrate.

#### **4.4. Backstop**

In order to avoid disturbing the gas flow near the substrate, and to allow undeposited powder to escape the deposition zone, in the following experiments the nozzle was directed to spray parallel to a backstop wall, similarly to the nozzle alignment section of the mask trials in Section 4.3.2.

The backstop components were made from tool steel, to reduce or eliminate deposition forming on the top surface of the backstop, depending on the depositing powder. Backstops of incrementally increasing heights, from 2 – 10 mm, were created to test whether the backstop height would affect the capability of the deposit to form adjacent to its surface, or alter the deposited layer height or surface finish. The nozzle was aligned perpendicular to the substrate with the face of the backstop being parallel to the axis of the nozzle, as shown in Figure 41.

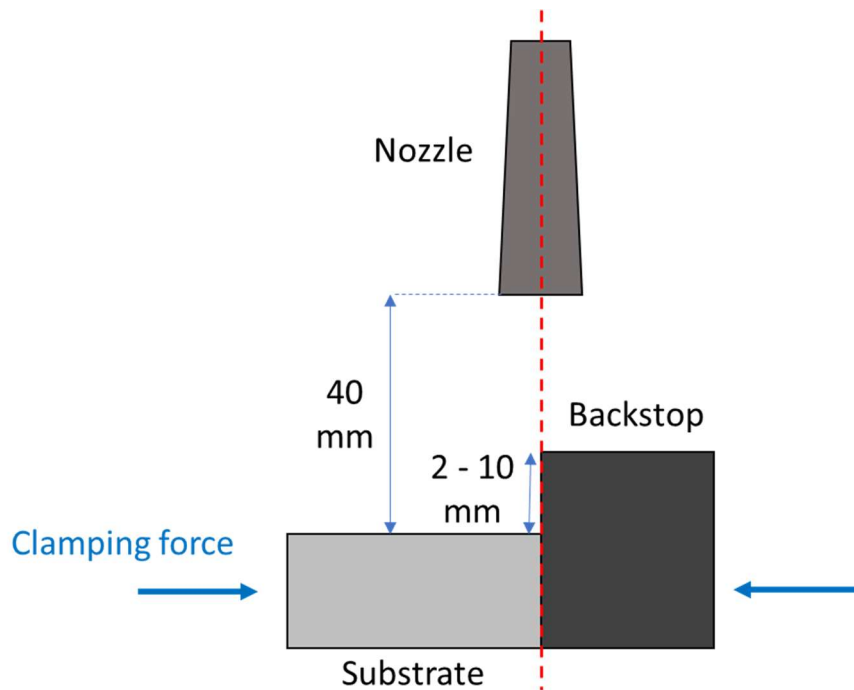


Figure 41 – Backstop design figure, nozzle traverse direction is into the page.

Spray parameters used for all experiments in this section are as described in Section 4.2.

#### 4.4.1. Backstop deposition results

Similarly to the parallel sections of the mask trials, a flat, vertical surface was achieved at all traverse rates for 2, 4 and 6 mm backstop heights, an example of which is shown in Figure 42.

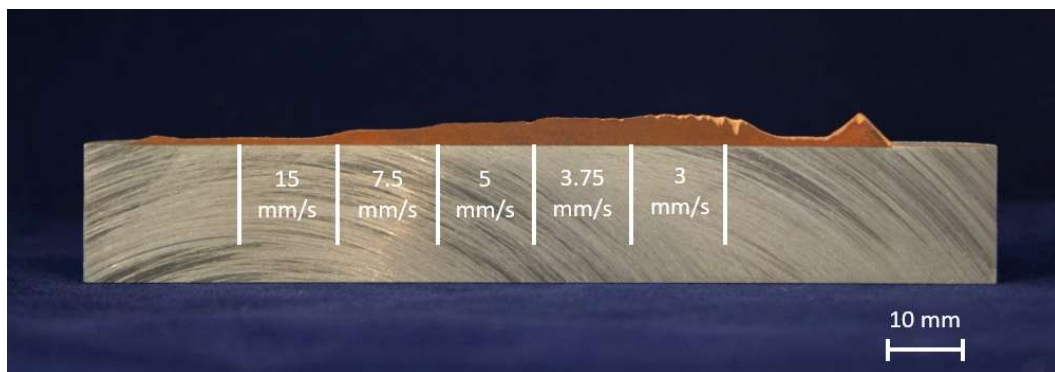


Figure 42 – Example of successful copper deposition against 6 mm backstop, with decreasing traverse rates of 15, 7.5, 5, 3.75 and 3 mm/s.

Successful vertical deposits were created in some experiments using 8 and 10 mm tall backstops, at all tested traverse rates, shown in Figure 43. The shape conformity and surface finish of the successful trials were the same as the successful smaller height backstop experiments.



*Figure 43 - Successful copper deposition against 10 mm backstop, at a steady declining traverse rate from 25 to 3.75 mm/s*

However, increasing the height of the backstop appeared to occasionally create greater inconsistencies in the successful deposition of a flat surface, shown in Figure 44's results using a 10 mm backstop, most commonly, though not solely, at the lower traverse rates.



*Figure 44 – Failed copper deposition adjacent to 10 mm height backstop at 25, 15, 7.5, 5 and 3.75 mm/s*

It is possible that the angle at which the nozzle was aligned to the backstop face, may have altered during operation, causing a “shadow” to be cast over the depositing region adjacent to the backstop face, as drawn in Figure 45. Evidently any shadow that impedes particles from reaching the substrate will cause problems with deposition in the wall adjacent zone.

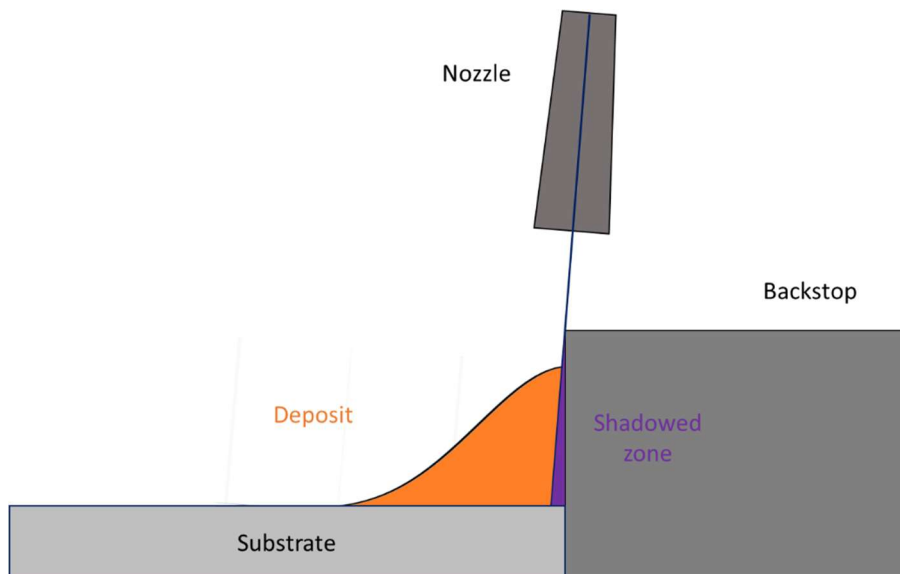


*Figure 45 - Nozzle alignment shadow*

A stepped backstop was created to study the effect of backstop height on the surface creation capability, whilst ensuring the process parameters and nozzle alignment during deposition were identical for each height, eliminating any minor variations from previous trials.

Figure 46 shows the similar inconsistent surface finish phenomenon in this trial as was demonstrated previously, with a flat, vertical wall being created in the 2, 4 and 6 mm tall backstop zones, while there was little success in the 8 and 10 mm zones, though the maximum build height remained consistent.

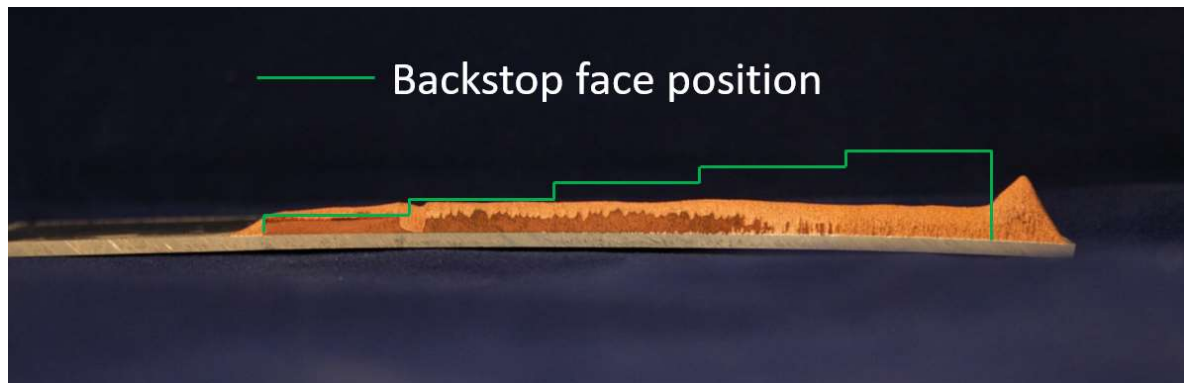


*Figure 46 – Stepped backstop result at heights of 2, 4, 6, 8 and 10 mm at 5 mm/s traverse rate*

It should also be noted that during these experiments there was build-up of deposited powder on the top surface of the backstop during deposition, despite using tool steel as the tool material. This is a feature of using a powder material that deposits so readily and would be reduced with other materials, but steps should be considered to minimize this build-up to avoid future interference with the desired deposition. This interference could come from nozzle collision, particle trajectory interference or the build-up detaching and obstructing with the deposition zone. This build up was triangular in cross section, approximately 4 mm wide and up to 2mm tall. During deposition it regularly detached from the top surface and was forced outwards away from the deposition site by the oncoming gas jet. This happened at all heights and was not observed to have altered the deposition in any way for any height of backstop.

#### **4.5. Flow separator**

As the forces involved in cold spray generated by the gas impacting on surfaces can cause strong vibrations, requiring everything within the path of the gas within the chamber to be firmly clamped, it was originally believed that the use of a thin sheet to define the desired deposit surface may lead to vibrations which would affect the deposition of the material, or potentially even bend the sheet. Following the success of the previous backstop experiments it was decided that the attempt should be made, as an effort to reduce interference with particle trajectory and gas dynamics as much as

possible, in addition to providing a less obtrusive and more easily positionable solution for a future production system.

A thin stainless steel sheet, 0.6 mm thick, termed the flow separator, was clamped to the side of a 12 mm thick machined substrate to ensure that its surface remained at 90° to the deposition zone on the nozzle facing substrate surface, as demonstrated in Figure 47. The nozzle was moved 50 mm along the flow separator at traverse rates of 3, 3.75, 7.5, 15, 25, 50 and 100 mm/s. It was then stepped away from the flow separator by 4 mm, and returned 50 mm back along the substrate whilst depositing an adjacent track to the first, and returned to the nozzle start position. Subsequent layers were then deposited in varying numbers (ranging from 2 to 50), with the intention of creating a similar total dwell time over the samples. For example, one layer deposited with nozzle traverse rate of 5 mm/s gives the substrate the equivalent dwell time as two layers at 10 mm/s.

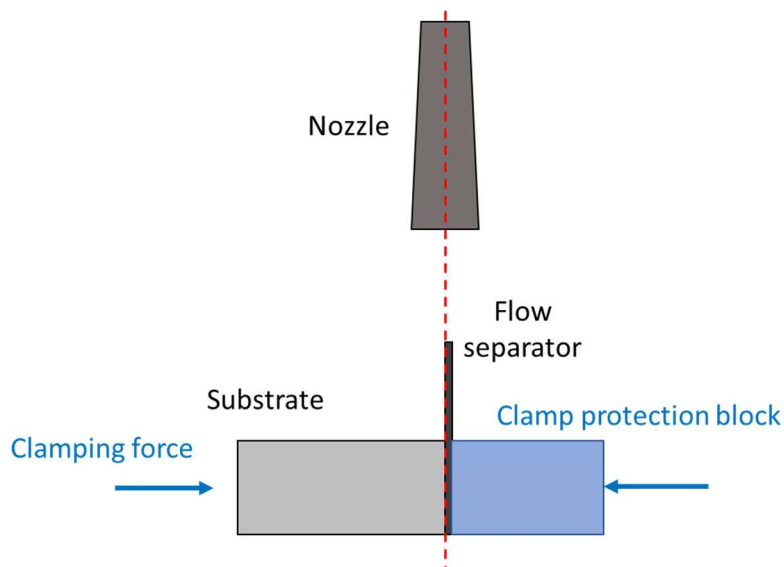
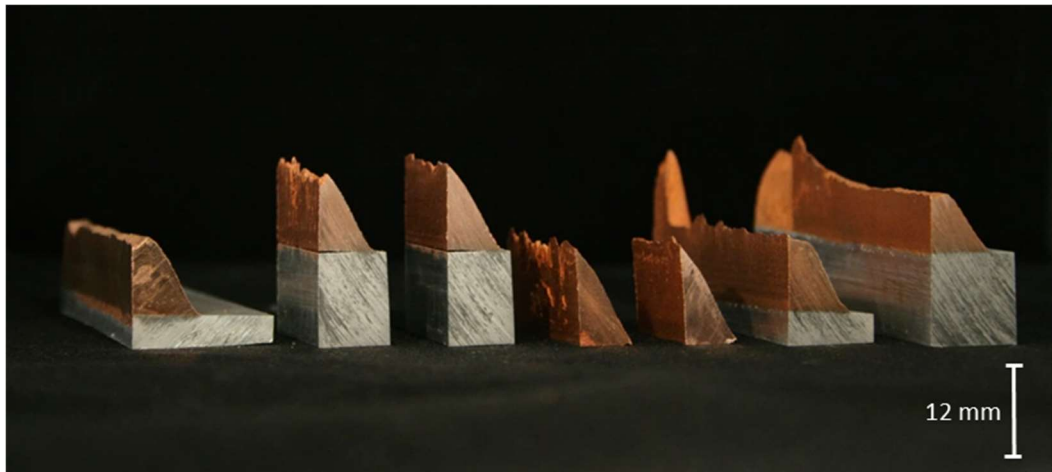


Figure 47 – Flow separator diagram

The height of the flow separator was chosen to be 19 mm. This height was chosen to allow a reasonable height of deposition for examination and measurement purposes, and to locate the leading edge of the flow separator just after the point of one of the diamond shocks in the simulated gas profile, as located by simulations in Chapter 5, where the pressure is already highest in the gas stream, hopefully avoiding the issues noted from the taller backstops in Section 4.4. It was hoped that this would cause the minimal interference with the gas and powder flow whilst allowing a height of surface to deposit. The results of test simulations for flow separators of different heights can be seen in Figure 70Section 5.6 in the simulation chapter.

#### 4.5.1. Flow separator deposition results

The flow separator experiments proved successful, repeatedly providing a flat, vertical walled deposit of 12 – 14 mm, adjacent to the flow separator face across a range of traverse rates from 3 – 100 mm/s, seen cross-sectioned to better show the straight surface in Figure 48. Taller spikes can be seen at the ends of some deposits, caused by signal delay in switching the powder feeder off as the nozzle is dwelling at the end of a deposition run.



*Figure 48 - Copper deposition cross sections [3, 3.75, 7.5, 15, 25, 50, 100 mm/s], with all parameters as described in Section 4.2.*

The defined, flow separator-adjacent surface of the copper deposits were observed to be reflective, achieving sub-micron surface roughness ( $R_a$ ) at all traverse rates, shown in Figure 49. There is not enough data to draw firm conclusions on how the traverse rate affects the surface roughness. It is likely that the deposits with a greater number of layers are presenting with a rougher surface, as the interface between the layers tends to be rougher and more porous than the deposition within a single layer. This is likely caused by the cooling of the previous layer, which could be countered by the addition of a preheating laser and optimisation of the deposition parameters.

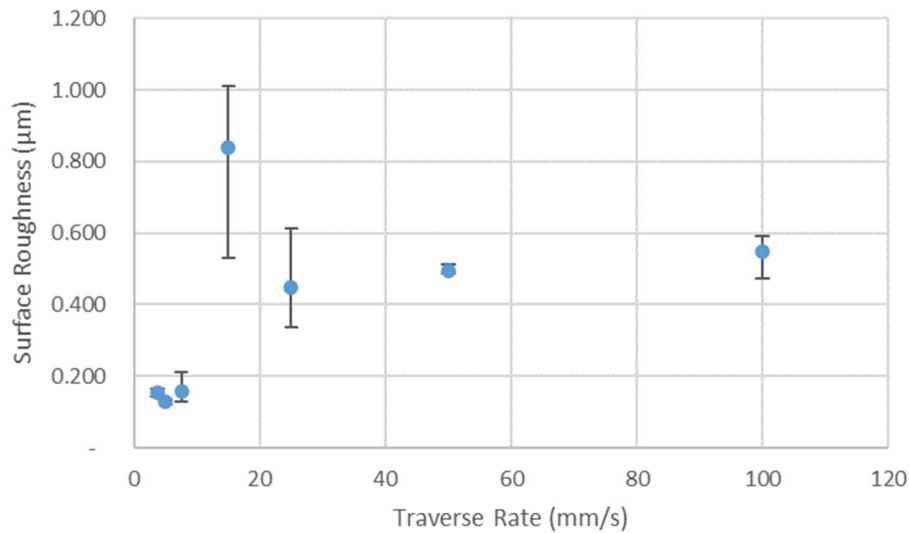


Figure 49 - Traverse rate vs surface roughness for copper flow separator deposits

While depositing, a thin layer of deposit can be seen building up on the top of the flow separator. This builds to a small height and then flakes off. This does not affect deposition, as the copper building up is only the width of the top of the flow separator, and as described in Section 6.2, the height of the separator makes little difference to the deposition.

## 4.6. Discussion

The results presented in this chapter have shown the advancements made in progressing the cold spray system from one incapable of any in-process shape control to one able to build high fidelity, controlled surfaces.

The highly limited deposition in the small feature sections shown in Section 4.3 of the masks despite the success in the alignment tests suggests that in order to facilitate the deposition of subsequent powder, there has to be an escape path any previously undeposited powder. Additionally, the use of masking plates to construct three-dimensional objects would limit the potential shapes, as this would require a fixed cross section of the component being built. Deposition on the top surface of the mask is also unwanted, as this may interfere with deposition at a later point, either affecting gas flow, powder clearance, laser interaction, nozzle clearance, or potentially breaking off and interfering with deposition.

With these considerations in mind, it was decided the next experiments would use tall, flat walls to spray adjacent to, and facilitate the clearing of powder from the deposition zone. These walls would be made from a harder material to avoid building up a deposition on the top surface of the shaping tool, as the incoming powder would deposit less readily to a harder material.

Subsequent experiments were conducted with the nozzle aligned centrally with the face of the tool, as this would locate the tallest part of the deposition at the tool face. This prevents subsequent layers from spraying into a channel between the previous deposit layer and tool face displayed in Figure 50, potentially hindering powder clearance and further deposition.

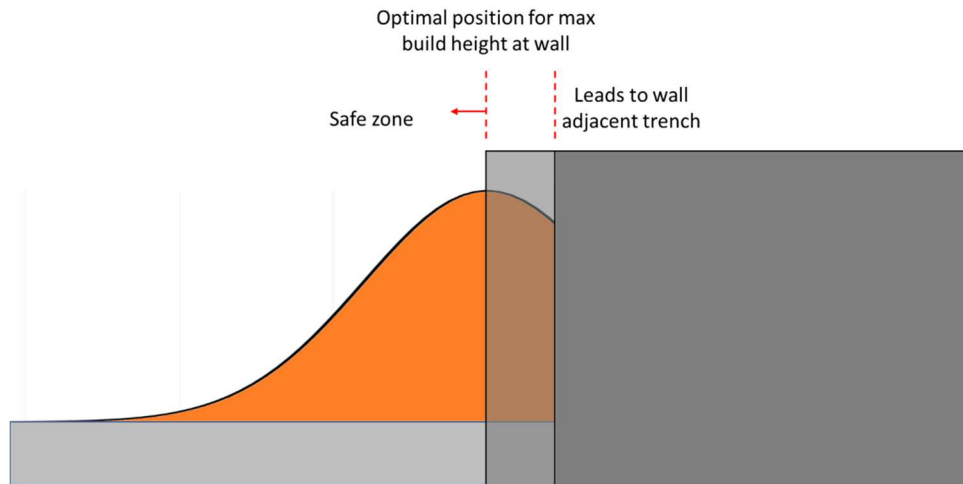


*Figure 50 - Diagram showing the effects of tool wall position on tool adjacent deposit shape*

During the backstop trials, conformal surfaces were successfully created across a range of traverse rates and backstop heights. The buildable height is only limited by the critical angle of the non-sculpted face of the deposit, building adjacent tracks or full layers with defined surfaces would allow the height to continue to increase, something that will be investigated in further chapters.

Whilst capability has been demonstrated, seemingly affected by height of the backstop, a solution requiring the positioning of a large flat backstop would further limit the achievable shapes in a future system. As the experiments are expensive and time consuming, it was decided to attempt to reduce the required size of the backstop tool, rather than optimise and explain the results achievable with this method.

Research has been unable to determine why the deposit was less consistently successful with a 10 mm backstop, than with a 2 mm backstop. It is possible that a larger volume of powder is hitting the taller vertical surface of the backstop prior to the substrate and, having lost velocity after this impact, is not bonding nor clearing the deposition zone, causing interference with the subsequent incoming particles. Alternatively, alignment issues could have caused the backstop to occlude the substrate, causing deposition issues. The gas dynamics surrounding the backstops will be considered in Chapter 5, to see if any conclusions can be drawn about why the particle trajectories were affected with taller backstops.

The flow separator experiments successfully and consistently produced smooth, flat and dense deposits that conformed to the surface of the tool face at a range of traverse rates. The deposits produced using a flow separator have the most consistently smooth and conformal surfaces, and used the tool that would lead to the least interference/most flexibility in terms of positioning capability. These deposits were further analysed to assess deposit structure and compared with standard cold spray, detailed in Section 6.3.1, and to allow better comparison to the subsequent experimentation.

The backstop experiments noted difficulties in producing successful, flat deposits when utilising taller backstops, especially at lower traverse rates. This however does not seem to be the case for equally tall or taller flow separators used to shape the deposition, and so further work is required to understand what phenomenon causes the instability at greater backstop heights.

#### **4.7. Powder recycling**

The deposition efficiency of the powder was not measured for the trials in this research, as the amount of powder used was not a measurement of success in this case, and this process by necessity involves diverting powder away from the deposition site in the surface regions of the component shape during deposition, thereby lowering the deposition efficiency compared to standard cold spray. In order to reduce material waste and therefore cost of this process, an investigation should be conducted into the recyclability of the powder which does not adhere during deposition. As the environmental chamber is enclosed, this powder would not be difficult to recollect for deposition, though it may be difficult to ensure its purity if different materials are used in the same system.

After one of the spray trials detailed in this thesis, titanium powder was collected from the chamber for a cursory visual inspection. Figure 51 shows the SEM images of the powder (a) before and (b) after spraying. As can be seen, the powder particles appear to remain largely spherical, however have lost most of the smaller satellite particles adhered to them, and generally appear to have smoother surfaces, although are faceted in places where impact with the substrate or deposit has likely occurred but not caused adherence. Some may have even shattered on impact into a number of smaller particles. Further work is needed to ensure that the particles behave in the same way as fresh powder before the powder can be deemed reusable. The powder properties are likely to have changed following the substrate impact from work hardening, though how significantly is unknown. It is possible that the powder could then be annealed to return the original material properties of the virgin powder.

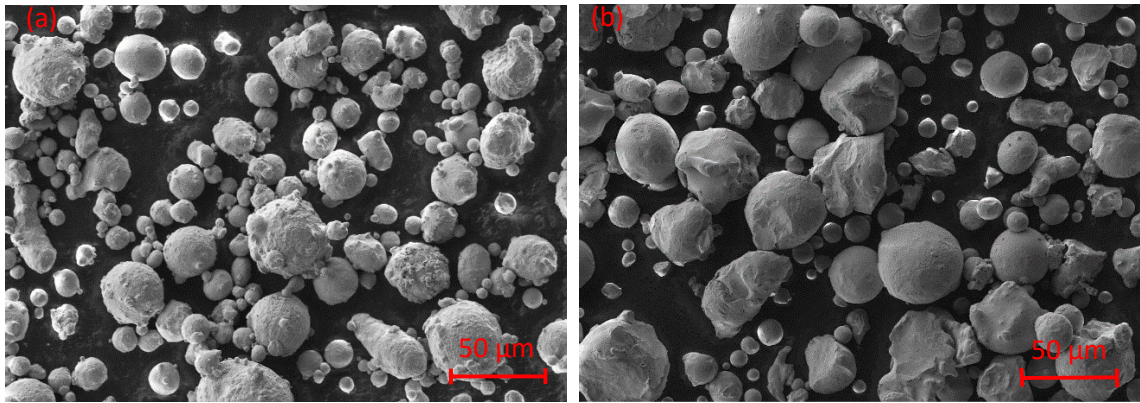


Figure 51 - Powder particles (a) before and (b) after spraying through the system

## 4.8. Summary

The results presented in this chapter have shown that the deposition of a defined, flat, vertical surface is possible using cold dynamic gas spraying of a copper powder, by spraying parallel to the surface of a tool with a flat, vertical side wall.

It has also been shown that the shape of the tool can affect the maximum height that the tool can be before affecting the deposition capability, though it has not been understood what causes this observation at lower traverse rates. It has been noted that in all cases, the deposition of a defined surface appears most affected by the presence of a shaping tool at lower traverse rates. This is not of major concern for the development of a future manufacturing system, as faster traverse rates create thinner, flatter layers which would be desirable to substrate-nozzle normalcy and retain maximum deposition efficiency.

The next logical step in this work is the expansion of the capabilities of this system when using the thin, flow separator tools. This includes the testing of other materials, the addition of laser substrate preheating, and the creation of further shapes with defined surfaces, all of which are examined in Chapter 6.

Before that, however, an attempt to understand the cold spray gas and particle dynamics, and resulting interference caused by obstacles, will be investigated in Chapter 5 to lend understanding to some of the affects seen in this chapter.



---

# Chapter 5 - Generation and validation of computational flow models

---

## 5.1. Introduction

After the inconsistent results during lower traverse rate experiments in Section 4.4, it seemed logical to gather a better understanding of the complex gas dynamics involved in cold spray deposition by simulating the gas flow, and to investigate the effect of placing obstacles into the flow path on the path of the particles. It was expected that understanding the effects on the trajectories of the particles would allow explanation of the inconsistencies found when depositing with backstops but not with flow separators.

In order to do this, a series of simulations were created to model the experimental setup of the cold spray system. The purpose of creating these models is to understand the gas velocity profiles, the shape of the shock structures that form and the effects that these have on the particle trajectory.

This work was undertaken in ANSYS FLUENT and described within this chapter is the method of establishing the model, and its subsequent validation through comparison with other simulations in literature, developed as part of this work. Once the gas structure had been accepted as accurate, the effects of these structures upon particle trajectory through the nozzle and through the exhaust region was added to the model.

The comparison of the generated gas flow models will generally focus on the centreline gas velocity, as is standard in cold spray simulation [84]–[86], [88], [89], [101], [102]. Once particle tracking has been implemented these results will also be part of the comparisons.

## 5.2. Model construction

The gas flow dynamics involved in cold spray were not well enough described in literature to inform the flow shaping methods being considered, and so models of the gas structure were developed to aid this understanding. Certain assumptions about the system were necessary to facilitate this simulation, and are justified below. The construction and validation of these models is discussed in this chapter, with the implications from these models on experimental design considered in the chapter summary.

### 5.2.1. Assumptions

- i. The gas flow is continuous. The pressure within the system is sufficiently high that the interactions of individual molecules do not have to be considered.
- ii. There are no chemical changes within the gas flow, e.g. combustion. The gases used in cold spray are inert.
- iii. Gravity acts along the nozzle length, but has been ignored as its effects are negligible compared to the other forces acting in the system.
- iv. Upon convergence of the model, the flow is expected to remain steady, i.e. the velocity, pressure and density are independent of time. Transient models do not provide significantly different results in this instance, but require much greater computing power. Whilst in reality the gas flow is likely to slightly fluctuate around an average case, the standard process for cold spray is to assume a steady state.
- v. The gas is treated as an ideal gas for density calculations.
- vi. The solid phase particles within the gas stream are not of sufficient volume to affect the flow conditions of the gas, allowing for a discrete phase Lagrangian method to be applied over an Eulerian method. This is standard practice for mixed phase flows with secondary phases comprising less than 10% of the volume flow rate. This is discussed further in this chapter.
- vii. The model is static. Though the nozzle is moving in reality, the velocity of the gas far exceeds the traverse velocity of the nozzle, by approximately 10,000 times. For this reason the assumption holds that this will have negligible effect on the instantaneous gas structure and velocity.

### 5.2.2. Dimensions

There are three available model types for analysis in Fluent 16.0: 2D profile, 2D axisymmetric or 3D volume. 2D profile modelling does not provide an accurate representation of the flow for this situation. The initial case of a nozzle plus an exhaust region is ideal for modelling as an axisymmetric simulation, but this would restrict all simulated obstacles in the later instances to being also axisymmetrical. The 3D volume model would be the optimal choice, however it is more resource intensive for both meshing and solution iteration, and the mesh needs more careful control when being created.

Initially, two-dimensional models were created to test the assumptions listed previously, and determine whether the initial parameters selected gave reasonable gas velocity and structure results. This approach was chosen as it would be the less resource intensive method, and allow for comparison with literature data, which is predominantly 2D, to examine the validity.

Following this, three-dimensional models were created in order to allow the introduction of non-axisymmetric obstacles into the flow, and create a more accurate model. These models were validated by comparison to the 2D models.

### 5.2.3. Geometry and meshing

Analysis conducted in ANSYS Fluent requires the geometry of the volume in which the fluid is located. The internal dimensions of the nozzle were therefore used to create a model of only the initial gas

pathway, starting at the nozzle inlet as the nitrogen arrives from the gas heater, through the throat and diverging section. Once this model had been tested, an exhaust section was added to the nozzle, with the option for including substrates and altering the standoff distances, seen in Figure 52.

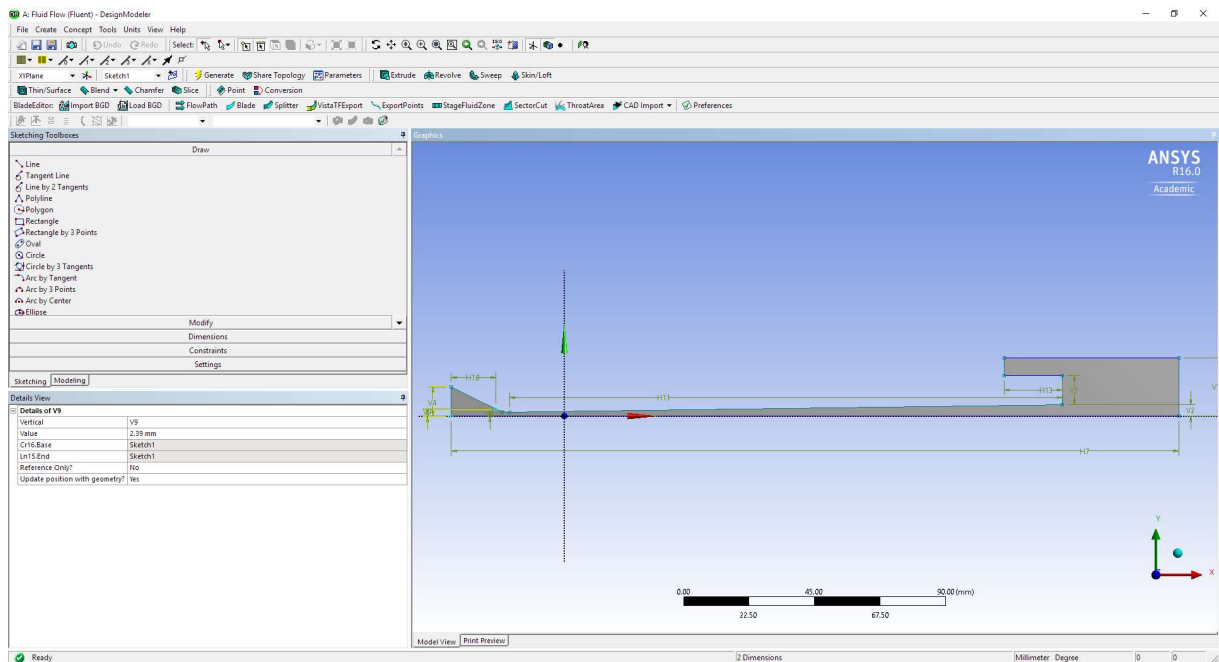


Figure 52 - Geometry creation screenshot

When creating a 2D mesh for the axisymmetric calculations, the most important definable parameters include the minimum edge size, maximum face sizes and the growth rate. The maximum face size allowed for these simulations was 0.2 mm. This would allow a minimum number of 10 cells across the narrowest part of the nozzle, including the smaller boundary layer cells. If the cell size is too large, flow structure will be lost between iterations. Alternatively, if the cell size is too small, the processing power required to calculate the flow structure will be too large to resolve the flow with the available resources, and is unnecessary to create a sufficiently accurate model. With these limitations in mind, the minimum edge length was set as 0.1 mm.

For the three-dimensional models, the maximum face size has been extended to 0.5 mm to allow for faster processing in the bulk of the model, while still creating a minimum of 20 cells in the cross section of the nozzle at the throat. In actuality the models had more than 20 cells at this point, as this is the minimum number. An unstructured mesh was used as it is more suitable in dealing with complex geometry when using compressible fluids, which can be seen in Figure 53, and has been previously employed in cold spray modelling [81], [95], [101].

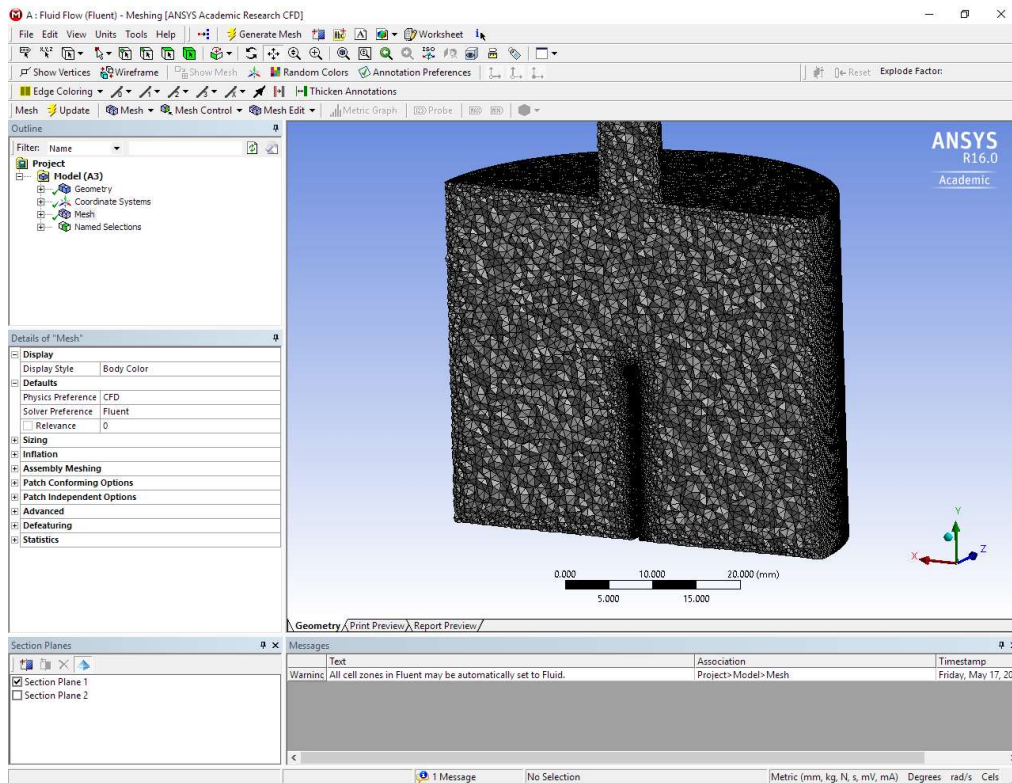


Figure 53 – Mesh creation screenshot of early mesh model

Once a body mesh has been established, the parameters were altered to provide a finer mesh, max edge length of 0.1 mm, and therefore better gas flow resolution at the most interesting areas, such as the throat and exhaust of the nozzle, or the surface of any flow altering implement.

## 5.2.4. Solver parameter selection

As the problem deals with supersonic flow, which is high-speed and compressible, the density-based solver option is employed in the FLUENT setup. Though Fluent is now capable of applying either density based and pressure-based solvers for calculation of compressible flows, the density based solvers are most commonly used as the velocity profile can be obtained directly from the momentum equations, and the pressure from the equations of state.

### 5.2.4.1. Energy equation

As the model is operating with compressible flow, the additional energy equation must be activated to ensure energy conservation throughout the model.

### 5.2.4.2. Discrete phase modelling

There are two types of particle tracking methodology in Fluent 16 [125], Euler-Lagrangian discrete phase model or Euler-Euler mixtures as described in Section 2.12.5. The one-way coupled Euler-

Lagrangian method is chosen for these models as the powder volume fraction is low, the particles are assumed to have no influence on the fluid, allowing for reduced computation time.

The injection site of the particles can be specified within the model, with particles given an initial temperature, velocity and size, and a mass flow rate given to the injection zone. The particles are typically assumed to be spherical, though some alteration can be made to provide a typical aspect ratio for particles if this is not the case. The particles used in this trial were gas atomised, and as shown in Figure 51 are spherical enough to be approximated to spherical without significant change to results. At the expense of further resources, a stochastic tracking principle can be applied, whereby multiple tracks will be modelled per injection point, based on random turbulent dispersions added to each track. The effects of the gas structure on the particle are then evaluated every 50  $\mu\text{m}$  along its path length, as this is half the minimum cell edge length allowing a minimum of 2 calculations per cell, to determine the velocity of the particle.

The spherical drag coefficient was applied in FLUENT for the particle velocity calculations, as is common throughout cold spray simulation with the particles typically being approximately spherical [53], [83], [86], [87], [95], [107], [126].

#### **5.2.4.3. Materials**

The fluid volume denoted by the mesh is set to be nitrogen. The density is set to follow the ideal-gas method, and the viscosity to use the Sutherland equations.

Though the initial conditions in reality would be an air environment, the steady state solution for the nozzle will be entirely nitrogen, and as this case would have been rapidly reached in a few iterations, there is no need to include another complicating factor.

The nozzle wall is designated to be tungsten carbide, and the heat transfer component disabled. When the system has been active during warmup, the nozzle reaches temperatures close to the inlet gas temperature of 300°C, meaning that there will be no energy loss through the wall, and the cooler gas further down the nozzle will be moving so quickly that there can be minimal heat transfer to the gas.

The inert particle materials and parameters are also chosen at this point, though can be altered later as the flow is not coupled. The chosen material was copper, and the particles were designated as spherical with diameters of 30 microns.

#### **5.2.4.4. Boundary conditions**

In all cases, the gauge pressure at the nozzle inlet was fixed at 30 bar as this is the maximum operating pressure of the system when using nitrogen as the carrier gas, and was the pressure used for all

experiments. The gauge pressure at the outlet of the system is initialised as 0 bar, with an operating pressure of 1 atm (101,325 Pa) throughout the system.

The nitrogen temperatures were also established, with the temperature at the nozzle inlet fixed at 300 °C, as it arrives from the gas heater, and initialised to 20 °C at the outlet.

#### **5.2.4.5. Turbulence model**

As mentioned in Section 2.12, the most commonly utilised turbulence model for cold spray simulations is standard k- $\epsilon$ .

As the development of these models were created with the intention of developing three-dimensional shock structures, the realizable k- $\epsilon$  model was chosen over standard k- $\epsilon$ . Despite the increase in processing power and time required to cope with this upgrade, one of the major benefits of using the realizable model is the more accurate predictions of the distribution of the dissipation rate of round jets and of boundary layers in large pressure gradients, both of which are features of a cold spray system, and around the obstacles intended to be introduced to the flow. This should allow a more accurate representation of the gas flow, and subsequently the particle trajectory in the three-dimensional simulations.

#### **5.2.4.6. Discretisation scheme**

The order of the discretisation scheme in cold spray modelling is rarely discussed in cold spray model generation, but can have a fundamental impact on the results, particularly on the generated shock structure [127]. Lower order schemes typically produce less accurate results at a faster convergence rate, and less resolved shock structures and vice versa for higher order schemes.

A comparison was made of models using first and second order upwind schemes, and subsequently, first and second order terms in the turbulence equations. Removing second order terms from the upwind calculations altered the resulting gas structure, providing less resolution of the diamond structure and larger irregularities around the walls and substrate, despite identical mesh sizes.

Figure 54 shows us that when the second and higher order terms were included in calculating the turbulence equations, minimal difference was noted in the gas velocity. This model does not rely heavily on turbulent zones, but since the inclusion of these terms did not significantly increase processing times, it was decided that the higher order terms would be included. This would also be useful for comparison purposes should sources of turbulence be added in future experimental setups.

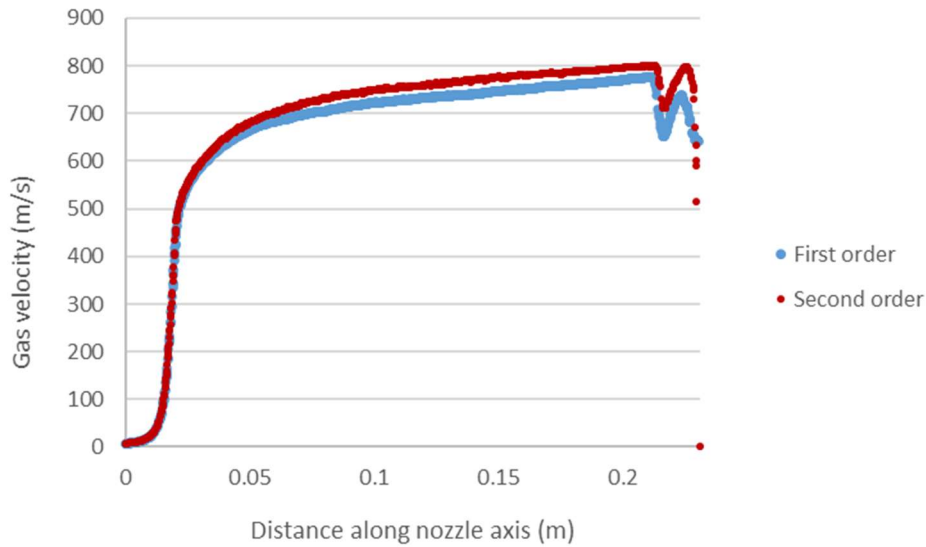


Figure 54 – Graph depicting the gas velocity along nozzle centreline for solutions including different order upwind equation terms

## 5.3. Two-dimensional modelling

### 5.3.1. Model progression

In order to establish that the correct parameters had been chosen for modelling, the initial model included only the nozzle with no exhaust zone, helping to reduce the processing power required for simulation. Once a sensible flow structure and velocity profile had been established, the geometries were then incrementally expanded to include an exhaust section, followed by a substrate, and finally flow structuring devices.

### 5.3.2. Initial results

Initial results show the nozzle used at the IfM to be over expanded as it was designed, with the gas jet collapsing from the exhaust, forming a diamond shock profile, as can be seen in Figure 55. Over-expansion allows the gas to reach greater velocities than those achievable with a perfectly expanded nozzle, and therefore will also allow the acceleration of the particles to a greater velocity. However, it is uncertain how the subsequent shock profile affects the trajectory of individual particles. The gas is shown to accelerate to over 900 m/s, which was near the expected value for this system from previous work using schlieren imaging and PIV.

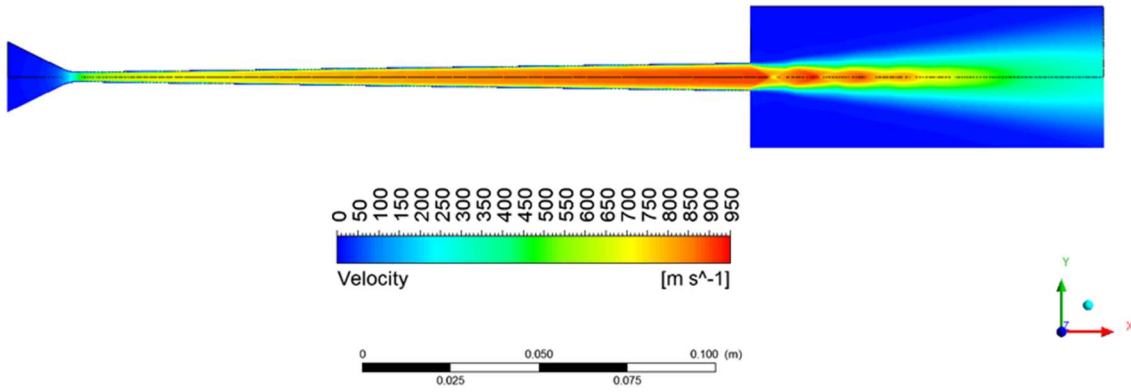


Figure 55 – Simulation generated gas velocity map of the cold spray nozzle with open exhaust area, with parameters as established in Section 5.2.4

When the substrate is introduced to the simulation at a 40 mm offset from the nozzle, the expected bow shock can be seen on the substrate and the radial shocks are formed parallel to the substrate as the nitrogen is blasted outwards from the nozzle centreline, shown in Figure 56.

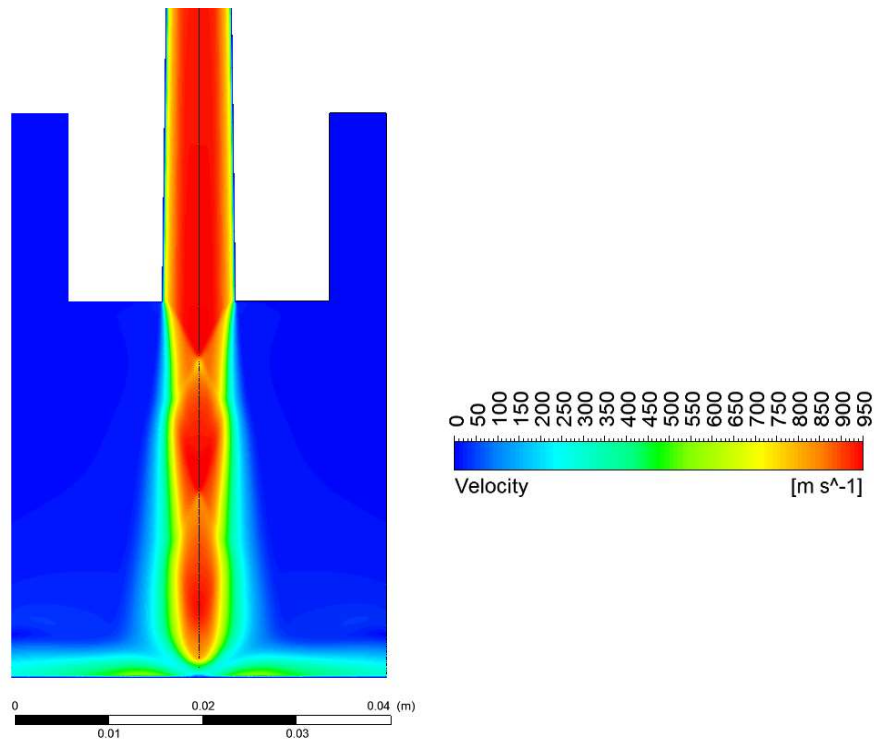


Figure 56 – 2D Simulation generated gas velocity map of cold spray nozzle and substrate at 40 mm stand-off distance

The shape of the diamond shocks is consistent with those seen in other simulations and previously published images of this setup using Schlieren photography, taken of the same system during operation, as shown in Figure 57.

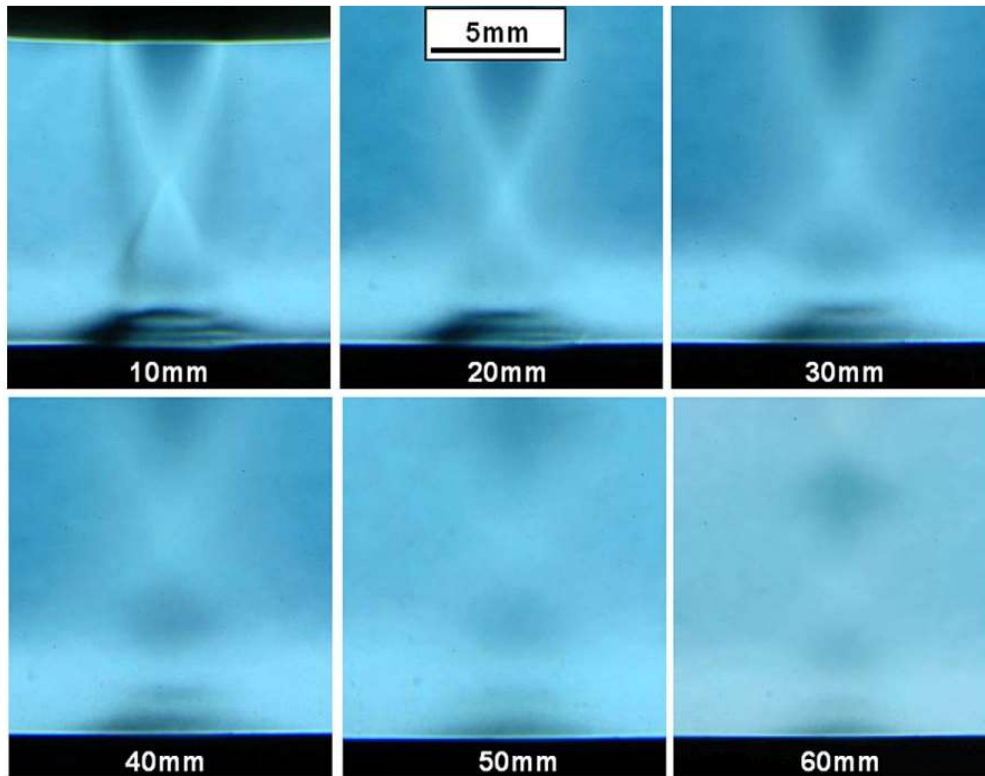


Figure 57 – Schlieren image of shock structure vs offset distance [128]

### 5.3.3. Two-dimensional mesh independence

When modelling the fluid region, the size of cells in the mesh must be constrained to provide sufficient resolution to the gas structure and accuracy in velocity calculations, without requiring unnecessary processing time.

To test whether altering the chosen mesh size would have an impact on the accuracy of the resulting model, after the model parameters had been established as detailed in Section 5.2.4 and a converging model generated, the same calculation was attempted with a mesh that was half of the size of the original. The mean absolute difference in generated centreline gas velocity was 0.3%, as shown in Figure 58.

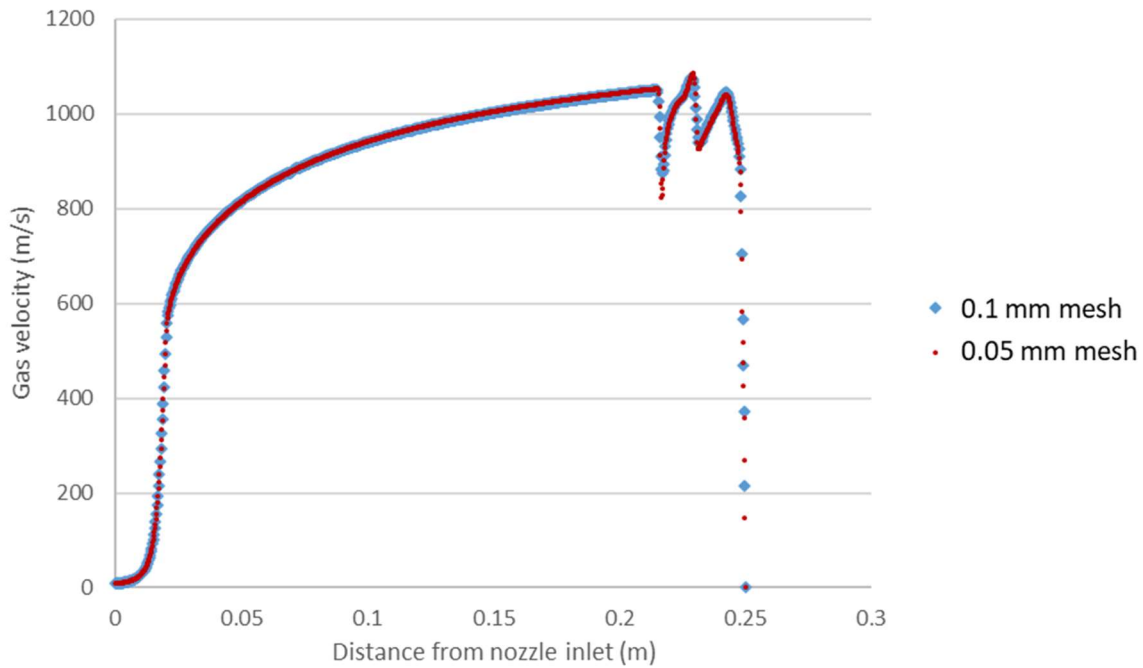


Figure 58 – Centreline gas velocity comparison for 2D mesh independence demonstration

Having demonstrated a minimal difference in results, there is no reason to further refine the mesh in an attempt to create more accurate simulations, allowing for savings on computational power without sacrificing clarity in results. Whilst an enlarged mesh could also be tested for comparison, it was felt that the gas shock structure could be lost if the mesh size were to be increased too much, and so the mesh would be kept in the same order of magnitude as the powder particles.

#### 5.3.4. Two-dimensional obstacle addition

As can be seen from Figure 59, the introduction of other obstacles into the gas flow causes alterations to the shock structure formed in the deposition zone, with the formation of larger subsonic zones or secondary radial shocks. Two-dimensional, axi-symmetric modelling of the gas flow limits the obstacles that can be introduced in the same manner. To determine the effects of non axi-symmetric obstacles, a three-dimensional model is required, which requires greater processing capability. As the initial solver parameters and boundary conditions have now been established by the two-dimensional model, they can now be re-implemented in the generation of three-dimensional models.

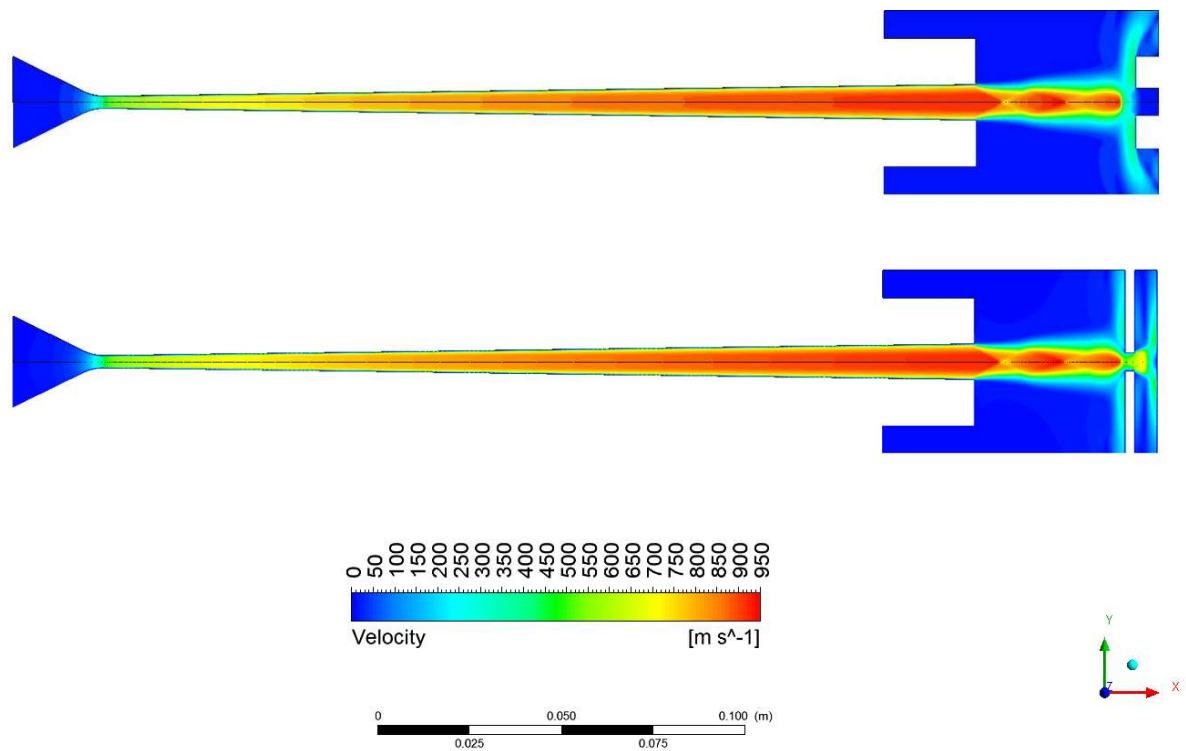


Figure 59 – Axisymmetric obstacles in nozzle exhaust

#### 5.4. Model validation with literature

In order to provide a degree of validation to the results generated from the two-dimensional simulations, an examination of literature was conducted in an attempt to find scenarios that could be replicated in this model. It was found to be very uncommon for papers to contain the full nozzle dimensions, parameters used for cold spray, and gas or powder velocities that would be necessary to allow replication of the simulation. Those that did state gas or particle velocities often gave only one measurement, usually at the centreline or averaged at the exhaust of the nozzle respectively [101].

Only one study was found in which the author had provided all of the required initial conditions of the simulation parameters, the nozzle dimensions and the gas and powder velocities, in a paper investigating particulate flow in cold spray nozzles by Meyer and Lupoi [89]. Data from this set of results was extracted from the graph presented in the paper and compared to a simulation conducted at the same temperature and pressure as that described. The model established for the Cambridge system was adapted to account for the different nozzle geometry (noted in Table 6), and the initial conditions adjusted to match those from the paper, however no alteration was made to the mesh generation settings or solution controls.

Table 6 - Geometric properties of Meyer and Lupoi nozzle

$A_i$ (mm <sup>2</sup> )	$L_c$ (mm)	$A^*$ (mm <sup>2</sup> )	$L_d$ (mm)	$A_e$ (mm <sup>2</sup> )
314	20	5.7	190	47.8

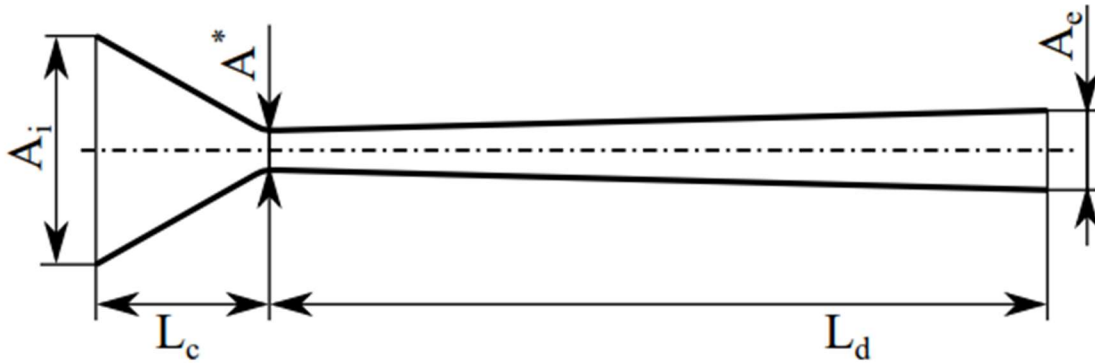


Figure 60 - Meyer and Lupoi nozzle diagram

The solution was then run to convergence, and a comparison of the centreline gas velocities from the resulting data and the published data can be seen in Figure 61 below.

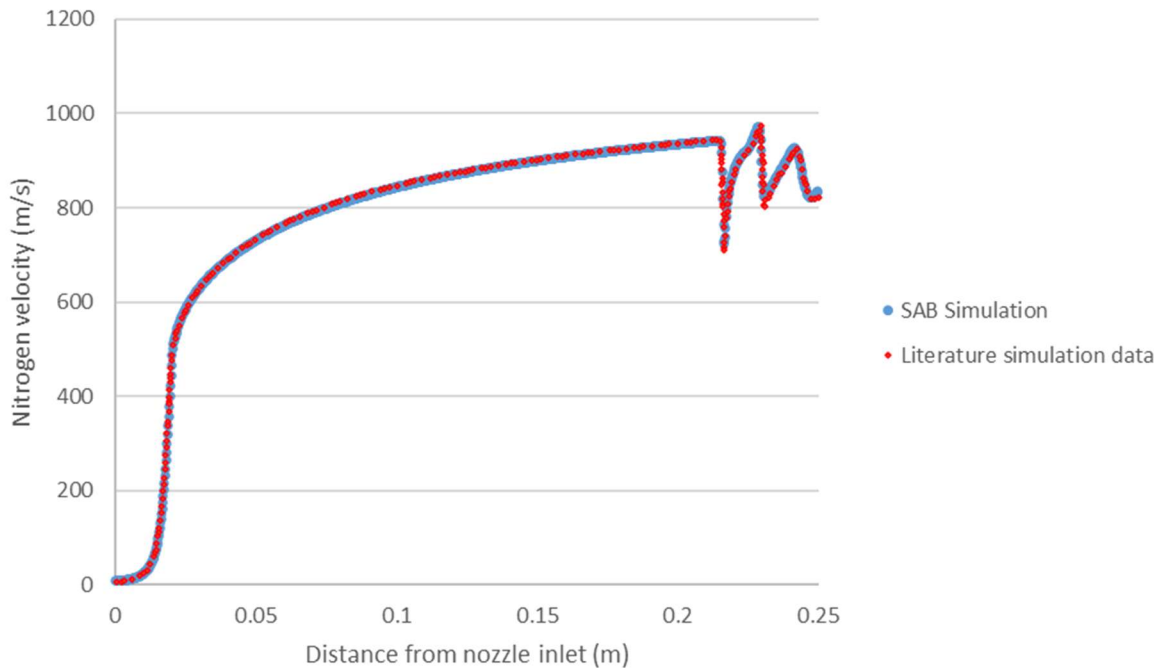


Figure 61 – Comparative centreline gas velocity results of simulation with literature

The gas velocity along the centreline of the model from inlet to substrate was compared at over 250 points, approximately every millimetre along the nozzle length, to the data from the paper. The similarity in the generated model can be seen in Figure 61. The mean absolute difference measured

between the points from the simulated model and the published model on this graph is 1.52%, which is well within acceptable error.

A further comparison was then conducted of the particle velocities. The paper in question mentions that unsatisfactory results for particle velocity were obtained when the solver was uncoupled. Figure 62 shows the comparison of the results of my uncoupled particle tracking method with the coupled particle tracking method utilised in the paper.

There should be no reason why the particle would decelerate during its path through the nozzle (up to 0.19 m path length) other than hitting the nozzle walls, and that would likely cause greater discrepancies than those shown below if well modelled, or have no effect at all depending on the modelling of the powder-wall interaction. Nevertheless, the final particle velocity appears to be similar, and follows a broadly similar velocity profile along its path length. It is likely therefore that the uncoupled method used in this paper did not use a fine enough mesh or small enough step length or time step to calculate the effect of the gas upon the powder particle. That being said, the similarity between the published coupled results and those simulated in this thesis suggests that the uncoupled particle tracking method used in this thesis is sufficiently accurate, and indeed is the most commonly used method for low volume fraction, particle-laden flows, as mentioned in Section 5.2.4.2.

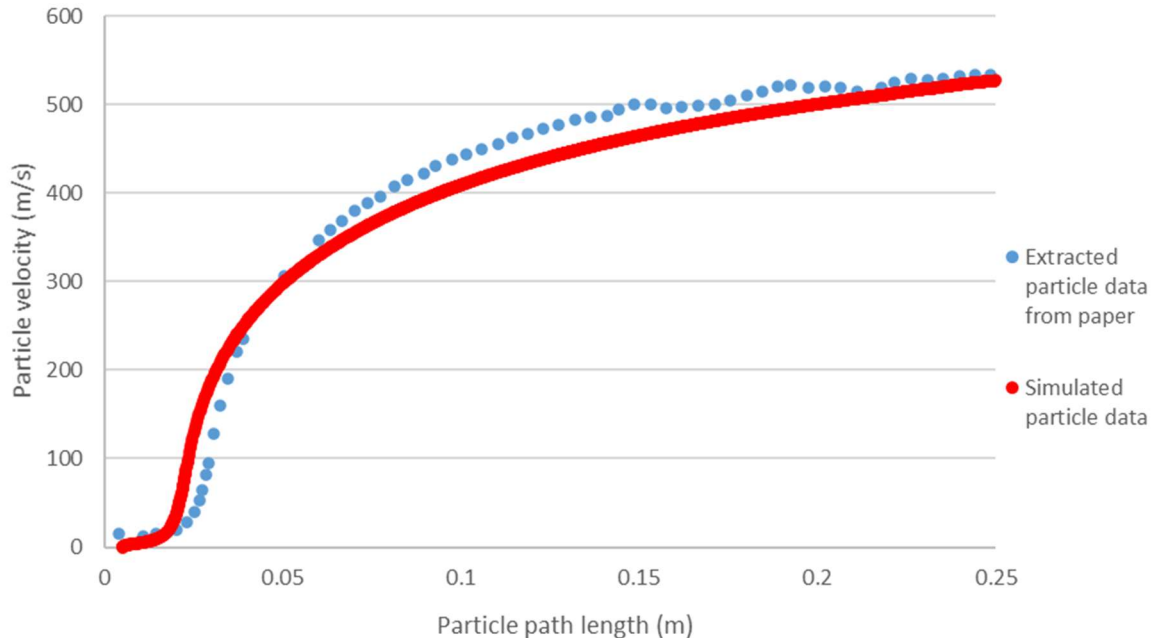


Figure 62 - Particle velocity comparison to literature data [89]

The correlation of the gas and particle data with the published model suggests that the solution parameters – including turbulence model, solution methods, initial conditions and boundary conditions – have been correctly established to produce a model comparable with the literature. This

will allow the use of these parameters in subsequent models with confidence in the accuracy of generated solutions.

## 5.5. Three-dimensional modelling

Once the two-dimensional model was accepted as an accurate representation of the process, a three-dimensional model was created using the same parameters and boundary conditions, barring the mesh adjustments noted in Section 5.2.3.

Similarly to the generation of two-dimensional models, three-dimensional models were built up from nozzle only, followed by the inclusion of an exhaust region and substrate, as shown in Figure 63, and finally the inclusion of obstacles to act as shaping devices for the deposition. This was to allow the investigation of each individual component region of the model for fault finding, which saved time in the long run for both meshing and solving. The initial measures of success of these models was the convergence of the model and the shape of the curve generated from the velocity magnitude of the gas along the model centreline. Subsequently they were compared to the 2D models for further validation.

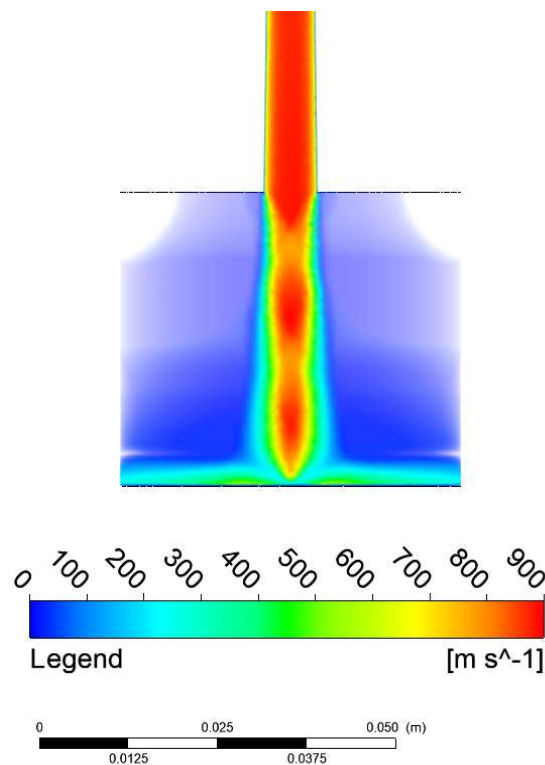


Figure 63 – 3D nozzle with open expansion/substrate

### 5.5.1. Three-dimensional mesh independence

Similarly to the two-dimensional model, there comes a point at which further refinement of the mesh only provides minimal difference in results at the expense of greater computational time.

The model was re-meshed with double the edge length, while keeping all model parameters and solution controls identical. Figure 64 shows the comparison of centreline gas velocity between the two models.

The mean absolute difference is 0.7%, but for this instance it was decided that the smaller mesh would be preferable as this would allow better resolution of the shock structures, especially around the obstacle and substrate surfaces.

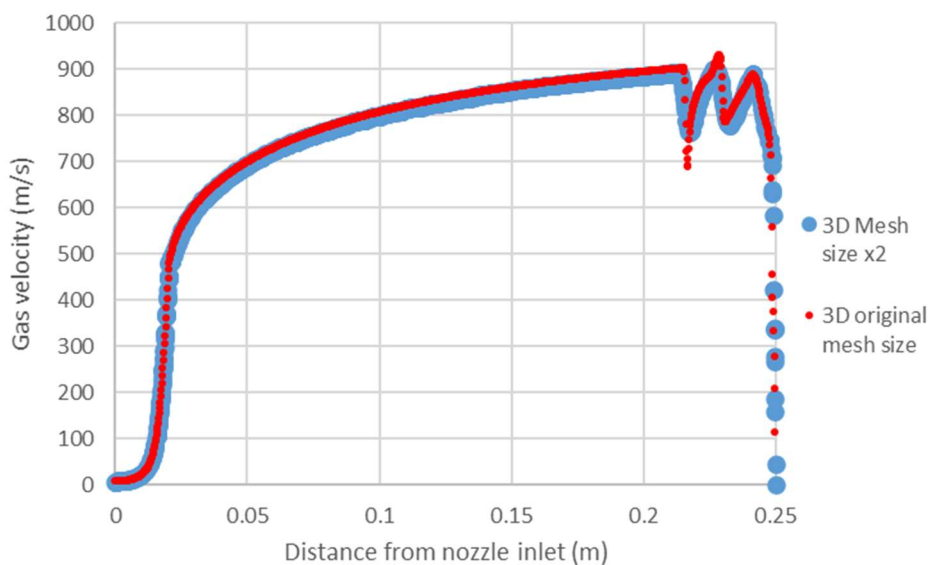


Figure 64 – 3D mesh independence test

### 5.5.2. Comparison with two-dimensional model

In order to validate the three-dimensional model, a comparison of the shock structure and centreline gas velocities was made for a nozzle directed perpendicularly at a substrate with 40 mm stand-off distance. All other parameters and boundary conditions were identical, except for the mesh sizing mentioned in Section 5.2.3. Figure 65 shows the structure comparison, and as can be seen the structures formed are identical in size and shape, as well as the measure of generated gas velocity magnitude.

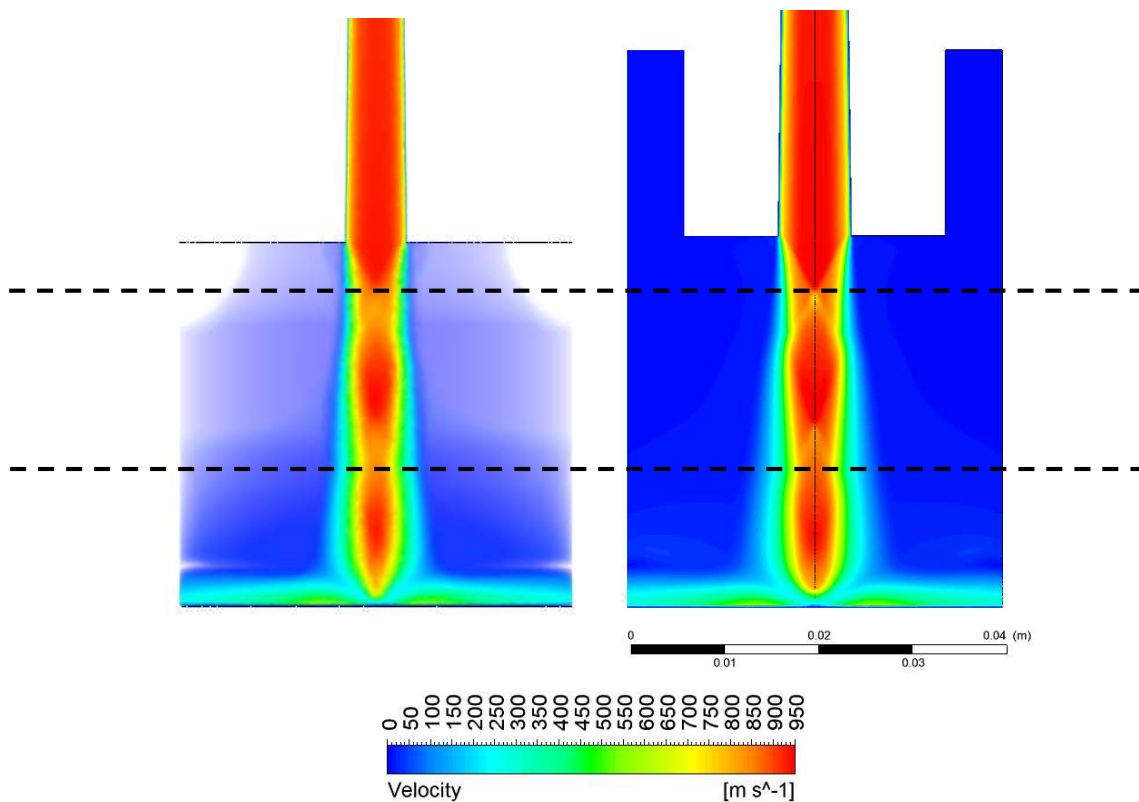


Figure 65 – Comparison of 3D and 2D nozzle simulations with substrate at 40 mm standoff

As can be seen in Figure 66, gas velocity data from the centreline path of the 3D model correlates well with the 2D results, with the gas velocity at the nozzle exit being 900 m/s and 893 m/s respectively.

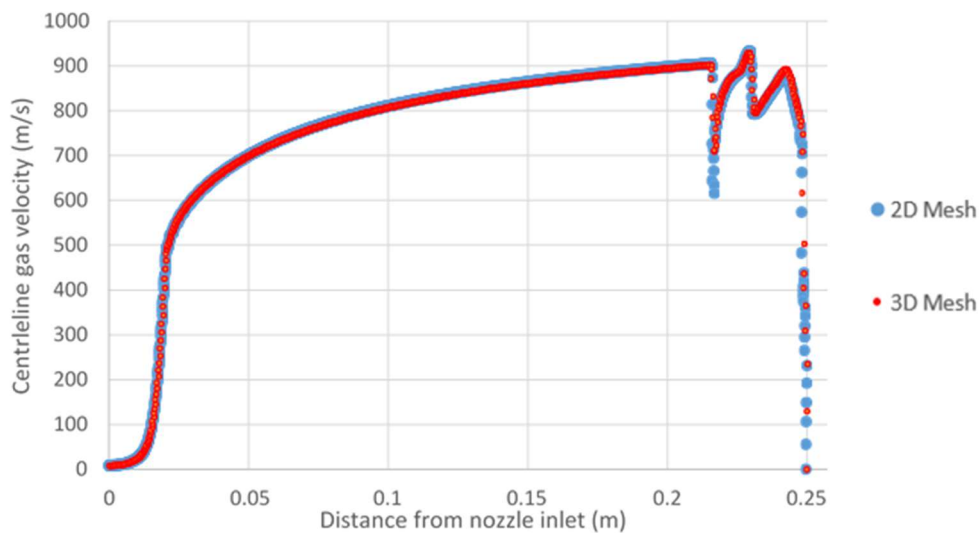
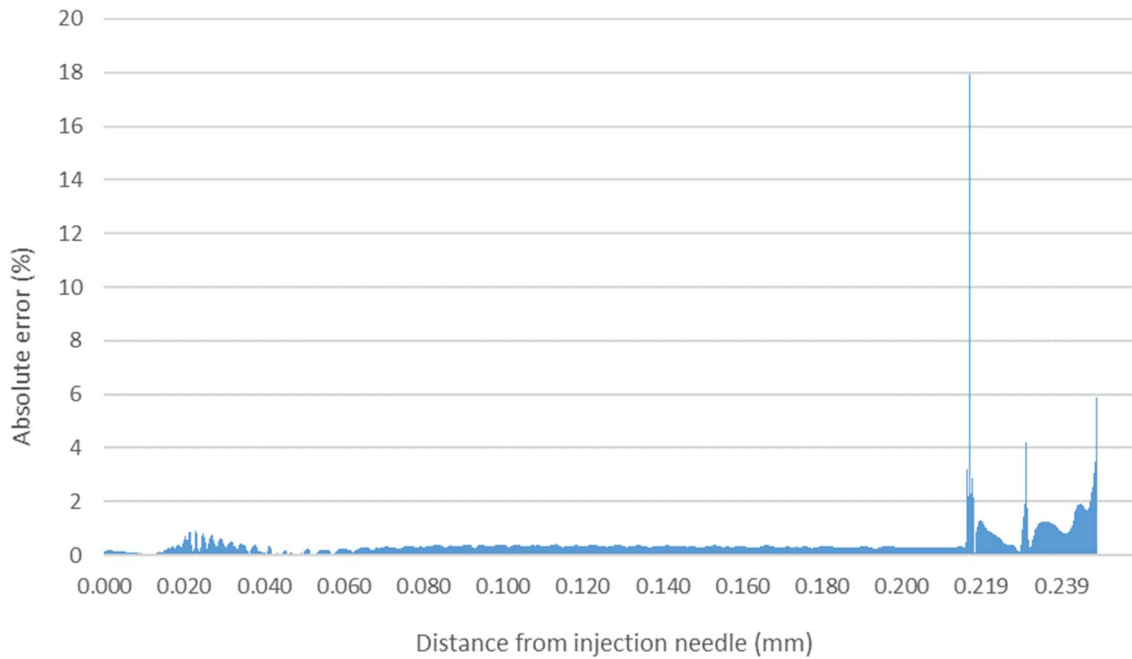


Figure 66 – Centreline gas velocity comparison of 2D and 3D FLUENT models

The mean absolute difference in values along the centreline between the two models is 0.26%, seen in Figure 67. As the two-dimensional model was provided a level of validation by comparison with literature, the correlation here suggests that the three-dimensional model is also an acceptable

representation of the real-world scenario, and that the modelling parameters have been appropriately selected. The measurements which show larger disparities are found in areas where the gas velocity is rapidly changing after the exhaust. The disparity between measurements is likely to be due to the different size of mesh between 2d and 3d models creating marginal short length differences between the models.



*Figure 67 – Absolute percentage difference between 2D and 3D models*

## **5.6. Three-dimensional obstacle addition**

Once satisfied with the construction of the three-dimensional model, obstacles were added into the gas stream geometry between the nozzle exhaust and model's substrate, and the model was re-meshed. These obstacles were aligned to have the face of the obstacle in line with axis of the nozzle. Initially a large block obstacle was tested to represent the flat-topped backstops used in Section 4.4, and subsequently a thin flow separator as used in Section 4.5, the velocity magnitude results of which are displayed in Figure 68 below. Models were tested across a range of obstacle heights, with the alteration to the gas structure shifting with the top edge of the tool, but the shape of the disturbance remained consistent.

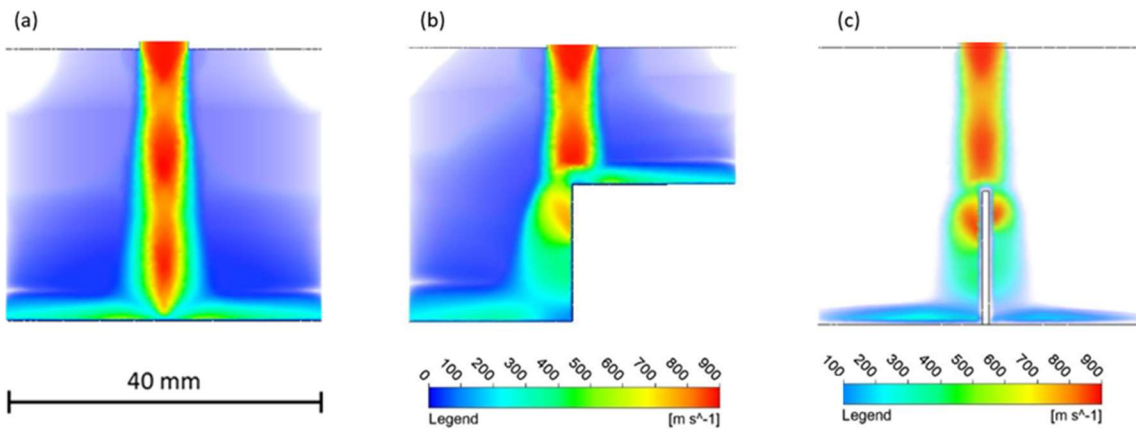


Figure 68 – Gas structure at the central plane of 3D model showing gas velocity magnitudes with (a) no obstacle, (b) with 19 mm backstop, and (c) with 19 mm flow separator

As can be seen in Figure 68, the generated gas structure and velocity magnitudes are identical in all cases up to the first 15 mm from the nozzle exhaust. The model with the backstop appears to have a larger subsonic section around the corner at the top surface, though the flow along the face of the tool remains supersonic as seen from the flow lines in Figure 69, between 400 and 800 m/s, for the majority of the distance to the substrate, for both backstop and flow separator. These speeds are higher than the expected particle velocities at this point, so should not cause any deceleration of the particles.

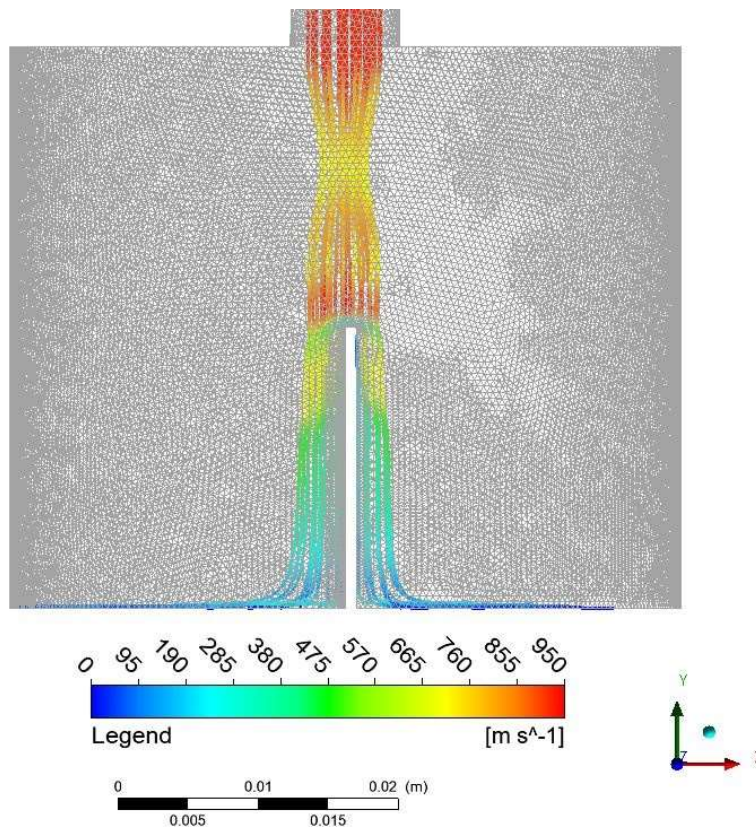


Figure 69 - Gas flow lines around flow separator

This subsonic regions at the backstop corner and top of the flow separator are of similar size to the subsonic region formed under the substrate bow shock in substrate only deposition, which itself is not sufficient to prevent deposition nor deflect the particles. At this point the particles will already be travelling at over 95% of its maximum achievable velocity in an open exhaust environment.

The observations made at this point made it unlikely that the gas flow structure around the various obstacles, being of comparable velocity to the particles and similar size to existing structures, would cause any significant difference in particle trajectory from their original paths.

Despite this, flow separators were also modelled at different heights to attempt to find the smallest disturbance to the gas flow structure, and therefore minimise any affects from unknown variables. As can be seen from Figure 70, and as would be expected, the shorter the flow separator, the smaller the difference from the original gas structure seen in (a). As the gas structure at 19 mm was still reasonably unaltered, this height was chosen as it allowed for a greater height of deposit to be built for our sample investigation.

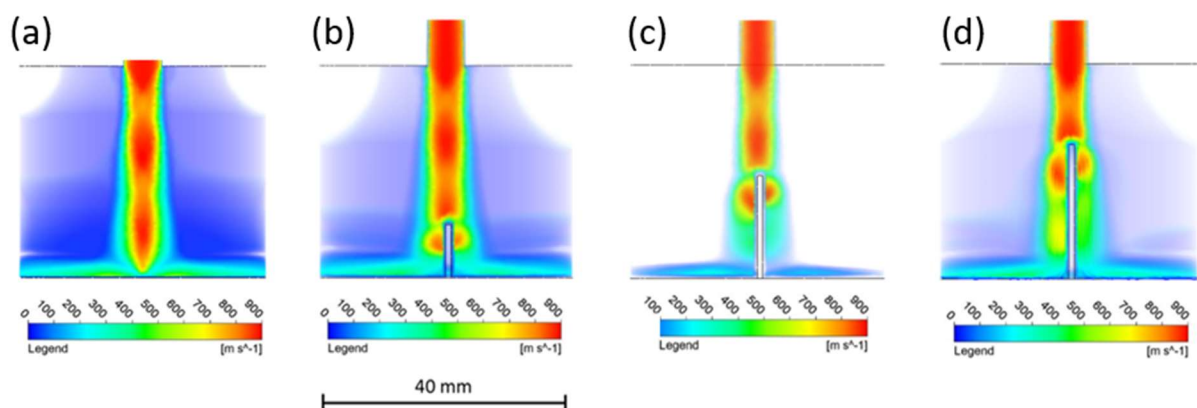
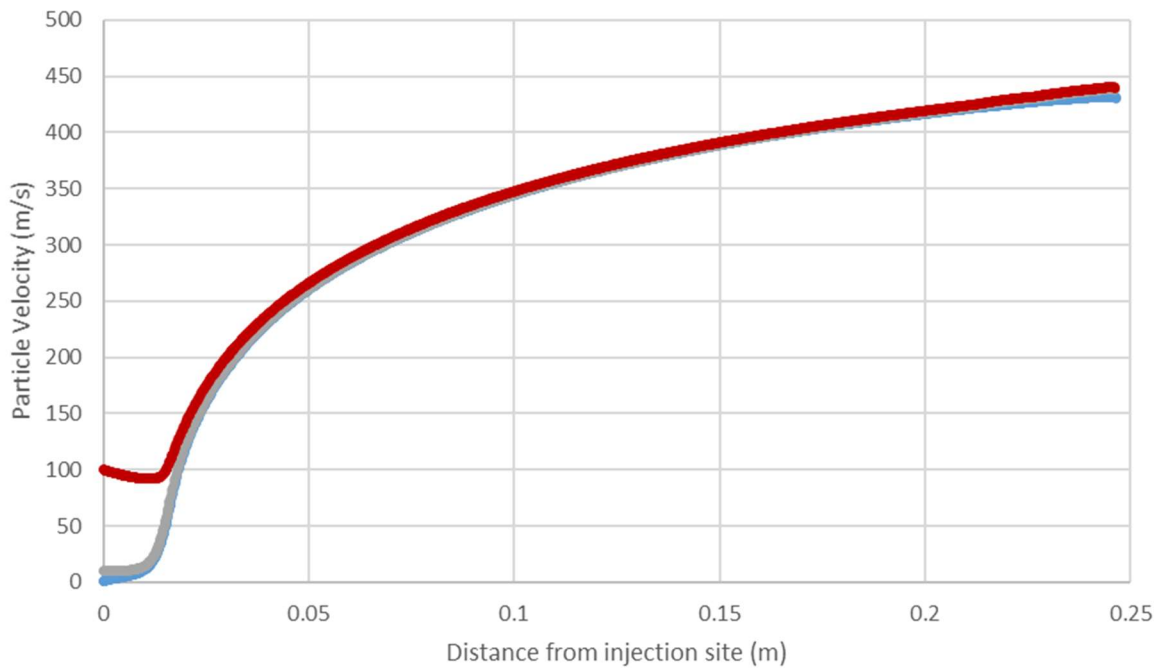


Figure 70 – Simulations of (a) nozzle and substrate at 40 mm stand-off distance, plus added flow separators at (b) 10 mm, (c) 19 mm and (d) 28 mm.

## 5.7. Particle tracking results

After establishment of the gas model was complete, the tracking of particle velocity and trajectory was added to the model as described in Section 5.2.4.2. The initial particle velocity is calculated to be 100 m/s determined from the recorded gas flow through the powder feeder. At this point the powder has been entrained in the gas jet from the powder feeder for long enough to be travelling at approximately the same speed as the gas at the exhaust of the needle, which enters the nozzle 5 mm from the nozzle entrance, leaving it 15 mm short of the throat. Though the initial particle velocity from the powder injection needle was calculated to be 100 m/s, the particle velocity and trajectory were calculated from the models using initial particle velocities of 1, 10 and 100 m/s to note any differences

and to account for errors in calculation of gas velocity and potential slower particles of greater mass or from needle collision, and the resulting differences in exit velocity from the nozzle were less than 3%, as can be seen in Figure 71.



*Figure 71 - Particle velocities calculated from differing initial velocities*

It had been expected that the particles would deflect significantly when they passed through the shock formations formed over the substrate. Arrays of particles were launched from the location of the injection needle tip, with stochastic direction variation, into the simulated gas structures developed in Section 5.6. The horizontal displacement from the centreline was plotted against the distance travelled along the centreline, an example graph of which can be seen in Figure 72. What was found was that the particles are travelling at a high enough velocity when they exit the nozzle, and therefore with so much momentum, that their trajectory remains relatively unaffected by the differing shock structures which they may pass through.

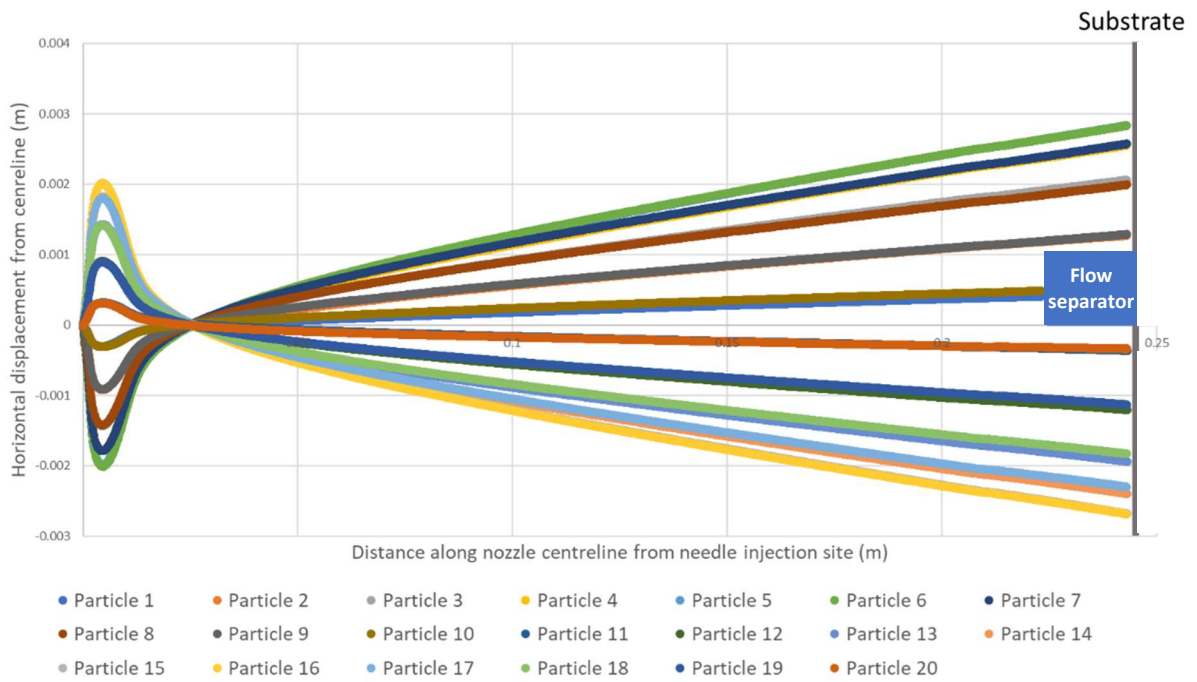


Figure 72 – Simulated 40-micron diameter particle trajectory past a 20 mm tall, 1 mm thick flow separator

Those passing more centrally also pass through more normally to the shock boundary, making it even less likely to deflect, as seen in Figure 73 by the increasing deflection as we move away from the backstop face at the axis.

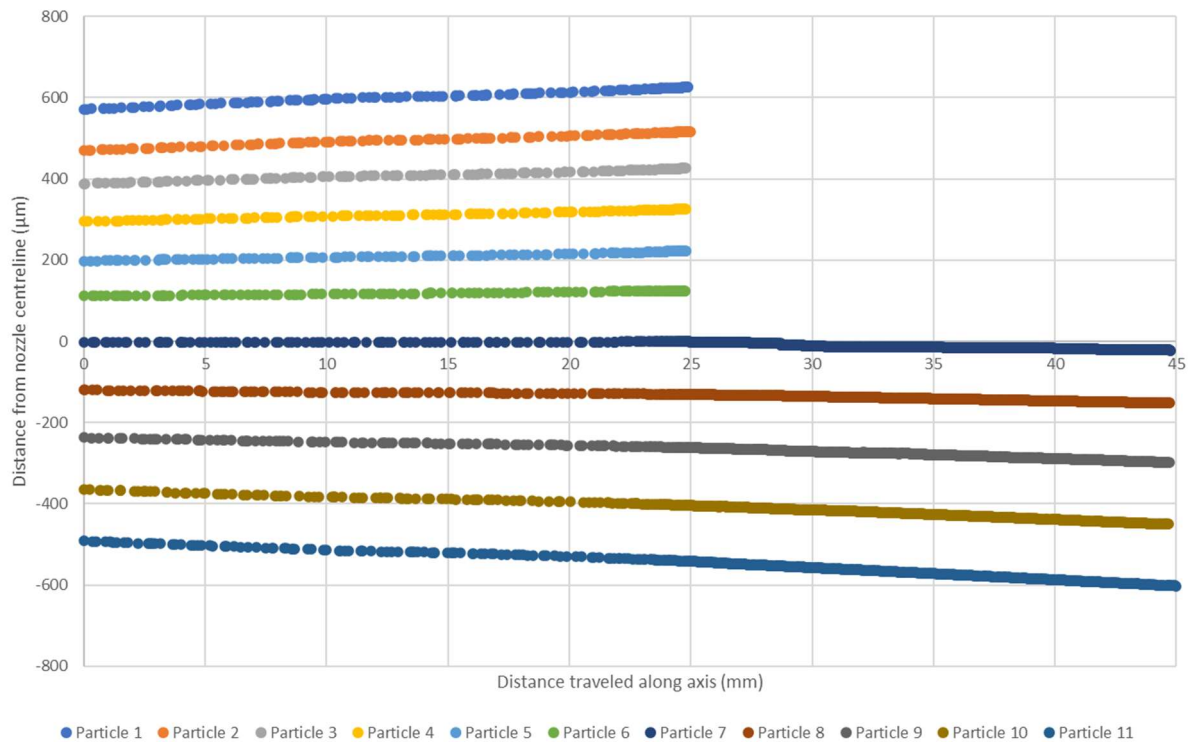


Figure 73 – Simulated 40-micron diameter particle trajectory from the nozzle exhaust, past a 20 mm tall backstop

The minimal deflection that is noted when compared to the standard, unobstructed flow, of 12 – 40 microns, is not significant enough to explain the irregularities caused when depositing with a backstop, especially as the model suggests that the resulting deflections should be no different to depositing alongside a flow separator. From this, it is unclear how great of a deflection of powder particles would cause the prevention of satisfactory deposition adjacent to the face of a flow separator or backstop.

At this point a calculation was made to determine the theoretical maximum force that could be acting on the particle due to the pressure gradient in the period that it passes the wall, and the maximum theoretical deflection that this would cause from the particle's original trajectory.

The deflection was calculated with the worst-case scenario in mind. The pressure gradient used represent the highest observed adverse gauge pressure gradient, as shown in the pressure maps in Figure 74. The maximum deflection was calculated as 16  $\mu\text{m}$ , as shown in Appendix A.

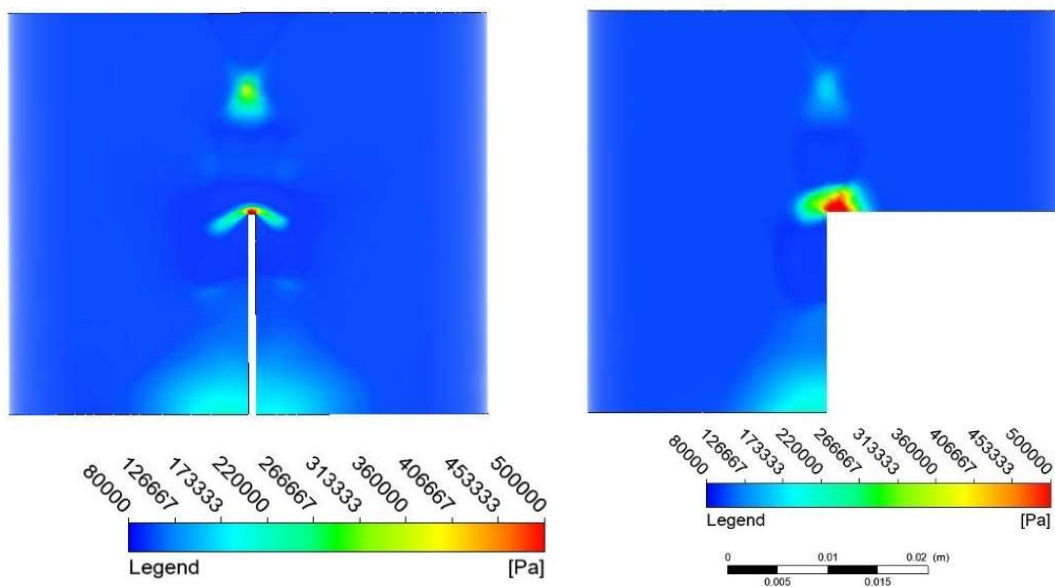


Figure 74 - Pressure maps for flow separator and backstop FLUENT models

After noting the lack of effect on the particles, previous work was further examined to see if anything could be learned. In the examined literature where the nozzle has been slotted, in Section 2.9.2.4, the spot width changed only from roughly 10 mm to roughly 12 mm, despite the allowance of rapid sideways expansion much farther up the nozzle [55].

That equates to 1 mm additional radial spread of the smallest particles at the nozzle's edge from the deposition centre, across a 60 mm travel to the substrate, when the gas is allowed to expand into free air. It is therefore understandable that the deflection caused by obstacle interference at the centre of the gas stream, when only 20 mm above the substrate in the centre of the gas stream would cause less displacement of the powder from its trajectory.

## 5.8. Confirmatory literature on particle trajectory models

Since conducting these simulations, Klinkov et al have published a paper on coating formation while spraying past a wire of 1 mm thickness, demonstrating using “three-exposition shadow flight-time method” that the powder particles are not greatly deflected by the shockwave, but do bounce off the wire [129].

Mean velocity and angle of approach before the shock region and after are shown in Table 7 from the paper in question. The copper and aluminium particles used in these experiments had average diameters of 60 and 30 microns respectively, so of a similar size to the particles used in the experiments contained within this thesis. As is noted in the study, the difference between particle speeds before and after the wire is negligible, with a maximum 3.2% between the mean values, and the difference in angles of 0.2 – 0.3 degrees.

*Table 7 – Particle trajectory parameters measured during shockwave interaction by Klinkov et al. [129]*

Position	Parameters	Al		Cu	
		$m$	$\sigma$	$m$	$\sigma$
Incoming	$v_p$ , m/s	394±4.6	28	371.5±2.3	30.7
	$\alpha_p$ , deg	1.65±0.31	1.9	1.96±0.11	1.48
Passing	$v_p$ , m/s	388±1.4	32.6	363±0.9	32.9
	$\alpha_p$ , deg	2.03±0.09	2.16	2.2±0.04	1.6
Rebounded	$v_p$ , m/s	165.5±6.2	45.5	196±3.2	57.4
	$\alpha_p$ , deg	42.2±2.2	16.2	42±0.8	14
	$v_{py}$ , m/s	106.5±6.4	47.5	121±2.0	35.8

It was concluded that the only significant effect on the particle flow from the masking structure is from direct collision of the particles into the mask, and that the shock structures around the mask have a negligible effect in altering the speed or trajectory of the particles greater than 1  $\mu\text{m}$  in diameter.

If these deflections are applied to the flow separator case, the likely displacement of the particles from the surface of the flow separator can be calculated. The leading edge of the flow separator should form a similar shock structure to that of a wire of similar thickness, 1 mm in this case.

A particle arriving before the shock being normal to the substrate and targeting the interface between the substrate and flow separator, could deflect up to a maximum of 0.3 degrees off from this trajectory, shown in Figure 75. At 20 mm height above the substrate, that would create a maximum displacement of 105 microns, a result consistent with that simulated and calculated in Section 5.7.

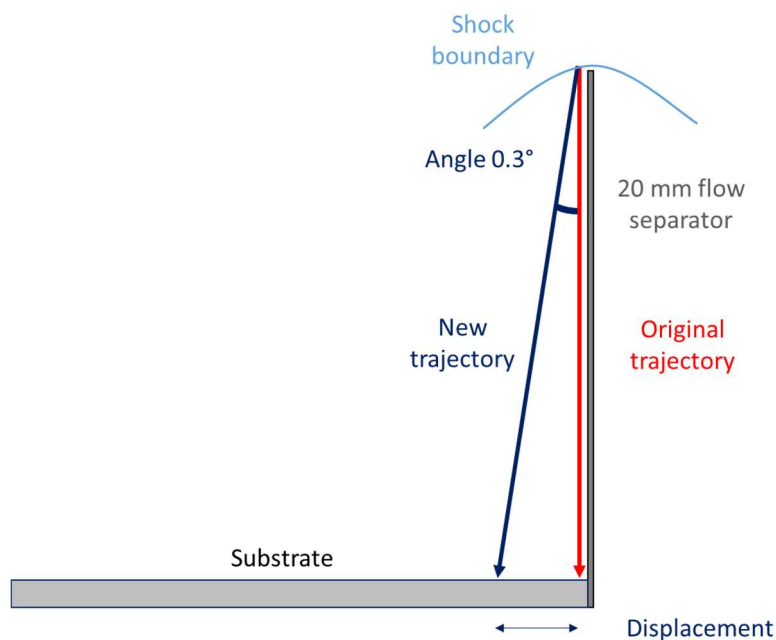


Figure 75 – Mean displacement of particle from original trajectory

## 5.9. Summary

At the outset of this work it was expected that the shock structures formed around the various shaping mechanisms would cause the powder particles to be deflected from their trajectories. The simulations presented in this chapter were designed to investigate the different occurring shock patterns, the gas velocities surrounding these shaping tools, and how this affected the particle trajectory.

Two- and three-dimensional models of the cold spray system at the IfM were created using ANSYS Fluent, including nozzles and exhaust regions for the purposes of gas velocity monitoring and shock structure visualisation. Subsequently, substrates and deposit shaping obstacles were introduced into

the exhaust region, and particle tracking was added to the model to determine how these obstacles would affect particle trajectory throughout the system.

Particle tracking showed the gas structure surrounding the substrate to have little impact upon the trajectory of the powder particles at this point. This should perhaps have been the more likely outcome, as particles are noted to have previously been able to reach the substrate in a satisfactory manner while passing through the diamond shocks that exist from the nozzle exhaust when there is no obstacle present, and the bow shock that exists over the substrate. If they are not significantly deflected by these structures then it is reasonable to assume that they would not be significantly affected by a minor alteration of these structures by the addition of obstacles into the flow, other than by collision with said obstacles.

As these simulations were conducted in parallel with experimentation, a number of design choices for experimental progression are noted in the Chapter 4 to have been made with the notion of minimising the effects on gas structure. Whilst it has now been demonstrated that this is likely to have been unnecessary, it remains good practice to maintain as consistent a set of variables as is possible to eliminate potential causes for disruption.

With the knowledge of the shock structures having minimal effect on the particle trajectory, an alternative cause for the inconsistent deposition from some shaping mechanisms, in Section 4.4, could be sought in the future work detailed in Section 7.3. As these inconsistencies did not continue to be a factor when using the thinner, flow-separator tools of the same height, it could be accepted that there was a short-term random unknown variable, perhaps concerning nozzle-flow separator alignment, that affected the deposition on this occasion, and that it may not be worth pursuing for future development of a capable system as the backstop was not determined to be the most appropriate method for other, additional reasons.



---

# Chapter 6 - Progression of structural control

---

## 6.1. Introduction

After successfully achieving control of the deposition structuring mechanism using copper, several further avenues of investigation were pursued to examine the capabilities of the system and assess the viability of progressing towards an industrial system. To this end, it was important to ensure that the process was not limited by material choice, nor disrupted by the addition of a laser interaction for substrate pre-heating. Once that had been established, structures of increased complexity were attempted to develop the system's capability.

## 6.2. Flow separator height

The flow separator height had been maintained at 19 mm throughout the trials in Section 4.5, resulting in successful deposition. To further test the effect of flow separator height on the deposited surface, a flow separator with constantly sloped edge was created with height from 2 to 24 mm above the substrate.

As can be seen from *Figure 76*, the height of the deposit was reasonably consistent across the range of flow separator height, with a flat, vertical deposit face being consistently created. The minor height variations of the deposit formed can be accounted for by the unevenness in the powder feed rate. The surface roughness and density of the sample was consistent along its length.

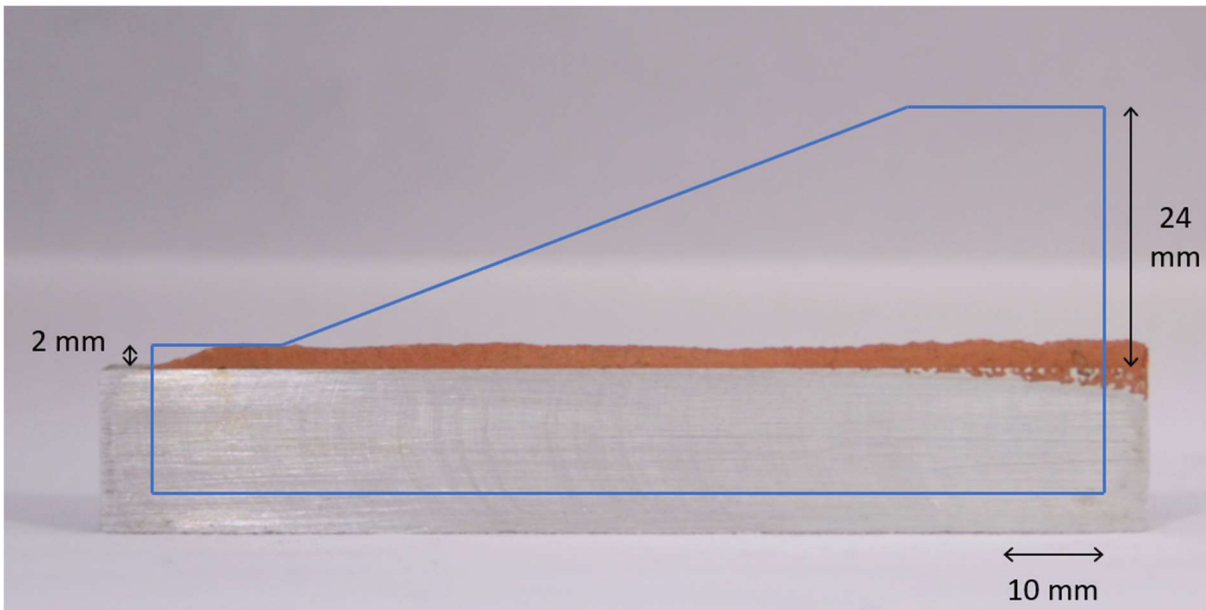


*Figure 76 – Single track, single layer deposit with variable height flow separator at 5 mm/s (Flow separator outline drawn in)*

The consistency of deposition height despite varying flow separator height may prove a useful feature for the deposition of consistently shaped surfaces as it will allow a larger separator to be positioned a single time and deposited against, rather than a smaller separator repeatedly requiring repositioning which may increase build time and decrease accuracy.

In future experiments, the initial backstop height was fixed at 19 mm above the substrate, as it was for the previous copper experiments to maintain a consistent experimental setup. This height places the top of the flow separator below the point of a diamond in the exhaust shock profile, as has been calculated in the simulations in Chapter 5 and measured experimentally in literature [128]. This is the location at which the gas flow is already beginning to expand again, so the intention is to minimise the disturbance to the shock structure, gas flow and powder trajectory.

### **6.3. Material investigation**

Following the successful construction of flat, vertical copper surfaces in the Chapter 4, the method required testing with alternate materials to verify that the noted shaping effects were not material dependent.

Titanium and steel (316L) were chosen as test materials in addition to the already demonstrated copper, as these represented a range of material properties, displayed in Table 8.

Table 8 – Material properties of test powders, from manufacturer data sheet

Material	Copper	Titanium (grade 2)	Steel (316L)
Hardness (Rockwell B)	55	98	81
Density (kg/m <sup>3</sup> )	8960	4510	8000
Yield strength (MPa)	320	400	205
Modulus of Elasticity (GPa)	110	105	193

These materials were trialed using the flow separator in the same experimental setup as in Section 4.5, with parameters as detailed in Table 9.

Table 9 - Parameters for deposition

Variable	Setting
Powder	Copper: - 38 + 15 $\mu\text{m}$ Titanium: - 45 $\mu\text{m}$ Steel (316L): 20-63 $\mu\text{m}$
Powder feed rate	20 cm <sup>3</sup> /min
Substrate	Aluminium – 12 mm thick plate
Gas Temperature	300 °C – Cu, Al, Ti 500 °C – Steel 316L
Gauge pressure	30 bar
Traverse rates	3.75, 5, 7.5, 15, 25 mm/s (plus 50, 100 for copper)
Flow separator Surface Roughness	26 nm

### 6.3.1. Copper

Having passed the initial success criteria for creating a defined cold spray deposit by the level of shaping control, the copper samples described in Section 4.5, shown again in Figure 77, were analysed to determine their quality, through analysis of the achieved surface roughness, build height and density.

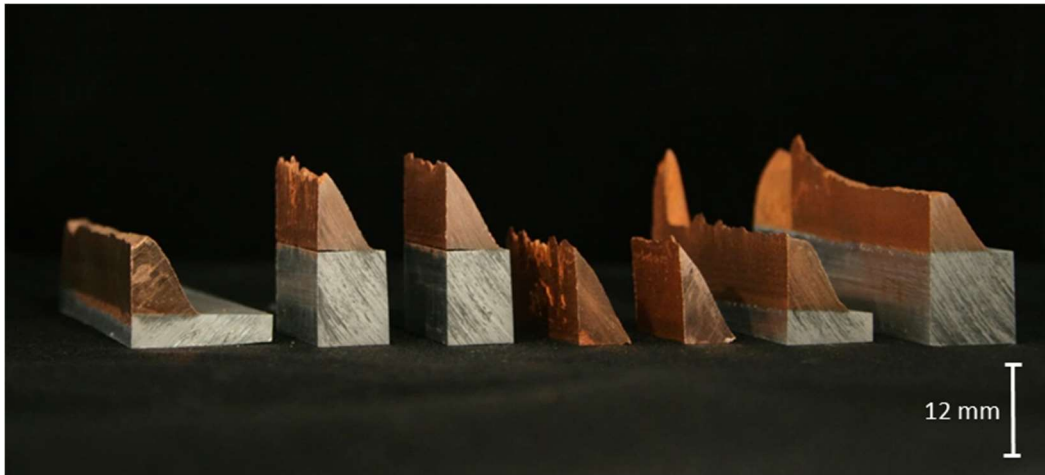


Figure 77 - Copper deposition cross sections [3, 3.75, 7.5, 15, 25, 50, 100 mm/s]

As is the case with standard, unrestricted cold spray deposition, the deposited layer height decreases with increasing traverse rate, as would be expecting from there being a lower volume of powder impacting per unit length of deposit. Subsequent layering of the same track causes the same final height to be built as a function of time. For example, a single track at 10 mm/s will be the same height as two layers at 5 mm/s. However, once parallel, overlapping adjacent tracks are deposited, the surface upon which the subsequent layers will be impacting will be changed, and so those with higher traverse rates may expect to build taller on average for the same deposition time.

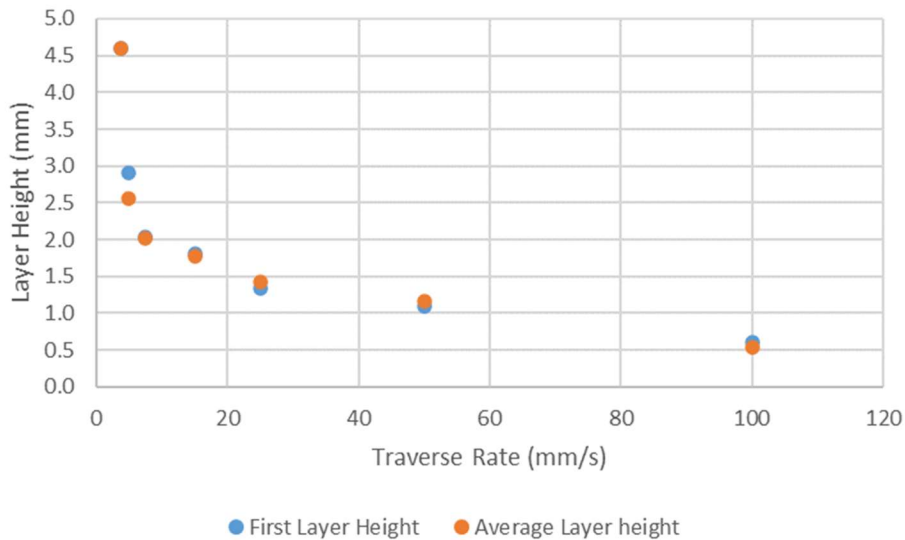
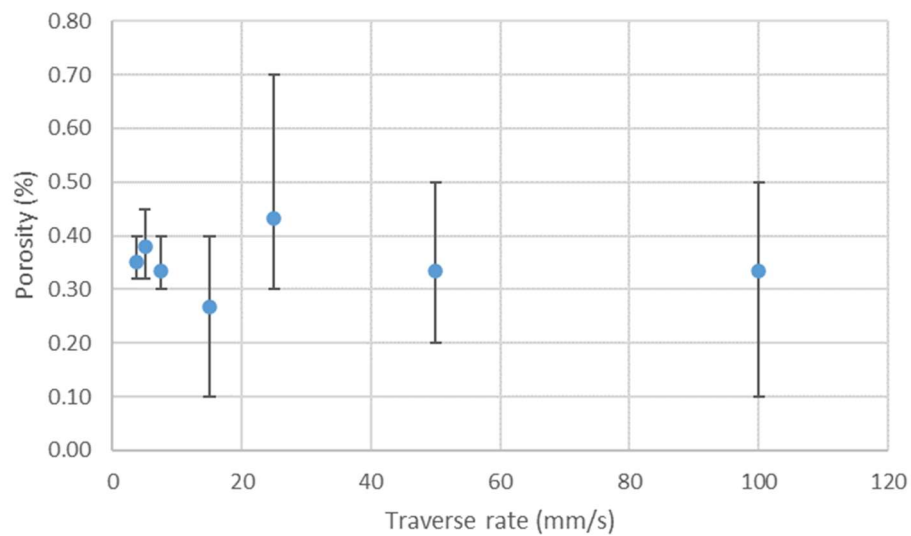


Figure 78 – Copper layer build height vs traverse rate

The average measured density of the copper cold spray deposits while depositing adjacent to the flow separator was 99.7%, with the porosity measurements shown in Figure 79. This is comparable to standard cold spray deposition of copper powder, typically achieving results of 99% and higher, showing that the density of the deposits has not been adversely affected by the presence of the flow

separator. With the development of optimisation experiments to determine the best parameters, including traverse rates, gas temperatures, and offsets, the density could likely be improved further to create near fully dense components.



*Figure 79 - Copper porosity vs traverse rate*

It was initially theorised that there may be a difference in porosity between the bulk sections of the deposit and the area within a few particle diameters of the surface for the deposit, as those impacting in the surface region may be inhibited in their deformation by the flow separator or uncleared powder particles trapped between the deposit and the flow separator surface. This would require components with tight tolerances to be made a few hundred microns oversize, and in need of slightly more rigorous finishing operations. Whilst this would not present a particular problem when machining copper, this could prove more problematic when working with materials that are more difficult to machine.

Figure 80 shows one of the images taken during density measurements of these copper trials, showing no discernible difference in porosity between the bulk sections of the deposit away from the flow separator, and near surface sections, both repeatedly measuring  $99.7 \pm 0.15$  % density in all samples. The surface built adjacent to the flow separator for this sample was at the copper-resin boundary in the image below, which also gives an indication of the flatness of the achieved surface.

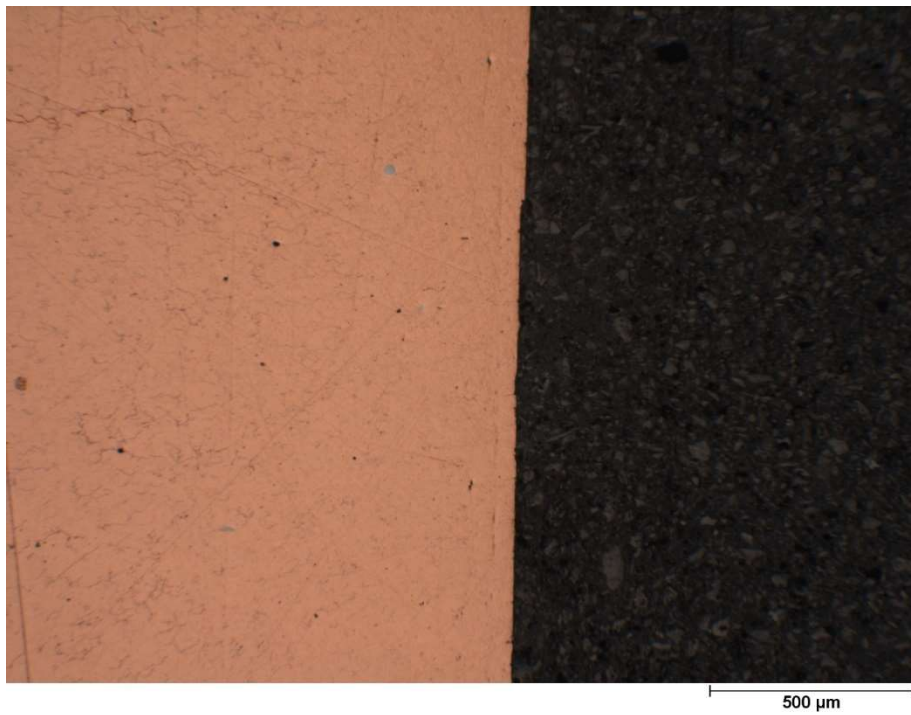


*Figure 80 – Microscope image showing surface and bulk density, 500 micron scale represents approximately 10-15 particle diameters*

Having decided to align the nozzle centrally with the tool face after the mask trials in Section 4.3, a further test was devised to investigate how the deposition shape was affected by the nozzle-flow separator alignment. This was done by traversing the nozzle diagonally across the flow separator while the powder spray was active. The nozzle was moved to deposit a track of 50 mm length parallel to the flow separator face at 5 mm/s, whilst moving 10 mm perpendicular to the face of the flow separator.

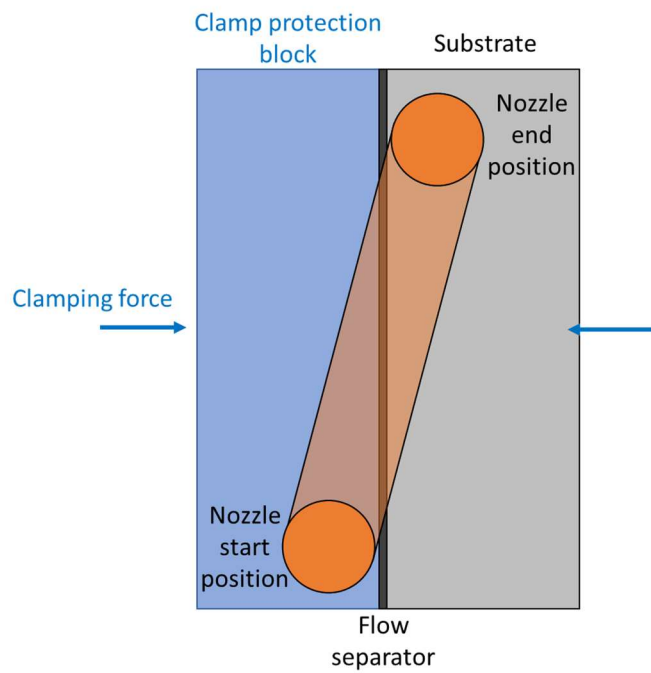


Figure 81 - Nozzle path diagram for diagonal height

The deposit that formed, shown in Figure 82, had a defined surface across the full range of alignment position, until the deposit was no longer forming adjacent to the flow separator, showing that perfect alignment of the nozzle's central axis with the face of the flow separator is not critical to the formation of a flat surface. However, the maximum height of copper deposited still occurred as the nozzle was centrally aligned with the face of the shaping tool, and ideally will be positioned no further than that halfway point to ensure that the tallest deposition occurs adjacent to the flow separator. This experiment also proved that the nozzle does not need to be pre-aligned with the flow separator before spraying commences, but can be brought into position over the separator with powder already flowing without detrimentally affecting the shaping capabilities.



Figure 82 - Copper diagonal test

### 6.3.2. Titanium

The second material to be explored was titanium, as titanium and its alloys are materials commonly available for metal additive manufacturing systems, and have uses in a wide range of applications from aerospace to medical implants and devices.

The powder used for deposition was Titanium Grade 2, - 45  $\mu\text{m}$  nominal size. The experimental setup was identical to that shown in Section 4.5, with the flow separator being clamped to the side of the substrate and the centre of the nozzle aligned at the substrate-flow separator interface.

As can be seen from the build height profile of the surface in Figure 83, the diagonal test of titanium also shows the optimum build height is achieved when the flow separator is aligned with the centre of the nozzle. Similarly to the copper deposition trials, in subsequent deposition experiments, the nozzle was actually aligned centrally with the face of the flow separator, to ensure the peak of the deposition was adjacent to the flow separator to allow for any minor misalignment of clamping and motor axes.

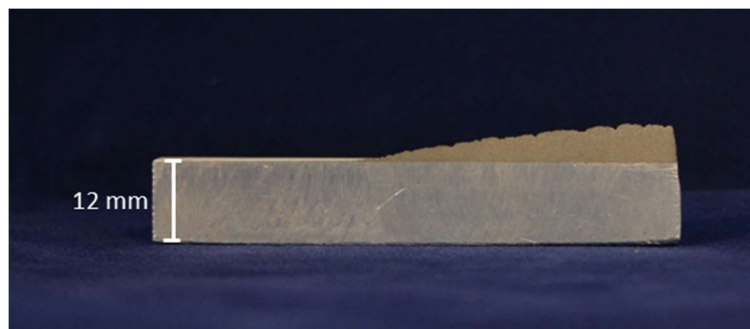


*Figure 83 – Build profile of titanium nozzle alignment test after sectioning at the centre*

The titanium readily deposits onto the substrate in the area immediately adjacent to the flow separator, depositing a flat vertical surface at all traverse rates tested seen in Figure 84. At 3.75 mm/s, the second layer of deposition was inconsistent and resulted in peaks and troughs building upon the first layer. It remains unclear why this occurs at lower traverse rates, as was the case in the copper deposits. One potential cause could be that the powder is able to clear better from the deposition zone at faster traverse rates, as the moving nozzle allows the radial gas jets that form as the gas hits the surface, to move over the area more frequently. Though this does not explain why the inconsistency is only seen on the second layer.

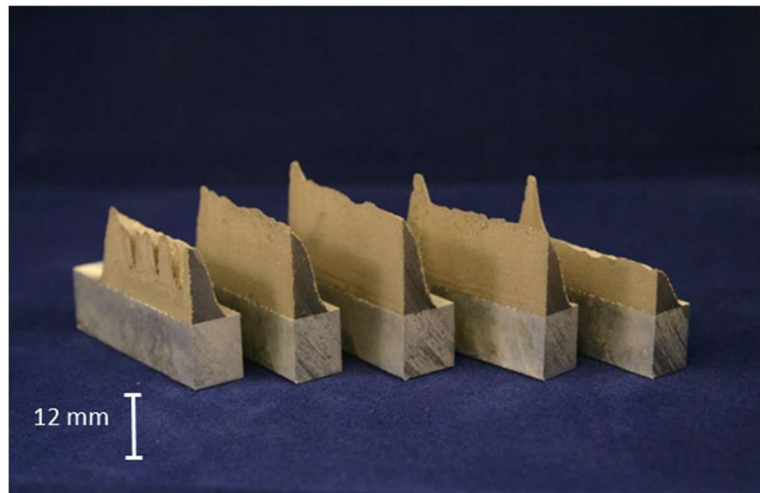


Figure 84 - Titanium deposits adjacent to flow separator at 3.75, 5, 7.5, 15 and 25 mm/s

Variation of the traverse rate did not appear to affect the surface roughness of the created titanium surfaces, seen in Figure 85, though the measured surface roughness for the titanium surfaces was higher than that of copper, at all traverse rates. This may be caused by the relative hardness of the titanium compared to the copper, as the particles deform less on impact, and so do not conform as closely to the surface of the flow separator as the copper particles.

Further development of the deposition parameters, such as increased gas temperature or pressure, and utilisation of the laser should reduce the surface roughness of the created surfaces by allowing the powder particles to deform farther during deposition.

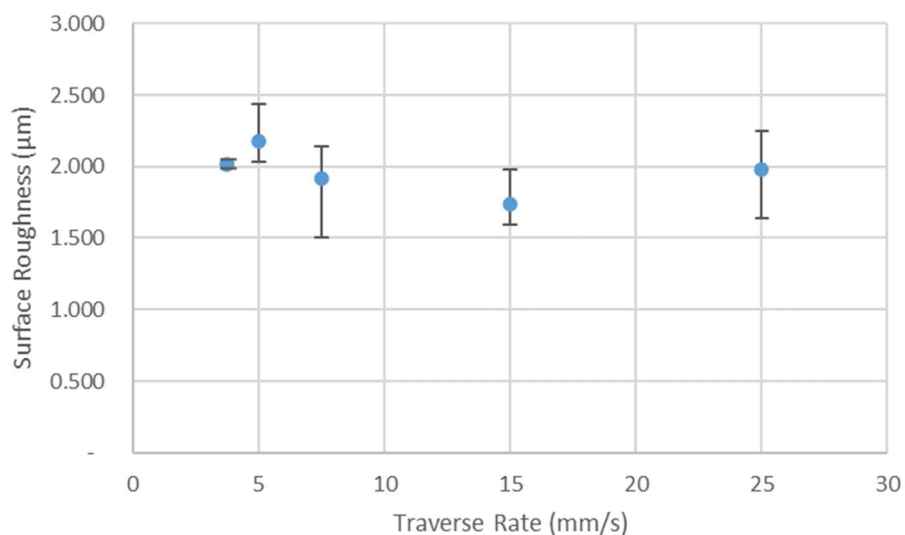


Figure 85 – Titanium deposits surface roughness vs traverse rate

Similarly to the copper deposits, the first layers deposited were marginally larger than subsequent layers causing a lower average layer build height. This was expected as the deposition efficiency of

each layer decreases as the powder is impacting a surface that is increasingly angled from the normal to the powder trajectory.

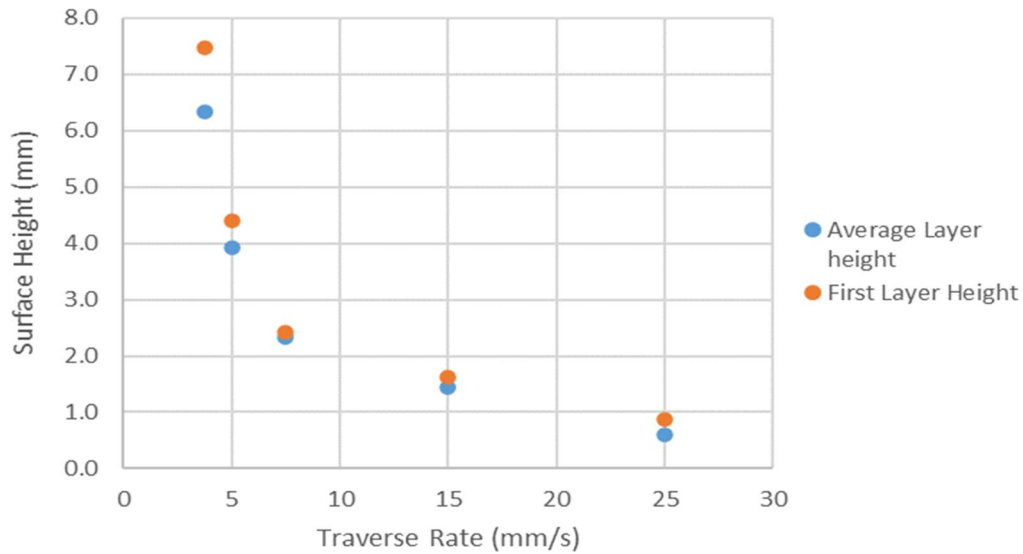


Figure 86 - Surface height vs traverse rate for Ti deposit

Cold spray deposition is capable of achieving titanium deposition with porosity as low as 0.2% when in a high pressure and high temperature system, but depending on coating requirement and optimisation can vary from 0.2 – 20 % [130]. As can be seen from Figure 87, the titanium experiments produced porosity measurements in the 2-3 % range, which is a respectable value for an unoptimized system. A free-standing track built with the same parameters during the same experimental trails was measured at 2.1 % porosity, indicating that the shaping method is having little impact on the porosity of the deposit.

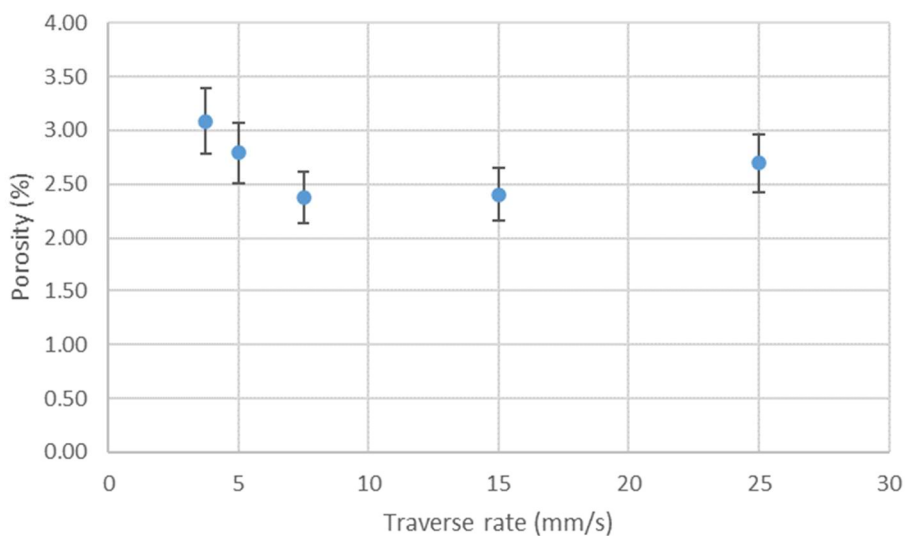


Figure 87 – Titanium sample porosity vs nozzle traverse rates

### 6.3.3. Stainless steel (316L)

As another commonly utilised engineering material, and a material often utilised by other additive manufacturing systems, stainless steel was chosen as the third test material. Specifically, 316L was chosen as it has previously been successfully deposited via cold spray.

As steel does not deposit readily at 300°C, building thin layers with a low deposition efficiency, the gas temperature for this test was raised to 500°C. This provided an opportunity to test whether the temperature of the cold spray carrier gas would affect the deposition capability.

As has come to be expected from the previously deposited materials, the alignment height test shows that the tallest build height for the vertical near wall section is when the nozzle is centrally aligned with the flow separator, as shown in Figure 88.



*Figure 88 – Build profile of steel nozzle alignment test*

The steel deposited adjacent to the flow separator at all traverse rates, conforming to the shape of the separator to create a flat vertical surface, shown in Figure 89. Raising the gas temperature to 500°C does not appear to have caused any adverse effects on the shaping capability of the system, nor caused any adherence of the deposit to the flow separator.

It is notable that the steel deposition did not produce the inconsistencies in deposit that were seen in the copper and titanium trails at the lowest traverse rate. The higher gas temperature will have created higher gas and subsequently powder velocities, perhaps mitigating the effect that was disrupting the powder deposition at slow traverse rates in other materials.

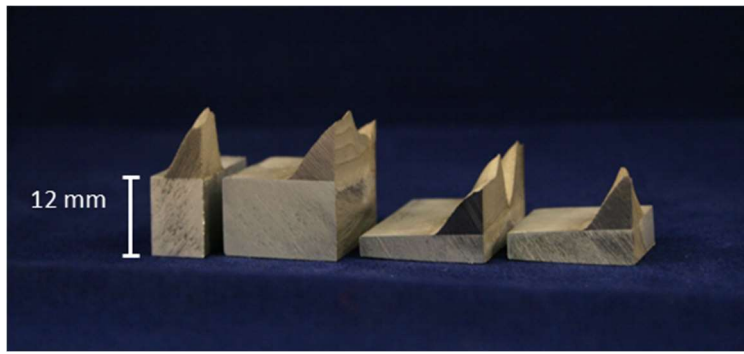


Figure 89 - Steel deposits, cross sectioned to display surface profile, at 3.75, 7.5, 15 and 25 mm/s

The steel deposition achieved sub-micron surface roughness (Ra) at all traverse rates. There are not enough data points to conclude if there is a trend in surface roughness when compared to traverse rate, but a reason for one is not readily apparent, allowing an assumption that similarly to the other materials, there is no effect.

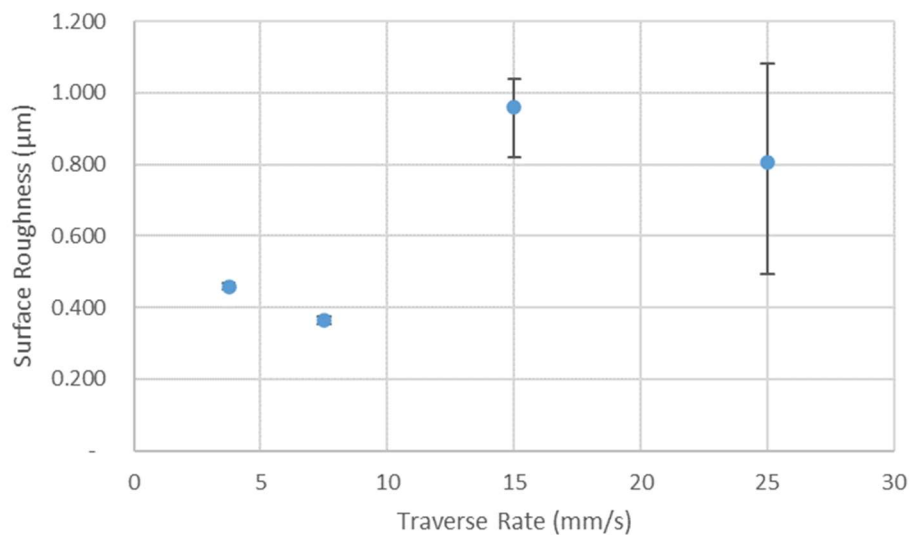


Figure 90 – Steel surface finish vs traverse rate

As with copper and titanium, the first layers of steel deposit were higher than the average layer height. The difference in the slowest traverse rate of 3.75 mm/s is minimal, as only 2 layers were deposited, skewing the average. The difference in the fastest traverse rate is also minimal, skewed as the first layers would not significantly alter the normalcy of the substrate from the powder trajectory, allowing a number of initial layers to measure similarly.

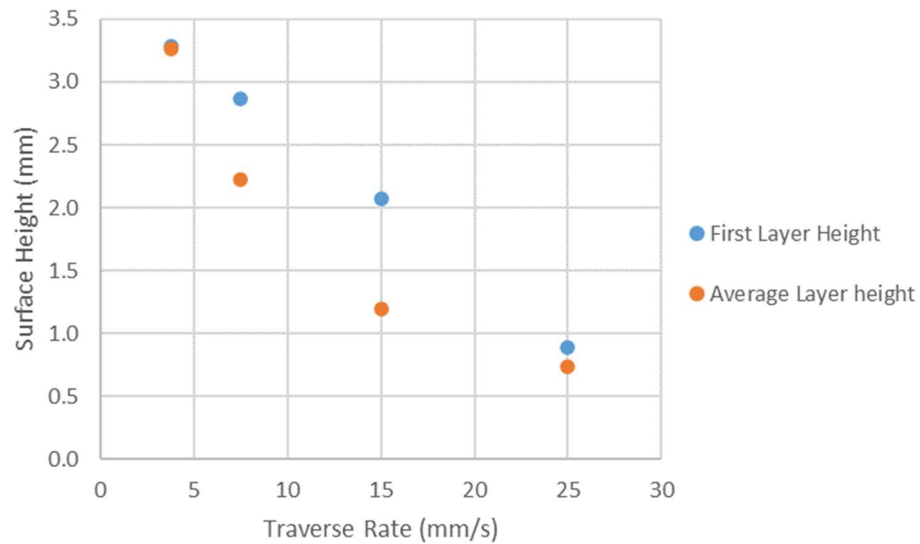


Figure 91 – Steel layer height vs traverse rate

The steel deposits proved more porous than both the copper and titanium deposition, shown in Figure 92, caused by the increased hardness of the steel powder particles and the lack of optimisation of the process, giving an average density of approximately 97%. Increased gas speeds from higher gas temperatures or alternative carrier gases, and increased particle temperature from a preheating stage, would allow reduction of the porosity of the deposition to that measured in standard cold spray deposits.

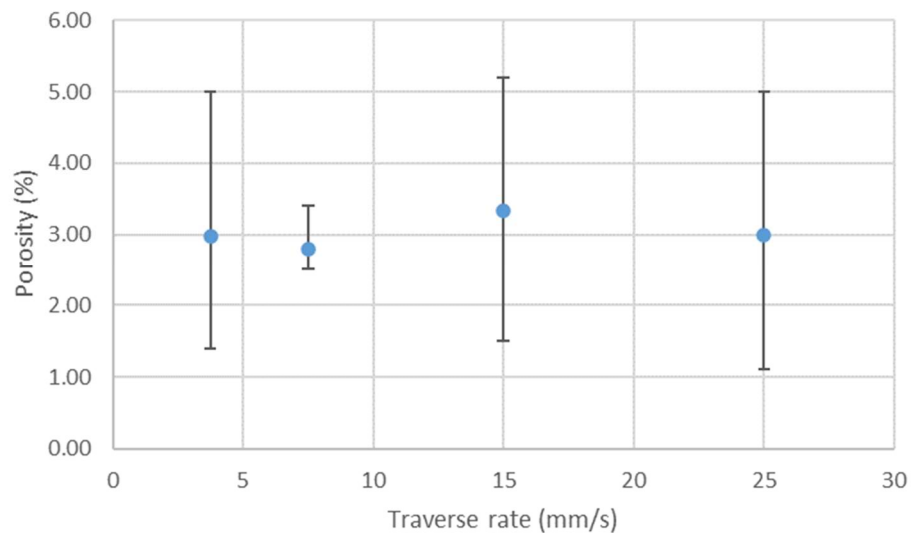


Figure 92 - Steel samples porosity vs traverse rate

## 6.4. Supersonic laser deposition

As the creation of definable surfaces has now been achieved using cold dynamic gas spraying without the use of a laser in the previous chapter and the previous sections of this chapter, the purpose of this

section is to examine whether the application of laser has any adverse effects on this capability. As mentioned in Section 3.3.4, the laser intensity at this spot size is in the heating range for materials used, not enough to cause melting.

Typically, literature shows that the addition of laser substrate heating to the cold spray process can give a variety of process benefits and increase the available material pool for deposition, as detailed in Section 2.11. As the flow separator does not interfere with the laser-substrate interaction, it was not expected to alter the deposition in any way other than that which is observed during standard supersonic laser deposition, while providing the same benefits over traditional cold spray. It was also not expected that the laser will cause any adherence of the deposit to the flow separator, nor alter the ability to deposit adjacent to a shaping tool.

#### **6.4.1. Titanium without laser vs with laser**

As shown in Section 6.3.2, Grade 2 titanium powder has been proven to successfully deposit at 300 °C adjacent to the flow separator. It has also been previously shown that titanium deposits with improved properties when utilising a laser substrate heating stage, compared to standard cold spray properties, noted in Section 2.11. Deposition of this powder was attempted with the flow separator in the same configuration as the titanium deposits in Section 6.3.2, to allow a direct comparison to the previous deposit, with the laser substrate heating. The traverse rate used was 15 mm/s with laser power of 600 W.

As can be seen in Figure 93, the addition of the laser has not affected the structured deposition of the titanium while using the flow separator. The deposition has still occurred flush to the flow separator without adhering to the face, building a flat surface feature on the adjacent side of the track.

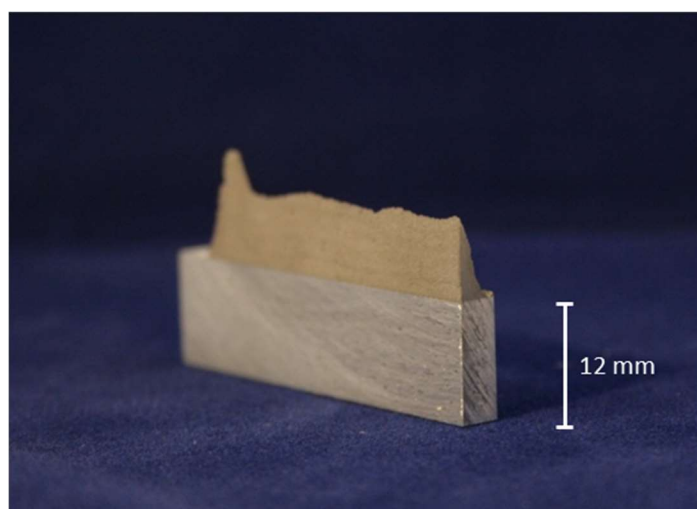


*Figure 93 – Supersonic laser deposition of titanium shaped with flow separator, sectioned to show shape*

Figure 94 below shows the achieved differences in surface roughness, porosity and build height between the previously deposited titanium samples and the titanium sample with laser assistance.

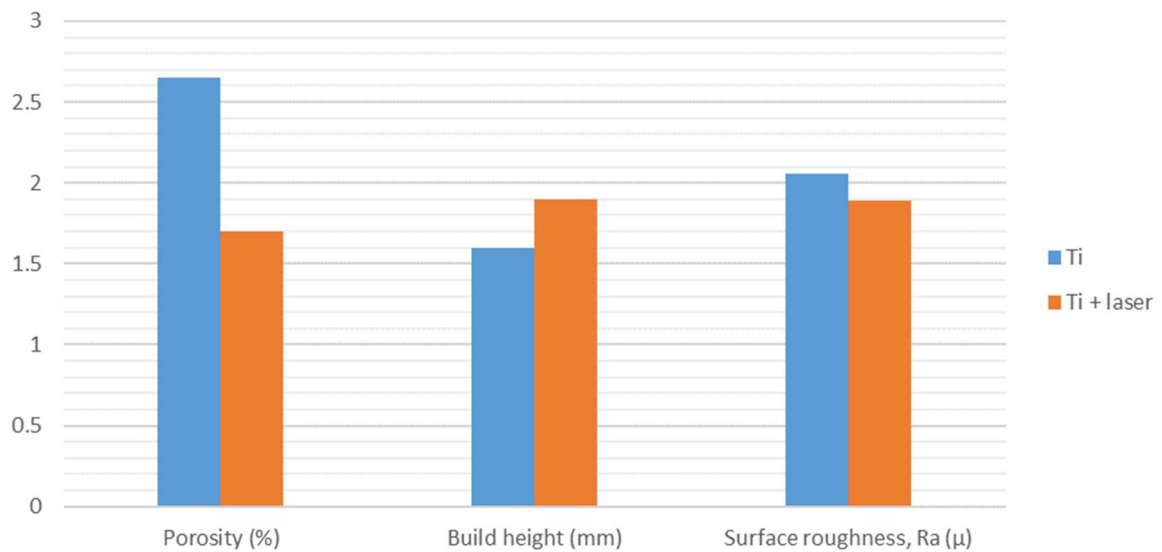


*Figure 94 – Comparison of Ti and Ti + laser assistance for porosity, average build height and surface roughness*

The porosity of the deposit has decreased with the addition of laser irradiation of the substrate due to the increased deformation of the particles and substrate/previous layer, allowing the particles to form a more dense coating as they deform into the available space. The build height of the laser assisted deposition experiment had also increased. Both of these results were to be expected as the addition of a laser assisted heating stage to standard cold spray also provides reduced porosity and increased deposition efficiency, and consequentially build height.

Additionally, the surface roughness of the deposit decreased. This could be due to the particles being more readily able to deform to the surface of the flow separator face, though further work is required to validate this as the measured difference was relatively small.

It appears likely that with optimisation of the laser parameters alongside the other cold spray parameters, an improvement similar to that seen in adding laser assistance to standard cold spray could be seen.

### 6.4.2. Controlled deposition of Stellite 21

Table 10 – Stellite 21 properties

Material	Stellite
Hardness (Rockwell B)	35
Density (kg/m <sup>3</sup> )	8330
Yield strength (MPa)	1050
Modulus of Elasticity (GPa)	245

Certain materials are not capable of being deposited with cold spray alone using this system, and require the addition of laser irradiation of the substrate, as detailed in Section 2.11. It was important to validate that the deposition of these materials was not affected by the addition of the flow separator. The material chosen for this purpose was Stellite 21, which leaves no deposit using the standard IfM cold spray system as the Nitrogen carrier gas does not allow for particle velocities above the critical velocity on a cold substrate, but forms dense coatings with laser irradiation of the substrate.

The laser power for these experiments was set to 1.5 kW, as this had been tested with this system previously for free-standing deposition. The gas temperature was set to 500 °C, the maximum value for the system to create the fastest carrier gas velocity. As can be seen from Figure 95, the deposition was successful and has still built flush to the flow separator. As with the titanium experiments, the laser irradiation has not caused the Stellite to bond to the flow separator.

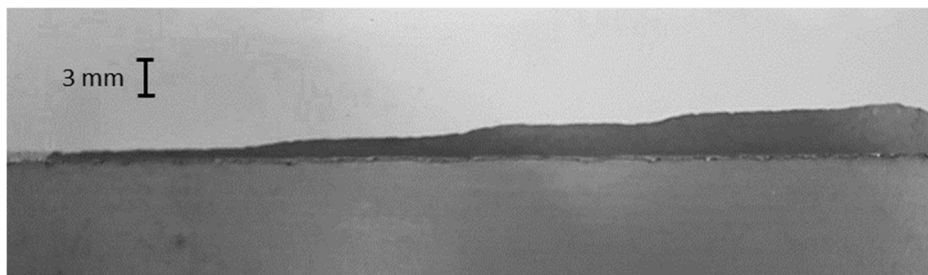


Figure 95 – Supersonic laser deposition of Stellite 21 shaped with flow separator at 25, 15, 7.5 and 3.75 mm/s, at 500 °C with additional 1.5 kW laser power

### 6.5. Effect of flow separator roughness

It was noted throughout Chapter 4 that the surface roughness of the backstop appeared to affect the surface roughness of the deposited surface. A test was conducted to see how the surface roughness of the backstop affected the roughness of the deposit surface formed. Copper was sprayed using the parameters as prior experimentation – 15 mm/s, 300 °C and 30 bar - along a flow separator that was

given a range of surface roughness values by grinding in sections with a variety of different roughing media.

As expected, the deposit roughness increased with increasing roughness of the shaping tool. In addition, Figure 96 appears to show an increasing disparity between the roughness of the deposit and the tool with increasing roughness, though this may be a proportional factor, there is not enough data to evaluate.

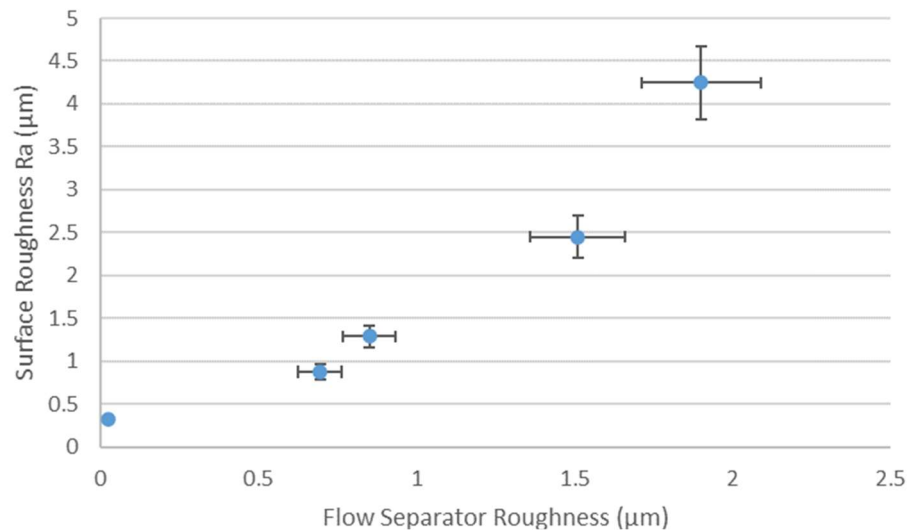


Figure 96 – Graph of initial tool face roughness vs deposit surface roughness (Ra)

The degree of difference between the surface finishes of the tool and deposit may be altered by material properties or by powder size, though this has not been investigated further in this work.

Additionally, the surface of the backstop is marginally detrimentally affected by the oblique impact of powder hitting it before impacting the substrate. This tool face roughening effect would be reduced for tools made from harder materials, and in a system with a reusable tool there would likely come an equilibrium point where further deposits would not further increase the surface roughness of the tool, creating a known and repeatable surface finish for the surfaces forming adjacent to the tool face.

As these trials used a new tool for each deposit to maintain the same parameters between experiments, this theory was not pursued in this work but should be examined for a more viable system.

## 6.6. Building block structures

Once a method for defining a straight, flat surface had been successfully achieved for a variety of materials, the development of further shapes was considered to further define the system capabilities.

It was decided that the development should be focussed on the creation of a range of “building block” structures, from which the creation of more complex shapes could be extrapolated. The shapes settled upon were: Projecting walls, thin wall sections, corners and curved surfaces.

The parameters used for deposition were the same as those used in Table 5 in Section 4.2, unless otherwise stated in the subsection.

## 6.6.1. Walls

### 6.6.1.1. Flat, defined walls

The production of flat, defined wall structures has been proven throughout Chapter 4 and previously in Chapter 6 of this thesis by positioning a thin, flow separator tool adjacent to the substrate.

### 6.6.1.2. Projecting walls

To allow more complex shape generation, the system must be shown capable of depositing material adequately onto existing geometry, not only when the shaping tool can be pressed alongside a substrate. In order to test this, a flow separator was positioned directly above the substrate with the face remaining perpendicular to the substrate and parallel to the axis of the nozzle. This was done by creating a U-shaped flow separator which could be clamped away from the face to be sprayed against.

Copper was used as the trial material with the same deposition parameters as in Section 6.3.1, using traverse rates of 7.5, 15 and 25 mm/s. The nozzle was centrally aligned with the open face of the flow separator as in the previous experimentation.

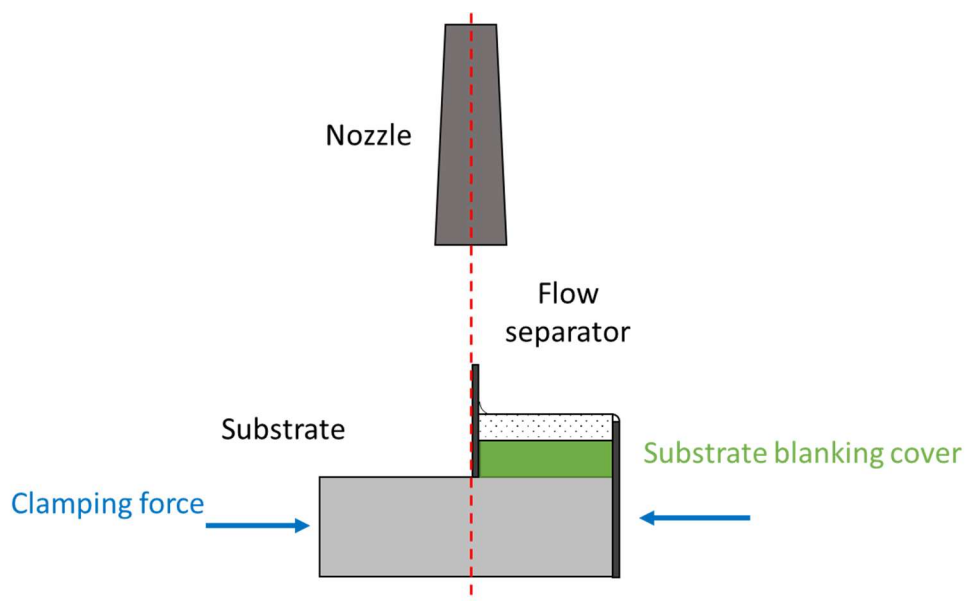
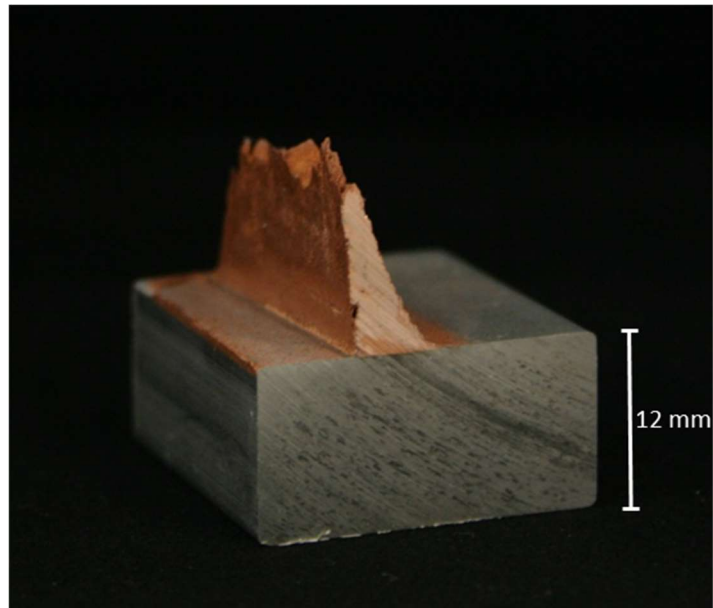


Figure 97 – Diagram of setup for flow separator to be positioned over the substrate

As can be seen from the sample in Figure 98, the defined surface was still deposited successfully with copper when the tool was placed over the substrate. A vertical wall was formed across the range of traverse rates without negatively affecting the density, surface finish or build height of the samples compared to samples with the flow separator adjacent to the substrate.

Initially there were concerns that the clamping forces were not close enough to the face of the separator that would be sprayed against, and this may lead to vibrations in the tool and interference with the deposition, however this proved not to be the case.



*Figure 98 – Separator positioning sample*

This is a significant capability demonstration for cold spray deposition, as it means that features can be built up from any existing surface at a sharp angle to the surface face, not just built up to continue the edge of a substrate with predetermined shape. The results displayed in Table 11 show that the alteration of the flow separator position has had little impact on the properties of the deposit, showing only a minor decrease in all quality of all measurements.

*Table 11 – Comparison of measurements for adjacent and above substrate flow separator positioning experiments*

<b>Measurement</b>	<b>Flow separator adjacent to substrate</b>	<b>Flow separator over substrate</b>
Surface Roughness, Ra ( $\mu\text{m}$ )	0.157	0.184
Porosity (%)	0.33	0.52
Average layer height (mm)	2.0	1.9



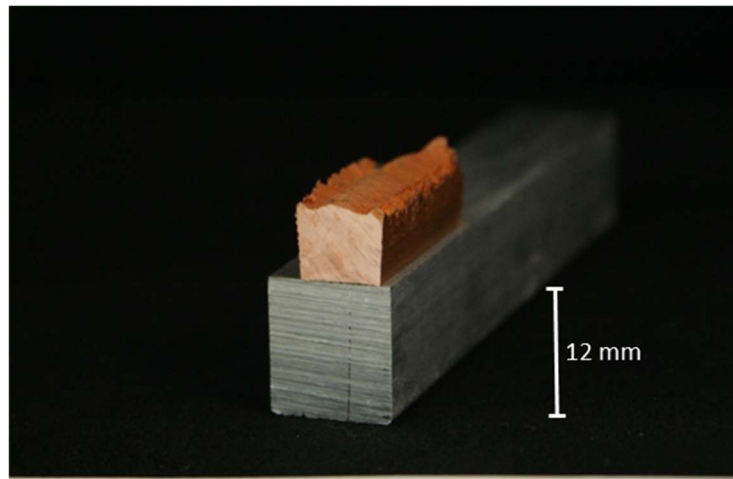


*Figure 100 – 8 mm copper wall section*

The surface finish and porosity measurements of these samples were consistent with those of the previously constructed copper samples, averaging  $0.164\ \mu\text{m}$  and  $0.39\ \%$  respectively.

### **6.6.3. Corners**

In order to build more complex shapes, it is clearly important that the surface is able to change direction while continuing deposition. To test this, two flow separators were created: one with a rounded corner, 2 mm radius, and the other with a squared corner. The nozzle was tracked along the flow separators along one axis up to the corner, and then followed the along the separator on the other axis. The space behind the wall was then filled in with a further 3 tracks to return to the starting position, at 4 mm spacing, half the track width.

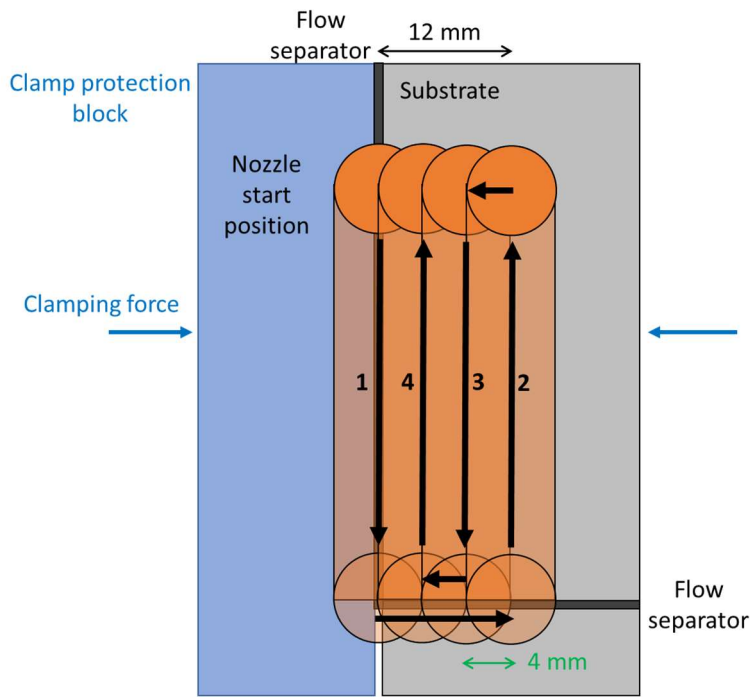


Figure 101 – Nozzle spray pattern for corner deposition

The samples were then sectioned to remove the top surfaces and better show the form of the deposit surfaces that formed adjacent to the flow separators. Figure 102 and Figure 103 show the successfully constructed surfaces when utilising both the rounded, 2 mm radius, and squared cornered flow separators respectively.

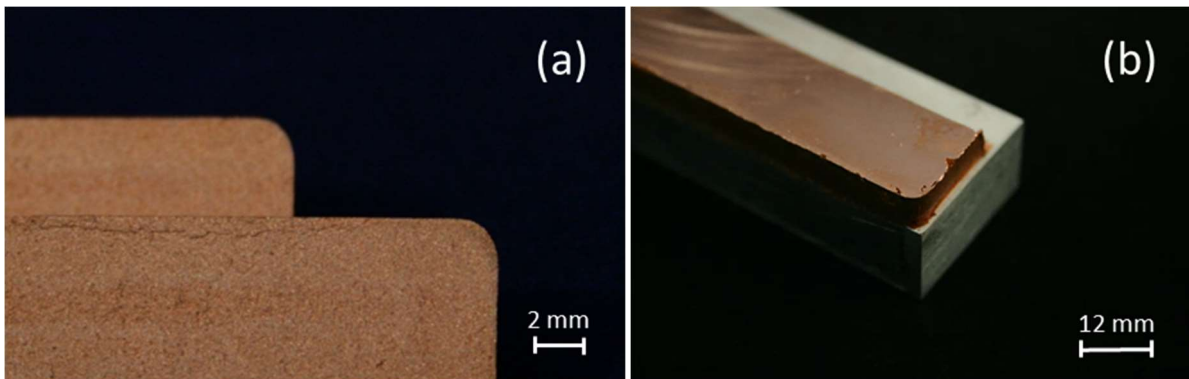
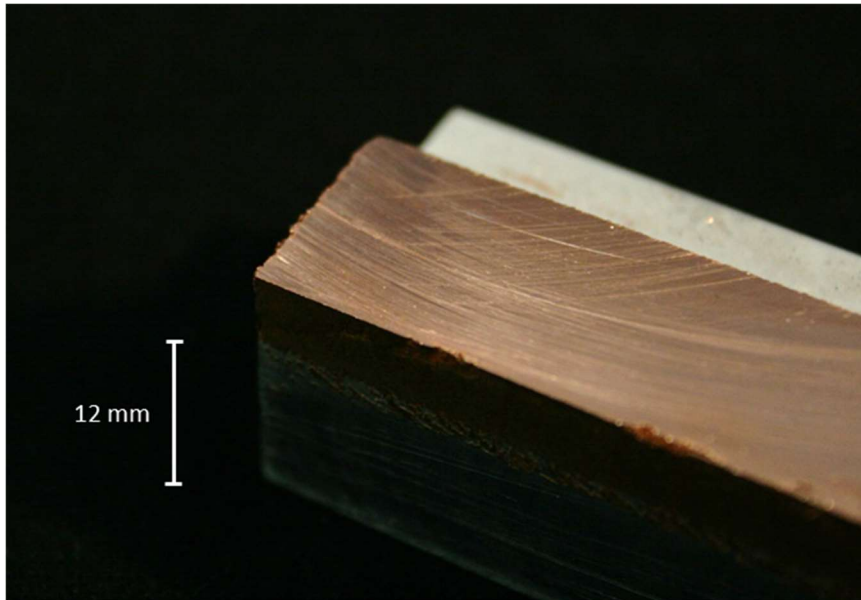


Figure 102 - Rounded corner deposit (a) prior to and (b) post sectioning



*Figure 103 - Square corner deposit formed using flow separator after sectioning*

#### **6.6.4. Curves**

As an example curve, the deposition of an arc was attempted in copper. A curved flow separator was fixed against a circular substrate, and the nozzle aligned centrally with the edge and tracked along the path of the separator. The deposition was successful, with Figure 104 showing the created arced surface after removal from the substrate and sectioning of the end to better show the surface form.



*Figure 104 – Curved copper surface*

Though the curve used in this particular trial was an arc of a circle, the nozzle could easily be programmed to follow a curved flow separator of any fixed or varying gradient, meaning the shape is only limited by the shape of available flow separator that may be placed during deposition.

## 6.7. Ring manufacture

As further proof of concept, to prove that the system could produce components with multiple layers, multiple tracks and with multiple controlled surfaces, a series of rings were developed to demonstrate the different capabilities highlighted in the previous “building blocks” section.

A cylindrical tube tool was designed and constructed from stainless steel tubing, leaving a thin section to act as flow separator at the top, chamfered to a thicker body below to provide rigidity and the ability to mount it to the rotary stage. The tube was 89.1 mm internal diameter, and gave a 19 mm original height above the substrate surface.

The substrate was then fixed inside the tool, and mounted to the rotary stage of the Aerotech CNC system which had been added to the platform. To keep the maximum track build height low and aid the building of adjacent tracks, a traverse rate close to 100 mm/s was desired. To simplify the timings in the programming, the stage was set to rotate at 120° per second, giving a traverse rate of 93 mm/s at the flow separator-substrate boundary and a full revolution every 3 seconds.

The nozzle was then aligned to the top of the flow separator tube. For the single-track rings, the nozzle then remained stationary in the X and Y axes. In subsequent trials when thicker rings were built, the nozzle was stepped across in X by 4 mm, half of the width of a single track, after every revolution of the substrate for a programmable number of times before returning to its original position.

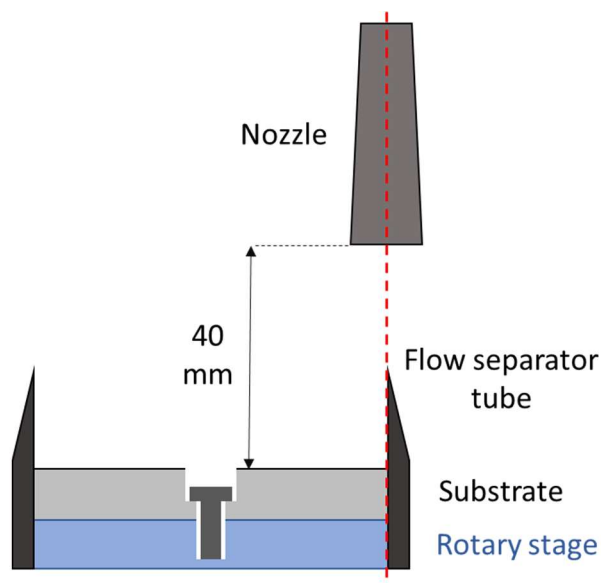
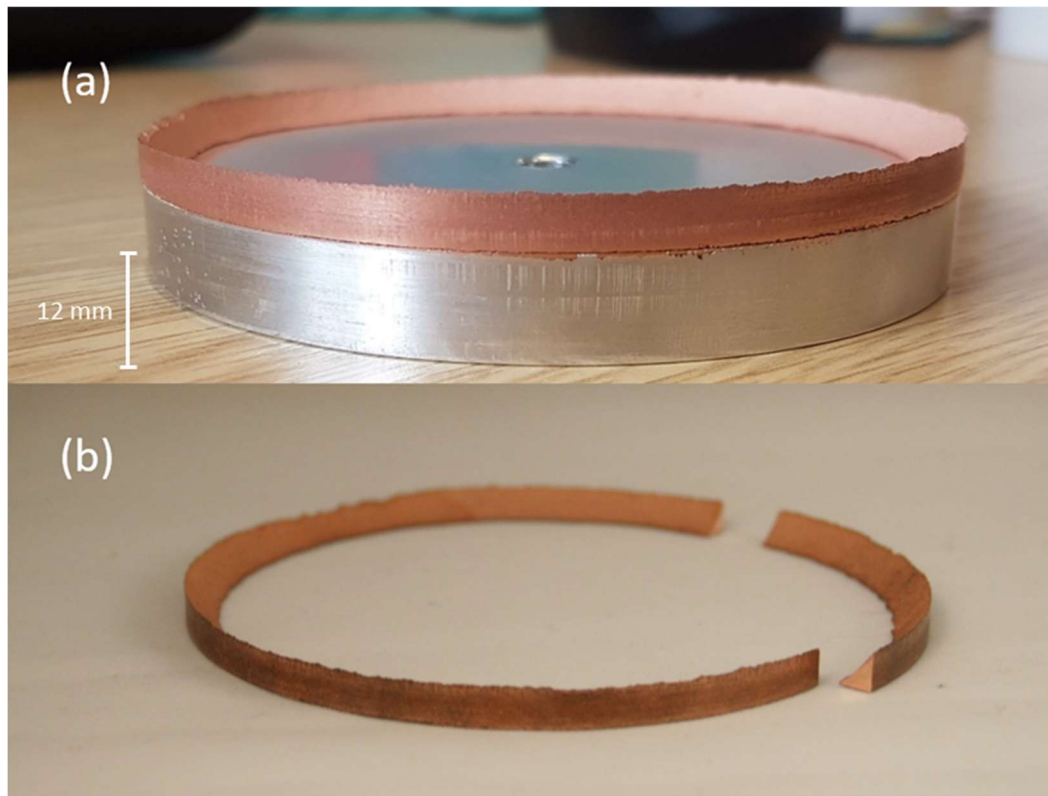


Figure 105 – Ring manufacture setup diagram

### 6.7.1. Copper ring

A copper ring was constructed first to ensure that the nozzle was correctly aligned with the tool on the rotary stage. Once constructed, some concern was held about residual stresses in the ring, and the

potential release of these stresses when sectioned, however, as can be seen in Figure 106, the ring suffered no deformation after being cut.



*Figure 106 – Copper ring (a) as deposited and (b) after sectioning*

Following this successful trial, a larger copper ring was attempted with several track widths, to ensure that there were no issues generated by the nozzle moving away from being centrally aligned with the flow separator or when moving back again. Figure 107 shows one of the taller, thicker rings that was also successfully deposited.

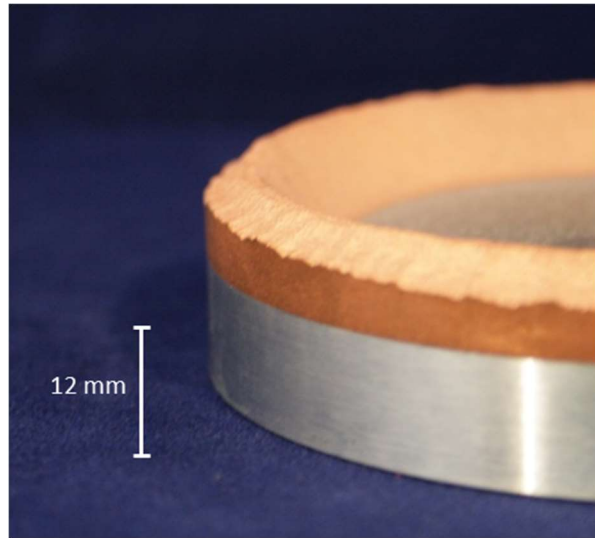


*Figure 107 - Thicker copper ring*

In both ring constructions, there was no bonding of the deposit to the tubular tool, which was easily removed from the deposit following the experiment.

### **6.7.2. Titanium rings and tool replacement**

As with the flat wall deposition trials, once the process had been successfully developed with copper powder, the process was attempted with titanium powder. With limited time and resources, it was decided that a taller, thicker ring would be constructed, allowing the testing of the replacement of the shaping tool mid-deposition.

The initial ring was constructed, seen in Figure 108, then the tool removed and a taller tool attached to the platform, allowing the nozzle to be raised and further deposition to increase the build height.

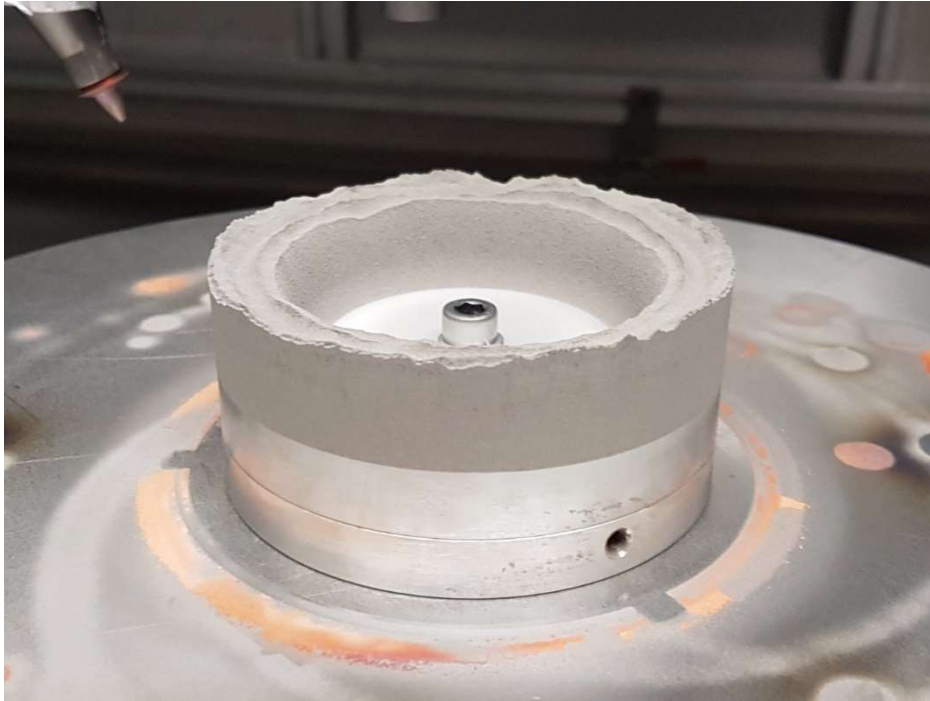


*Figure 108 - Titanium ring after first stage of construction*

A faint line of increased porosity can be seen around the titanium ring in Figure 109, at the point where the experiment was stopped to replace the tool. This likely is due to the titanium cooling before spray was recommenced, causing less successful bonding on the first layer of the restarted deposition due to the hardness of the material. This problem would likely not occur when running the system continuously, as can be seen from the many other layers contained in each half, and could also be eliminated by a heating stage or the addition of the laser for substrate preheating.

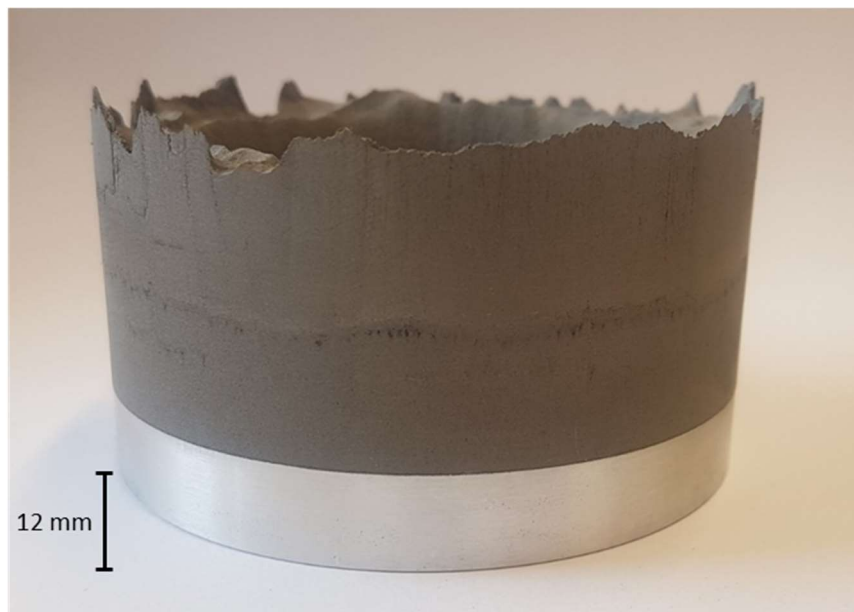


*Figure 109 – Deposited titanium tube, 55 mm height, 89 mm diameter*

The top surface of the constructed tube can be seen to have a somewhat uneven profile. This is caused by the repositioning of the nozzle in X after every revolution as the rotary stage continues to rotate over a hundred layers. As the nozzle was moved in X at 50 mm/s and was revolving to give a speed under the nozzle of 93 mm/s, when it had to move the 12 mm back to the outside, the ring had already rotated approximately 24 mm. With a better controlled system, able of switching the powder on/off faster or faster movement in X, this feature would be avoided providing a more consistent finish as seen in the previous experiments.

### 6.7.3. Ring with centre

It is important for a future manufacturing system developed from this idea to be able to construct internal features as well as shaping the exterior walls, so an experiment was conducted to extend the work of Section 6.7.2 and create a ring with both internally and externally defined walls.

A smaller tool was designed to be mounted in the centre of the substrate on the rotary stage, shown in Figure 110. This tool was also made from stainless steel tube that was turned to leave a thin section to act as a flow separator. The nozzle was then programmed to create one layer at the outer and inner surfaces, before returning to the outer surface and stepping across by half of the track width per revolution (4 mm), to fill in the central region.

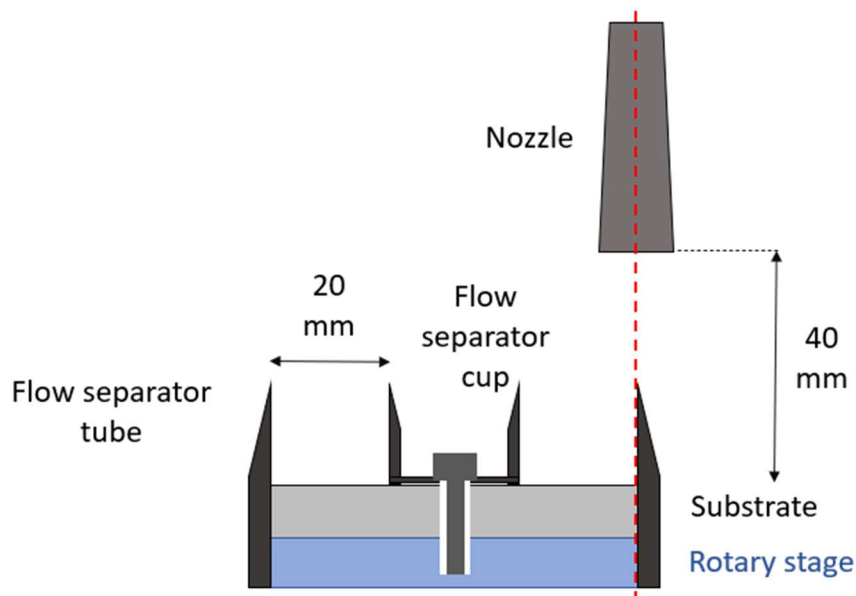
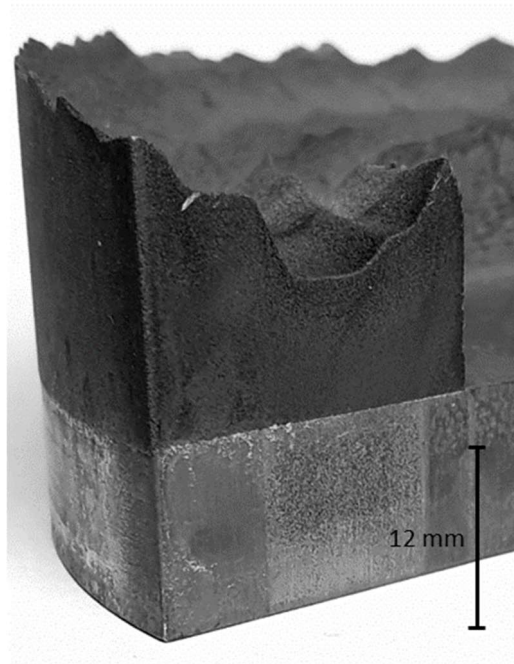


Figure 110 - Titanium ring creation with defined inner and outer surfaces, using flow separator tube and centre cup

As can be seen from the cross-sectioned ring image in Figure 111, parallel, vertical walls have been successfully built at the inner and outer surfaces. The reduced height of the central section between

the walls was due only to a coding error which excluded some layers in the central 2 tracks during deposition.



*Figure 111 – Sectioned titanium ring with inner and outer face sculpted*

#### **6.7.4. Ring with flange**

In order to establish that the structuring capabilities were not constrained to creating shapes simply built out with the same cross section as the substrate, a titanium ring with a 90° protruding flange was manufactured, by positioning the flow separator over the surface as detailed in Section 6.6.1.2.

A titanium ring was constructed in the same manner as in Section 6.7.2, and the top machined flat for ease of handling. This ring was then re-attached to the rotary axis, and the whole rotary axis rotated to be mounted horizontally onto the cold spray platform. The nozzle was then aligned with the flow separator as shown in Figure 112 and remained stationary, while the rotary axis was rotated at 120° per second, giving a surface traverse rate of 93 mm/s.

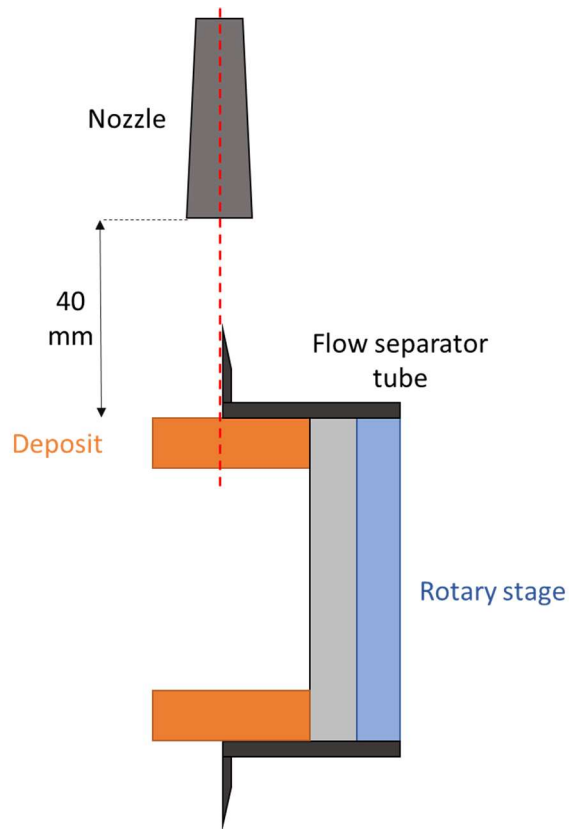


Figure 112 - System setup diagram for flange creation

As expected from the results in Section 6.6.1.2, the flange was deposited without issue onto the previously constructed titanium ring, creating the object shown in Figure 113.

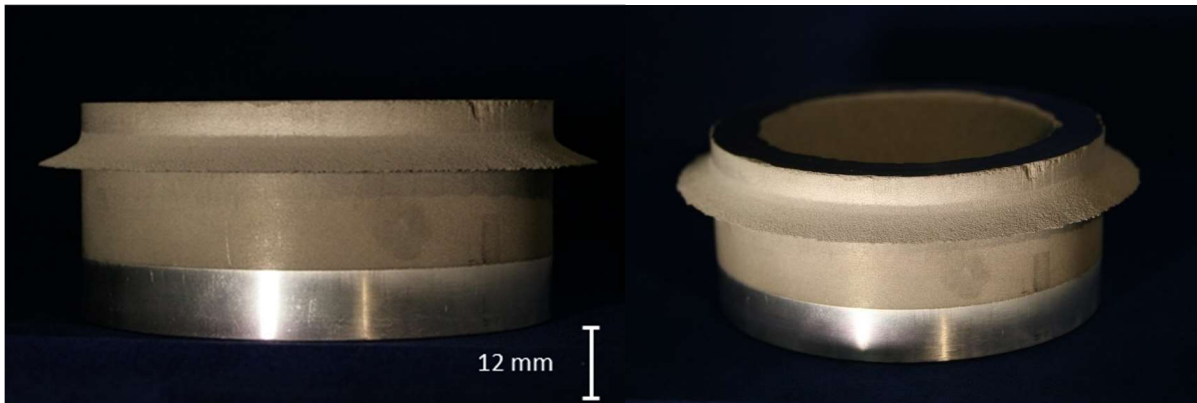


Figure 113 - Titanium ring with protruding flange

## 6.8. Discussion

It would appear that the material choice for deposition does not affect the potential for structuring of a surface in the deposited zone, and there is no apparent reason to suggest why any material that can be deposited via cold spray could not be deposited with this method. The surfaces created were all

markedly smoother than those created during typical cold spray deposition, and are comparable to or exceed those produced by other additive manufacturing processes.

The materials that were deposited did not show an appreciable difference in density when compared to standard cold spray, which is typically regarded as the main indicator of success in cold spray deposition. Further tests on other mechanical and material properties, such as hardness and conductivity, are desirable to ensure that the shape forming process has no effect on the properties of the deposits created.

The addition of laser substrate heating to the cold spray process did not prove detrimental to the shape formation of the deposit, but did provide an increase in the density of the deposit as would be expected when comparing standard cold spray with laser assisted cold spray.

The alteration of flow separator height between 2 and 24 mm above the substrate with a fixed 40 mm nozzle-substrate distance was shown to have no effect on the shaping capability of the depositing powder, nor the layer height. The positioning of the flow separator above the substrate surface, rather than clamped adjacent to it, also does not affect the deposit shaping capabilities.

The surface roughness of the deposit was found to be correlated to the roughness of the flow separator surface against which the deposition forms. Further investigation would likely determine a minimum achievable surface roughness for each material determined by the variables that would affect powder deformation upon impact such as powder size, impact velocity and hardness. Further investigation is also required to determine how the surface roughness of the flow separator is affected by the deposition process.

With the capability of constructing flat walls, corners, curves and projections from a surface, a vast array of shapes can be extrapolated from the combination of these features. Some shapes will need further investigation and careful consideration of build strategy and order to determine their viability, for example to create small, enclosed or overlapping features where powder may become trapped or nozzle/flow separator positioning may become difficult.

There are potential solutions for these issues that cold spray could utilise, including the use of a sacrificial filler material – as cold spray is capable of bonding dissimilar metals without compromising the desired material properties of the main component – or from the creation of additional support structures similar to those commonly used in other additive manufacturing techniques. The use of support material has been previously attempted using Titanium and aluminium, in the spraying of a hemisphere of titanium in an aluminium mould, as mentioned in Section 2.9.2.5.

The addition of a rotating stage to allow deposition using a tubular flow separator successfully created copper and titanium structures with defined outer surfaces that did not bond to the tool face.

Replacing the tool with a taller flow separator to extend the height of the ring did not cause complications with the formation of the ring shape, allowing a taller titanium ring to be constructed and showing that tool repositioning is possible during deposition.

Rings were also created with defined inner surfaces and protruding flanges to show that the process would not be restricted to creating a single defined surface during deposition, but could accommodate multiple surfaces in different and changing axes.

## **6.9. Summary**

The results presented in this chapter have shown that the successful creation of a defined surface is not limited to the use of copper for material choice. Whilst only 4 materials were tested in this thesis, they were chosen for their range of material properties, and the fact that they readily deposit when using standard cold spray techniques.

It was found that the deposition capability was not detrimentally affected by positioning the flow separator above the substrate, the height of the flow separator, or addition of a substrate heating laser. Nor was the method of deposition control developed in Chapter 4 limited to the creation of flat walled surfaces, with corners, curves and thin walls having been built in copper. The work here stands only as proof that different shapes are possible, the limits of each of these shapes have yet to be fully explored. For example, it is not known how narrow a thin wall section could be made, or how this would be affected by using different height flow separators to facilitate powder clearance.

Copper rings were created to trial the addition of a rotary axis stage onto the cold spray system, successfully depositing adjacent to the tubular flow separator mounted onto the stage. Subsequently, larger ring constructs were formed using titanium grade 2 powder, to explore some of the achievable shapes when combining the building block structures, not being limited to a constant cross-section, and showing that the repositioning of a flow separator during deposition does not inhibit the construction.

---

# Chapter 7 - Conclusions and recommendations

---

## 7.1. Introduction

The purpose of this research was to determine the viability of using the cold gas dynamic spray metal deposition system to create defined surfaces, with a view to developing a system capable of the near net shape creation of 3D structures, while retaining all of the material benefits that cold spray has over the competing manufacturing technologies.

To achieve this goal, a systematic review into the currently available metal additive manufacturing systems was conducted, and the place of a cold spray system within this field was suggested. Subsequently a series of methods for shaping the deposition were tested, and a computational fluid dynamics model created to aid in understanding of the gas dynamics of the system.

## 7.2. Summary and conclusions from analysis

An investigation of the additive manufacturing landscape and current cold spray deposition structure capabilities was conducted, determining that there was a viable niche for a net-shape capable additive system using cold spray. This thesis then presents the progress through the concepts developed for shaping the deposition of cold spray coatings, achieving the greatest success with the positioning of a thin sheet of stainless steel, termed a flow separator, and progressing a clear step beyond the control previously manageable with cold spray deposition. Using this novel method, a series of samples were successfully created with flat surface features, and analysed for comparison of material properties with standard cold spray deposits.

Computational fluid dynamics models were then created to simulate the supersonic gas structure and powder particle trajectory, which suggest that alteration of the gas dynamics of the exhaust area alone have little consequence on the final impact position of the particles. The inclusion of obstacles into a 3D flow model for cold spray, other than a substrate, was an original contribution to the field. This was then demonstrated to be a mathematically sensible discovery, and was subsequently noted experimentally by a researcher investigating particle deflection at a shock boundary.

This developed process was then further shown to be viable for a range of materials covering an array of material properties, without detrimentally effecting the deposition properties that give cold spray its competitive placement within the additive manufacturing landscape. Alteration of the carrier gas temperature to increase the deposition efficiency for steel deposition did not affect the shaping capability of the system. There is no obvious reason to suggest that any material capable of being

deposited by a standard cold spray system would not also be capable of shaped deposition using this process.

Further to this, a range of viable shapes were achieved successfully to prove that the shaping capability was not limited to flat, featureless walls, another advancement in the process. Deposition was tested against flow separators of different shapes, namely corners, curves, thin sections, and projections, to create a set of sample components. As further proof of concept, to demonstrate that the system could produce components with multiple layers, multiple tracks and with multiple controlled surfaces, a series of rings were developed to demonstrate the different capabilities highlighted in the previous “building blocks” section.

These developments clearly demonstrate that it is both possible to control the shape of the depositing material during cold spray to a greater extent than is currently accepted, and possible to do so without adversely affecting the deposit characteristics that would offer cold spray a unique place in the additive manufacturing landscape. With more advanced control processes, a net shape cold spray system is a viable solution for creating components additively. The work done in this thesis has laid the foundations for the system, including demonstrating a range of materials and shapes to be built upon.

### **7.3. Future Recommendations**

The results achieved in this thesis have detailed a solid foundation for the development of a cold spray additive manufacturing system, capable of producing near net-shape components of low complexity, by the demonstrated construction of building block shapes.

There remains a number of significant challenges in progressing this work to a fully realised 3D construction capable system, in particular with process control.

#### **7.3.1. Positional control**

Greater positional control of both the cold spray nozzle and the flow separator will allow for more complex shape generation. There are several approaches to this issue:

- Mounting the substrate on a 5 or 6 axis platform. This would allow precise positioning of the component as it is deposited, which would be particularly useful if the component is built more free-form and not built in a layer-by-layer approach. However, for the manufacture of much larger components, the mass of the component may make this more complicated, especially if it must be moved rapidly to maintain a high effective traverse rate.
- Nozzle mounted on an articulated arm, with flow separator not fixed relative to the bed, but fixed relative to the nozzle.

### **7.3.2. Shape control**

Demonstration of greater control of the deposit formation zone is required to construct more complicated components with this method. There are several options available to achieve these shapes, but it is likely that precise control of the powder dosage to the nozzle will be required, to allow the changing and repositioning of the flow separator shape that is being followed.

As the deposit does not adhere to the flow separator, there is no requirement for the flow separator to be stationary relative to the substrate, rather than to the nozzle. This method was chosen for the trials in this thesis for ease of positioning on the substrate and alignment with the nozzle, but the trials with consistent shape requirements of the flow separator could have utilised a flow separator mounted stationary relative to the nozzle, and had the substrate moved underneath as the deposition occurred.

Further avenues of investigation include:

- A range of flow separator shapes for creating different surfaces
- A flexible flow separator that could be bent to the appropriate shape to sculpt different shapes
- A flow separator that is mounted to the nozzle for ease of positioning
- The smallest features that can be created
- The acutest angles that can be sprayed into

### **7.3.3. Parameter exploration and process control**

In order to avoid any shadowing issues demonstrated in Figure 45, it may be possible to intentionally angle the nozzle in the opposite direction. However, it is not yet known to what angle,  $\alpha$  in Figure 114, the nozzle could be tilted away from the flow separator in the opposite direction and still allow for controlled, layer-able deposition without adherence to the flow separator surface, which should form part of any future work on the subject and potentially mitigate any similar problems.

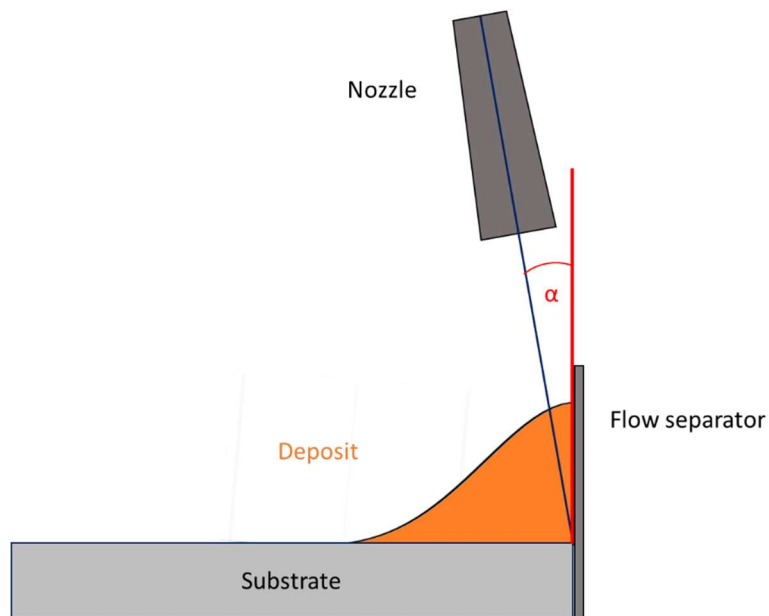


*Figure 114 – Flow separator-nozzle alignment angle*

- A comprehensive array of parameters must be constructed to detail the build height of different powders for each traverse rate, laser power, material choice, powder size and other parameters.
- Once this has been completed a build strategy must be developed for the most efficient construction of the component, considering the feature deposition order to allow rapid construction while not blocking line of sight for feature creation, whether created with a layer by layer, or in bulk sections.
- Investigation of sacrificial materials for feature creation assistance or support structures.
- Examine tool degradation, dependant on tool material and depositing powder.

---

## References

- [1] '4. Design for metal additive manufacturing for aerospace applications | Elsevier Enhanced Reader'.  
<https://reader.elsevier.com/reader/sd/pii/B9780128140628000054?token=17EF026F15E12F66A55C864795F0463AAE6E388CC548FBC3FE4CEFFA5152C5518746F024597F26B6875336F518321AE7> (accessed Jun. 07, 2020).
- [2] W. Gleeson, 'THE BENEFITS OF ADDITIVE MANUFACTURING AND ITS USE BY GENERAL ELECTRIC FOR AEROENGINE APPLICATIONS', p. 8.
- [3] T. Kellner, 'How 3D Printing Will Change Manufacturing', *GE Reports*, Nov. 13, 2017. <https://www.ge.com/reports/epiphany-disruption-ge-additive-chief-explains-3d-printing-will-upend-manufacturing/> (accessed Jun. 07, 2020).
- [4] W. E. Frazier, 'Metal Additive Manufacturing: A Review', *J. Mater. Eng. Perform.*, vol. 23, no. 6, pp. 1917–1928, Jun. 2014, doi: 10.1007/s11665-014-0958-z.
- [5] S. Singamneni, Y. Lv, A. Hewitt, R. Chalk, W. Thomas, and D. Jordison, 'Additive Manufacturing for the Aircraft Industry: A Review', vol. 8, p. 1, Feb. 2019, doi: 10.4172/2329-6542.1000214.
- [6] 'EBM Hardware', *Arcam AB*. <http://www.arcam.com/technology/electron-beam-melting/hardware/> (accessed May 30, 2015).
- [7] M. Shiomi, K. Osakada, K. Nakamura, T. Yamashita, and F. Abe, 'Residual Stress within Metallic Model Made by Selective Laser Melting Process', *CIRP Ann. - Manuf. Technol.*, vol. 53, no. 1, pp. 195–198, 2004, doi: 10.1016/S0007-8506(07)60677-5.
- [8] 'Sandia - Laser Engineered Net Shaping (TM)'. [Online]. Available: <http://www.sandia.gov/mst/pdf/LENS.pdf>.
- [9] R. R. Unocic and J. N. DuPont, 'Process efficiency measurements in the laser engineered net shaping process', *Metall. Mater. Trans. B*, vol. 35, no. 1, pp. 143–152, Feb. 2004, doi: 10.1007/s11663-004-0104-7.
- [10] 'Sciaky - Metal Additive Manufacturing Systems', *Sciaky*. <http://www.sciaky.com/additive-manufacturing/metal-additive-manufacturing-systems>.
- [11] Granta Design, *CES Edupack*. 2015.
- [12] 'Thermal Spraying Techniques', in *The Science and Engineering of Thermal Spray Coatings*, Wiley-Blackwell, 2008, pp. 67–113.
- [13] Hypertech, 'Titanium Forging', *Hypertech Medical*, May 28, 2015. <http://hiperteknoloji.com.tr/technology/titanium-forging/> (accessed Jun. 02, 2015).
- [14] A. P. Alkhimov, A. N. Papyrin, and V. F. Kosarev, 'A method of "cold" gas-dynamic deposition'. *Doki. Akad. Nauk SSSR* 318, Dec. 1990.
- [15] A. Papyrin, V. Kosarev, S. Klinkov, A. Alkhimov, and V. M. Fomin, *Cold spray technology*. Elsevier, 2006.
- [16] CSAT, 'Cold Spray Process', Aug. 28, 2015. <http://www.coldsprayteam.com/aboutcoldspray.html>.
- [17] *Treatise on Materials Science and Technology. Vol. 16: Erosion*. Academic Press, 1979.
- [18] R. C. Dykhuizen, M. F. Smith, D. L. Gilmore, R. A. Neiser, X. Jiang, and S. Sampath, 'Impact of high velocity cold spray particles', *J. Therm. Spray Technol.*, vol. 8, no. 4, pp. 559–564, Dec. 1999, doi: 10.1361/105996399770350250.
- [19] D. L. Gilmore, R. C. Dykhuizen, R. A. Neiser, M. F. Smith, and T. J. Roemer, 'Particle velocity and deposition efficiency in the cold spray process', *J. Therm. Spray Technol.*, vol. 8, no. 4, pp. 576–582, Dec. 1999, doi: 10.1361/105996399770350278.
- [20] M. Grujicic, C. L. Zhao, C. Tong, W. S. DeRosset, and D. Helfritsch, 'Analysis of the impact velocity of powder particles in the cold-gas dynamic-spray process', *Mater. Sci. Eng. A*, vol. 368, no. 1–2, pp. 222–230, Mar. 2004, doi: 10.1016/j.msea.2003.10.312.

- [21] C.-J. Li, W.-Y. Li, and H. Liao, 'Examination of the critical velocity for deposition of particles in cold spraying', *J. Therm. Spray Technol.*, vol. 15, no. 2, pp. 212–222, Jun. 2006, doi: 10.1361/105996306X108093.
- [22] R. C. Dykhuizen and M. F. Smith, 'Gas dynamic principles of cold spray', *J. Therm. Spray Technol.*, vol. 7, no. 2, pp. 205–212, Jun. 1998, doi: 10.1361/105996398770350945.
- [23] H. Assadi, F. Gärtner, T. Stoltenhoff, and H. Kreye, 'Bonding mechanism in cold gas spraying', *Acta Mater.*, vol. 51, no. 15, pp. 4379–4394, Sep. 2003, doi: 10.1016/S1359-6454(03)00274-X.
- [24] T. Schmidt, F. Gärtner, H. Assadi, and H. Kreye, 'Development of a generalized parameter window for cold spray deposition', *Acta Mater.*, vol. 54, no. 3, pp. 729–742, Feb. 2006, doi: 10.1016/j.actamat.2005.10.005.
- [25] S. Kuroda, J. Kawakita, M. Watanabe, and H. Katanoda, 'Warm spraying—a novel coating process based on high-velocity impact of solid particles', *Sci. Technol. Adv. Mater.*, vol. 9, no. 3, p. 033002, Jul. 2008, doi: 10.1088/1468-6996/9/3/033002.
- [26] T. Han, Z. Zhao, B. A. Gillispie, and J. R. Smith, 'Effects of spray conditions on coating formation by the kinetic spray process', *J. Therm. Spray Technol.*, vol. 14, no. 3, pp. 373–383, Sep. 2005, doi: 10.1361/105996305X59369.
- [27] T. V. Steenkiste and J. R. Smith, 'Evaluation of coatings produced via kinetic and cold spray processes', *J. Therm. Spray Technol.*, vol. 13, no. 2, pp. 274–282, Jun. 2004, doi: 10.1361/10599630419427.
- [28] T. H. Van Steenkiste, J. R. Smith, and R. E. Teets, 'Aluminum coatings via kinetic spray with relatively large powder particles', *Surf. Coat. Technol.*, vol. 154, no. 2, pp. 237–252, May 2002, doi: 10/drdh5p.
- [29] T. H. Van Steenkiste *et al.*, 'Kinetic spray coatings', *Surf. Coat. Technol.*, vol. 111, no. 1, pp. 62–71, Jan. 1999, doi: 10.1016/S0257-8972(98)00709-9.
- [30] S. V. Klinkov, V. F. Kosarev, and M. Rein, 'Cold spray deposition: Significance of particle impact phenomena', *Aerosp. Sci. Technol.*, vol. 9, no. 7, pp. 582–591, Oct. 2005, doi: 10.1016/j.ast.2005.03.005.
- [31] F. Raletz, M. Vardelle, and G. Ezo'o, 'Critical particle velocity under cold spray conditions', *Surf. Coat. Technol.*, vol. 201, no. 5, pp. 1942–1947, Oct. 2006, doi: 10.1016/j.surfcoat.2006.04.061.
- [32] 'Li et al\_2003\_Effect of spray angle on deposition characteristics in cold spraying.pdf' .
- [33] 'Li et al\_2007\_Effect of different incidence angles on bonding performance in cold spraying.pdf'. Accessed: May 29, 2015. [Online]. Available: <http://www.sciencedirect.com/science/article/pii/S1003632607600582/pdf?md5=ff42075cd1b62b1036e67390a2a666bc&pid=1-s2.0-S1003632607600582-main.pdf>.
- [34] T. Hussain, D. G. McCartney, P. H. Shipway, and D. Zhang, 'Bonding Mechanisms in Cold Spraying: The Contributions of Metallurgical and Mechanical Components', *J. Therm. Spray Technol.*, vol. 18, no. 3, pp. 364–379, Feb. 2009, doi: 10.1007/s11666-009-9298-1.
- [35] M. Grujicic, C. L. Zhao, W. S. DeRosset, and D. Helfritch, 'Adiabatic shear instability based mechanism for particles/substrate bonding in the cold-gas dynamic-spray process', *Mater. Des.*, vol. 25, no. 8, pp. 681–688, Dec. 2004, doi: 10.1016/j.matdes.2004.03.008.
- [36] M. Grujicic, J. R. Saylor, D. E. Beasley, W. S. DeRosset, and D. Helfritch, 'Computational analysis of the interfacial bonding between feed-powder particles and the substrate in the cold-gas dynamic-spray process', *Appl. Surf. Sci.*, vol. 219, no. 3, pp. 211–227, Dec. 2003, doi: 10/frs2wv.
- [37] C. Chen *et al.*, 'Evaluation of the interfacial bonding between particles and substrate in angular cold spray', *Mater. Lett.*, vol. 173, pp. 76–79, Jun. 2016, doi: 10.1016/j.matlet.2016.03.036.
- [38] T. Schmidt, F. Gärtner, H. Assadi, and H. Kreye, 'Development of a generalized parameter window for cold spray deposition', *Acta Mater.*, vol. 54, no. 3, pp. 729–742, Feb. 2006, doi: 10.1016/j.actamat.2005.10.005.
- [39] P. C. King, C. Busch, T. Kittel-Sherri, M. Jahedi, and S. Gulizia, 'Interface melding in cold spray titanium particle impact', *Surf. Coat. Technol.*, vol. 239, pp. 191–199, Jan. 2014, doi: 10.1016/j.surfcoat.2013.11.039.
- [40] M. V. Vidaller, A. List, F. Gaertner, T. Klassen, S. Dosta, and J. M. Guilemany, 'Single Impact Bonding of Cold Sprayed Ti-6Al-4V Powders on Different Substrates', *J. Therm. Spray Technol.*, vol. 24, no. 4, pp. 644–658, Apr. 2015, doi: 10.1007/s11666-014-0200-4.

- [41] M. Hassani-Gangaraj, D. Veysset, K. A. Nelson, and C. A. Schuh, 'In-situ observations of single micro-particle impact bonding', *Scr. Mater.*, vol. 145, pp. 9–13, Mar. 2018, doi: 10/gfz4z4.
- [42] J. Vlcek, L. Gimeno, H. Huber, and E. Lugscheider, 'A Systematic Approach to Material Eligibility for the Cold-Spray Process', *J. Therm. Spray Technol.*, vol. 14, no. 1, pp. 125–133, Mar. 2005, doi: 10.1361/10599630522738.
- [43] M. Hassani-Gangaraj, D. Veysset, V. K. Champagne, K. A. Nelson, and C. A. Schuh, 'Adiabatic shear instability is not necessary for adhesion in cold spray', *Acta Mater.*, vol. 158, pp. 430–439, Oct. 2018, doi: 10.1016/j.actamat.2018.07.065.
- [44] P. C. King, S. H. Zahiri, and M. Jahedi, 'Focused ion beam micro-dissection of cold-sprayed particles', *Acta Mater.*, vol. 56, no. 19, pp. 5617–5626, Nov. 2008, doi: 10.1016/j.actamat.2008.07.034.
- [45] Y. Xie, S. Yin, C. Chen, M.-P. Planche, H. Liao, and R. Lupoi, 'New insights into the coating/substrate interfacial bonding mechanism in cold spray', *Scr. Mater.*, vol. 125, pp. 1–4, Dec. 2016, doi: 10.1016/j.scriptamat.2016.07.024.
- [46] R. Lupoi and W. O'Neill, 'Deposition of metallic coatings on polymer surfaces using cold spray', *Surf. Coat. Technol.*, vol. 205, no. 7, pp. 2167–2173, Dec. 2010, doi: 10.1016/j.surfcoat.2010.08.128.
- [47] C. Stenson *et al.*, 'Cold spray deposition to prevent fouling of polymer surfaces', *Surf. Eng.*, vol. 34, no. 3, pp. 193–204, Mar. 2018, doi: 10.1080/02670844.2016.1229833.
- [48] J. Villafuerte, 'Considering Cold Spray for Additive Manufacturing', *Adv. Mater. Process.*, vol. 172, no. 5, pp. 50–52, 2014.
- [49] A. Sova, S. Grigoriev, A. Okunkova, and I. Smurov, 'Potential of cold gas dynamic spray as additive manufacturing technology', *Int. J. Adv. Manuf. Technol.*, vol. 69, no. 9–12, pp. 2269–2278, Aug. 2013, doi: 10.1007/s00170-013-5166-8.
- [50] J. Pattison, S. Celotto, R. Morgan, M. Bray, and W. O'Neill, 'Cold gas dynamic manufacturing: A non-thermal approach to freeform fabrication', *Int. J. Mach. Tools Manuf.*, vol. 47, no. 3–4, pp. 627–634, Mar. 2007, doi: 10.1016/j.ijmachtools.2006.05.001.
- [51] Y. Cormier, P. Dupuis, B. Jodoin, and A. Corbeil, 'Net Shape Fins for Compact Heat Exchanger Produced by Cold Spray', *J. Therm. Spray Technol.*, vol. 22, no. 7, pp. 1210–1221, Jul. 2013, doi: 10.1007/s11666-013-9968-x.
- [52] P. Dupuis, Y. Cormier, M. Fenech, A. Corbeil, and B. Jodoin, 'Flow structure identification and analysis in fin arrays produced by cold spray additive manufacturing', *Int. J. Heat Mass Transf.*, vol. 93, pp. 301–313, Feb. 2016, doi: 10.1016/j.ijheatmasstransfer.2015.10.019.
- [53] A. Sova, M. Doubenskaia, S. Grigoriev, A. Okunkova, and I. Smurov, 'Parameters of the Gas-Powder Supersonic Jet in Cold Spraying Using a Mask', *J. Therm. Spray Technol.*, vol. 22, no. 4, pp. 551–556, Apr. 2013, doi: 10.1007/s11666-013-9891-1.
- [54] S. P. Kiselev, V. P. Kiselev, and V. N. Zaikovskii, 'Effect of gas flow swirling on coating deposition by the cold gas-dynamic spray method', *J. Appl. Mech. Tech. Phys.*, vol. 53, no. 2, pp. 207–217, Mar. 2012, doi: 10.1134/S0021894412020083.
- [55] V. N. Zaikovskii, S. V. Klinkov, V. F. Kosarev, B. M. Melamed, and G. V. Trubacheev, 'Control of spray spot shape in cold spray technology. Part 2. Spraying process', *Thermophys. Aeromechanics*, vol. 21, no. 2, pp. 223–230, Apr. 2014, doi: 10.1134/S0869864314020085.
- [56] M. E. Lynch *et al.*, 'Design and topology/shape structural optimisation for additively manufactured cold sprayed components', *Virtual Phys. Prototyp.*, vol. 8, no. 3, pp. 213–231, Sep. 2013, doi: 10.1080/17452759.2013.837629.
- [57] T. Hussain, 'Cold Spraying of Titanium: A Review of Bonding Mechanisms, Microstructure and Properties', *Key Eng. Mater.*, vol. 533, no. 53, pp. 53–90, 2012, doi: 10.4028/www.scientific.net/KEM.533.53.
- [58] T. Marrocco, D. G. McCartney, P. H. Shipway, and A. J. Sturgeon, 'Production of titanium deposits by cold-gas dynamic spray: Numerical modeling and experimental characterization', *J. Therm. Spray Technol.*, vol. 15, no. 2, pp. 263–272, Jun. 2006, doi: 10/d6t54x.
- [59] S. H. Zahiri, C. I. Antonio, and M. Jahedi, 'Elimination of porosity in directly fabricated titanium via cold gas dynamic spraying', *J. Mater. Process. Technol.*, vol. 209, no. 2, pp. 922–929, Jan. 2009, doi: 10/cr6mph.

- [60] W. Wong, E. Irissou, A. N. Ryabinin, J.-G. Legoux, and S. Yue, 'Influence of Helium and Nitrogen Gases on the Properties of Cold Gas Dynamic Sprayed Pure Titanium Coatings', *J. Therm. Spray Technol.*, vol. 20, no. 1–2, pp. 213–226, Jan. 2011, doi: 10.1007/s11666-010-9568-y.
- [61] G. Bae *et al.*, 'Bonding features and associated mechanisms in kinetic sprayed titanium coatings', *Acta Mater.*, vol. 57, no. 19, pp. 5654–5666, Nov. 2009, doi: 10.1016/j.actamat.2009.07.061.
- [62] R. S. Lima, J. Karthikeyan, C. M. Kay, J. Lindemann, and C. C. Berndt, 'Microstructural characteristics of cold-sprayed nanostructured WC–Co coatings', *Thin Solid Films*, vol. 416, no. 1–2, pp. 129–135, Sep. 2002, doi: 10.1016/S0040-6090(02)00631-4.
- [63] M. Kumar *et al.*, 'Development of nano-crystalline cold sprayed Ni–20Cr coatings for high temperature oxidation resistance', *Surf. Coat. Technol.*, vol. 266, pp. 122–133, Mar. 2015, doi: 10.1016/j.surfcoat.2015.02.032.
- [64] L. Ajdelsztajn, B. Jodoin, and J. M. Schoenung, 'Synthesis and mechanical properties of nanocrystalline Ni coatings produced by cold gas dynamic spraying', *Surf. Coat. Technol.*, vol. 201, no. 3–4, pp. 1166–1172, Oct. 2006, doi: 10.1016/j.surfcoat.2006.01.037.
- [65] C.-J. Li and G.-J. Yang, 'Relationships between feedstock structure, particle parameter, coating deposition, microstructure and properties for thermally sprayed conventional and nanostructured WC–Co', *Int. J. Refract. Met. Hard Mater.*, vol. 39, pp. 2–17, Jul. 2013, doi: 10.1016/j.ijrmhm.2012.03.014.
- [66] L. Ajdelsztajn, J. M. Schoenung, B. Jodoin, and G. E. Kim, 'Cold spray deposition of nanocrystalline aluminum alloys', *Metall. Mater. Trans. A*, vol. 36, no. 3, pp. 657–666, Mar. 2005, doi: 10.1007/s11661-005-0182-4.
- [67] P. Richer, M. Yandouzi, L. Beauvais, and B. Jodoin, 'Oxidation behaviour of CoNiCrAlY bond coats produced by plasma, HVOF and cold gas dynamic spraying', *Surf. Coat. Technol.*, vol. 204, no. 24, pp. 3962–3974, Sep. 2010, doi: 10.1016/j.surfcoat.2010.03.043.
- [68] Q. Zhang, C.-J. Li, C.-X. Li, G.-J. Yang, and S.-C. Lui, 'Study of oxidation behavior of nanostructured NiCrAlY bond coatings deposited by cold spraying', *Surf. Coat. Technol.*, vol. 202, no. 14, pp. 3378–3384, Apr. 2008, doi: 10.1016/j.surfcoat.2007.12.028.
- [69] C. Borchers, F. Gärtner, T. Stoltenhoff, H. Assadi, and H. Kreye, 'Microstructural and macroscopic properties of cold sprayed copper coatings', *J. Appl. Phys.*, vol. 93, no. 12, pp. 10064–10070, Jun. 2003, doi: 10.1063/1.1573740.
- [70] B. Jodoin, L. Ajdelsztajn, E. Sansoucy, A. Zúñiga, P. Richer, and E. J. Lavernia, 'Effect of particle size, morphology, and hardness on cold gas dynamic sprayed aluminum alloy coatings', *Surf. Coat. Technol.*, vol. 201, no. 6, pp. 3422–3429, Dec. 2006, doi: 10.1016/j.surfcoat.2006.07.232.
- [71] J. Karthikeyan, '4 - The advantages and disadvantages of the cold spray coating process', in *The Cold Spray Materials Deposition Process*, V. K. Champagne, Ed. Woodhead Publishing, 2007, pp. 62–71.
- [72] X.-T. Luo, C.-X. Li, F.-L. Shang, G.-J. Yang, Y.-Y. Wang, and C.-J. Li, 'High velocity impact induced microstructure evolution during deposition of cold spray coatings: A review', *Surf. Coat. Technol.*, vol. 254, pp. 11–20, Sep. 2014, doi: 10.1016/j.surfcoat.2014.06.006.
- [73] W. B. Choi *et al.*, 'Integrated characterization of cold sprayed aluminum coatings', *Acta Mater.*, vol. 55, no. 3, pp. 857–866, Feb. 2007, doi: 10.1016/j.actamat.2006.09.006.
- [74] V. Luzin, K. Spencer, and M.-X. Zhang, 'Residual stress and thermo-mechanical properties of cold spray metal coatings', *Acta Mater.*, vol. 59, no. 3, pp. 1259–1270, Feb. 2011, doi: 10.1016/j.actamat.2010.10.058.
- [75] S. Celotto, J. Pattison, J. S. Ho, A. N. Johnson, and W. O'Neill, '5 - The economics of the cold spray process', in *The Cold Spray Materials Deposition Process*, V. K. Champagne, Ed. Woodhead Publishing, 2007, pp. 72–101.
- [76] M. Bray, A. Cockburn, and W. O'Neill, 'The Laser-assisted Cold Spray process and deposit characterisation', *Surf. Coat. Technol.*, vol. 203, no. 19, pp. 2851–2857, Jun. 2009, doi: 10.1016/j.surfcoat.2009.02.135.
- [77] B. Li *et al.*, 'Beneficial Effects of Synchronous Laser Irradiation on the Characteristics of Cold-Sprayed Copper Coatings', *J. Therm. Spray Technol.*, vol. 24, no. 5, pp. 836–847, May 2015, doi: 10.1007/s11666-015-0246-y.

- [78] Y. Danlos, S. Costil, X. Guo, H. Liao, and C. Coddet, 'Ablation laser and heating laser combined to cold spraying', *Surf. Coat. Technol.*, vol. 205, no. 4, pp. 1055–1059, Nov. 2010, doi: 10.1016/j.surfcoat.2010.06.018.
- [79] S. Yin, M. Meyer, W. Li, H. Liao, and R. Lupoi, 'Gas Flow, Particle Acceleration, and Heat Transfer in Cold Spray: A review', *J. Therm. Spray Technol.*, vol. 25, no. 5, pp. 874–896, Jun. 2016, doi: 10.1007/s11666-016-0406-8.
- [80] B. Jodoin, F. Raletz, and M. Vardelle, 'Cold spray modeling and validation using an optical diagnostic method', *Surf. Coat. Technol.*, vol. 200, no. 14, pp. 4424–4432, Apr. 2006, doi: 10.1016/j.surfcoat.2005.02.209.
- [81] T. Han, Z. Zhao, B. A. Gillispie, and J. R. Smith, 'Effects of spray conditions on coating formation by the kinetic spray process', *J. Therm. Spray Technol.*, vol. 14, no. 3, pp. 373–383, Sep. 2005, doi: 10/b543t6.
- [82] T. Han, B. A. Gillispie, and Z. B. Zhao, 'An Investigation on Powder Injection in the High-Pressure Cold Spray Process', *J. Therm. Spray Technol.*, vol. 18, no. 3, pp. 320–330, Sep. 2009, doi: 10/cpc22s.
- [83] S. Yin, X. Wang, and W. Li, 'Computational analysis of the effect of nozzle cross-section shape on gas flow and particle acceleration in cold spraying', *Surf. Coat. Technol.*, vol. 205, no. 8, pp. 2970–2977, Jan. 2011, doi: 10.1016/j.surfcoat.2010.11.002.
- [84] W.-Y. Li *et al.*, 'Effect of standoff distance on coating deposition characteristics in cold spraying', *Mater. Des.*, vol. 29, no. 2, pp. 297–304, Jan. 2008, doi: 10/dkwds9.
- [85] H. Katanoda, M. Fukuhara, and N. Iino, 'Numerical Study of Combination Parameters for Particle Impact Velocity and Temperature in Cold Spray', *J. Therm. Spray Technol.*, vol. 16, no. 5, pp. 627–633, Dec. 2007, doi: 10/bqrrz2.
- [86] X. K. Suo, T. K. Liu, W. Y. Li, Q. L. Suo, M. P. Planche, and H. L. Liao, 'Numerical study on the effect of nozzle dimension on particle distribution in cold spraying', *Surf. Coat. Technol.*, vol. 220, pp. 107–111, Apr. 2013, doi: 10/f4vnhc.
- [87] W.-Y. Li and C.-J. Li, 'Optimal design of a novel cold spray gun nozzle at a limited space', *J. Therm. Spray Technol.*, vol. 14, no. 3, pp. 391–396, Sep. 2005, doi: 10/fjwpgq.
- [88] E. H. Kwon, S. H. Cho, J. W. Han, C. H. Lee, and H. J. Kim, 'Particle behavior in supersonic flow during the cold spray process', *Met. Mater. Int.*, vol. 11, no. 5, p. 377, Oct. 2005, doi: 10/cqsw7h.
- [89] M. Meyer and R. Lupoi, 'An analysis of the particulate flow in cold spray nozzles', *Mech. Sci.*, vol. 6, no. 2, pp. 127–136, Aug. 2015, doi: 10/f7r86b.
- [90] S. V. Klinkov, V. F. Kosarev, A. A. Sova, and I. Smurov, 'Calculation of Particle Parameters for Cold Spraying of Metal-Ceramic Mixtures', *J. Therm. Spray Technol.*, vol. 18, no. 5, p. 944, Jun. 2009, doi: 10/bdv8fs.
- [91] S. Yin, Q. Liu, H. Liao, and X. Wang, 'Effect of injection pressure on particle acceleration, dispersion and deposition in cold spray', *Comput. Mater. Sci.*, vol. 90, pp. 7–15, Jul. 2014, doi: 10/f55fg8.
- [92] H.-B. Jung, J.-I. Park, S.-H. Park, H.-J. Kim, C. Lee, and J.-W. Han, 'Effect of the expansion ratio and length ratio on a gas-particle flow in a converging-diverging cold spray nozzle', *Met. Mater. Int.*, vol. 15, no. 6, pp. 967–970, Dec. 2009, doi: 10/dtzqg.
- [93] T.-C. Jen, L. Li, W. Cui, Q. Chen, and X. Zhang, 'Numerical investigations on cold gas dynamic spray process with nano- and microsize particles', *Int. J. Heat Mass Transf.*, vol. 48, no. 21, pp. 4384–4396, Oct. 2005, doi: 10/fbvc6s.
- [94] S. Yin, M. Zhang, Z. Guo, H. Liao, and X. Wang, 'Numerical investigations on the effect of total pressure and nozzle divergent length on the flow character and particle impact velocity in cold spraying', *Surf. Coat. Technol.*, vol. 232, pp. 290–297, Oct. 2013, doi: 10/f5jc64.
- [95] G. Huang, D. Gu, X. Li, L. Xing, and H. Wang, 'Numerical simulation on syphonage effect of laval nozzle for low pressure cold spray system', *J. Mater. Process. Technol.*, vol. 214, no. 11, pp. 2497–2504, Nov. 2014, doi: 10/gg7r6z.
- [96] M.-W. Lee *et al.*, 'Numerical Studies on the Effects of Stagnation Pressure and Temperature on Supersonic Flow Characteristics in Cold Spray Applications', *J. Therm. Spray Technol.*, vol. 20, no. 5, pp. 1085–1097, Sep. 2011, doi: 10/d4wngm.

- [97] J.-J. Park *et al.*, 'Supersonic Nozzle Flow Simulations for Particle Coating Applications: Effects of Shockwaves, Nozzle Geometry, Ambient Pressure, and Substrate Location upon Flow Characteristics', *J. Therm. Spray Technol.*, vol. 20, no. 3, pp. 514–522, Mar. 2011, doi: 10/b6rctc.
- [98] 'ANSYS FLUENT 12.0 Theory Guide - 4.4.2 RNG - Model'. <https://www.afs.enea.it/project/neptunius/docs/fluent/html/th/node59.htm> (accessed Jun. 10, 2020).
- [99] M. Karimi, A. Fartaj, G. Rankin, D. Vanderzwet, W. Birtch, and J. Villafuerte, 'Numerical simulation of the cold gas dynamic spray process', *J. Therm. Spray Technol.*, vol. 15, no. 4, pp. 518–523, Dec. 2006, doi: 10/dx2m82.
- [100] R. Lupoi and W. O'Neill, 'Powder stream characteristics in cold spray nozzles', *Surf. Coat. Technol.*, vol. 206, no. 6, pp. 1069–1076, Dec. 2011, doi: 10/dg4kzz.
- [101] H. Tabbara, S. Gu, D. G. McCartney, T. S. Price, and P. H. Shipway, 'Study on Process Optimization of Cold Gas Spraying', *J. Therm. Spray Technol.*, vol. 20, no. 3, pp. 608–620, Mar. 2011, doi: 10/bvvcn8.
- [102] V. K. Champagne, D. J. Helfritch, S. P. G. Dinavahi, and P. F. Leyman, 'Theoretical and Experimental Particle Velocity in Cold Spray', *J. Therm. Spray Technol.*, vol. 20, no. 3, pp. 425–431, Mar. 2011, doi: 10/d4zt8p.
- [103] A. Balabel, A. M. Hegab, M. Nasr, and S. M. El-Behery, 'Assessment of turbulence modeling for gas flow in two-dimensional convergent–divergent rocket nozzle', *Appl. Math. Model.*, vol. 35, no. 7, pp. 3408–3422, Jul. 2011, doi: 10/dgdq24.
- [104] A. Hadjadj, Y. Perrot, and S. Verma, 'Numerical study of shock/boundary layer interaction in supersonic overexpanded nozzles', *Aerosp. Sci. Technol.*, vol. 42, pp. 158–168, Apr. 2015, doi: 10/f68mjv.
- [105] P. H. Shipway and I. M. Hutchings, 'A method for optimizing the particle flux in erosion testing with a gas-blast apparatus', *Wear*, vol. 174, no. 1, pp. 169–175, May 1994, doi: 10/b89h64.
- [106] V. Shukla, G. S. Elliott, and B. H. Kear, 'Nanopowder deposition by supersonic rectangular jet impingement', *J. Therm. Spray Technol.*, vol. 9, no. 3, pp. 394–398, Sep. 2000, doi: 10/c9wsd3.
- [107] S. Yin, X. Wang, W. Li, and Y. Li, 'Numerical Study on the Effect of Substrate Size on the Supersonic Jet Flow and Temperature Distribution Within the Substrate in Cold Spraying', *J. Therm. Spray Technol.*, vol. 21, no. 3, pp. 628–635, Jun. 2012, doi: 10/bk9kfk.
- [108] B. Samareh, O. Stier, V. Lüthen, and A. Dolatabadi, 'Assessment of CFD Modeling via Flow Visualization in Cold Spray Process', *J. Therm. Spray Technol.*, vol. 18, no. 5, p. 934, Aug. 2009, doi: 10/d88jx4.
- [109] K. Taylor, B. Jodoin, and J. Karov, 'Particle loading effect in cold spray', *J. Therm. Spray Technol.*, vol. 15, no. 2, pp. 273–279, Jun. 2006, doi: 10/c87xn4.
- [110] B. Samareh and A. Dolatabadi, 'Dense Particulate Flow in a Cold Gas Dynamic Spray System', *J. Fluids Eng.*, vol. 130, no. 8, Aug. 2008, doi: 10/bz2xt4.
- [111] R. N. Raelison, Ch. Verdy, and H. Liao, 'Cold gas dynamic spray additive manufacturing today: Deposit possibilities, technological solutions and viable applications', *Mater. Des.*, vol. 133, pp. 266–287, Nov. 2017, doi: 10.1016/j.matdes.2017.07.067.
- [112] F. Luo, A. Cockburn, R. Lupoi, M. Sparkes, and W. O'Neill, 'Performance comparison of Stellite 6<sup>®</sup> deposited on steel using supersonic laser deposition and laser cladding', *Surf. Coat. Technol.*, vol. 212, pp. 119–127, Nov. 2012, doi: 10.1016/j.surfcoat.2012.09.031.
- [113] R. Lupoi, A. Cockburn, C. Bryan, M. Sparkes, F. Luo, and W. O'Neill, 'Hardfacing steel with nanostructured coatings of Stellite-6 by supersonic laser deposition', *Light Sci. Appl.*, vol. 1, no. 5, p. e10, May 2012, doi: 10.1038/lsa.2012.10.
- [114] F. Luo, R. Lupoi, A. Cockburn, M. Sparkes, W. O'Neill, and J. Yao, 'Characteristics of Stellite 6 Deposited by Supersonic Laser Deposition Under Optimized Parameters', *J. Iron Steel Res. Int.*, vol. 20, no. 2, pp. 52–57, Feb. 2013, doi: 10.1016/S1006-706X(13)60056-4.
- [115] F. Luo *et al.*, 'Simulation Analysis of Stellite 6<sup>®</sup> Particle Impact on Steel Substrate in Supersonic Laser Deposition Process', *J. Therm. Spray Technol.*, vol. 24, no. 3, pp. 378–393, Dec. 2014, doi: 10.1007/s11666-014-0176-0.
- [116] R. C. McCune, '15 - The use of cold spray coating for corrosion protection', in *The Cold Spray Materials Deposition Process*, V. K. Champagne, Ed. Woodhead Publishing, 2007, pp. 302–314.

- [117] E. Calla, 'System and Method of Joining Metallic Parts Using Cold Spray Technique', US20100170937 A1, Jul. 08, 2010.
- [118] S. Cadney, M. Brochu, P. Richer, and B. Jodoin, 'Cold gas dynamic spraying as a method for freeforming and joining materials', *Surf. Coat. Technol.*, vol. 202, no. 12, pp. 2801–2806, Mar. 2008, doi: 10.1016/j.surfcoat.2007.10.010.
- [119] VRC Metal Systems, 'VRC Gen III technology', *VRC Metal Systems*, May 31, 2015. <http://www.vrcmetalsystems.com/technology.html>.
- [120] 'GE Cold Spray Manufacturing', *GE Additive TEchnology*. <http://www.geglobalresearch.com/news/press-releases/ge-researchers-experiment-with-3d-painting-to-build-up-and-repair-parts>.
- [121] 'Development of Cold Spray towards the next generation of Additive Manufacturing'. <http://www.tcd.ie/mecheng/research/manufacturing-tech-systems/projects/cold-spray.php>.
- [122] Veeco Metrology Group, 'Wyko NT3300 Spec-sheet'. [https://www.equipnet.com/mp\\_data/media/nt3300specsheetsheet\\_20171130\\_95939\\_1.pdf](https://www.equipnet.com/mp_data/media/nt3300specsheetsheet_20171130_95939_1.pdf) (accessed Aug. 26, 2018).
- [123] Y. Cormier, P. Dupuis, B. Jodoin, and A. Corbeil, 'Net Shape Fins for Compact Heat Exchanger Produced by Cold Spray', *J. Therm. Spray Technol.*, vol. 22, no. 7, pp. 1210–1221, Jul. 2013, doi: 10.1007/s11666-013-9968-x.
- [124] P. Dupuis, Y. Cormier, M. Fenech, A. Corbeil, and B. Jodoin, 'Flow structure identification and analysis in fin arrays produced by cold spray additive manufacturing', *Int. J. Heat Mass Transf.*, vol. 93, pp. 301–313, Feb. 2016, doi: 10.1016/j.ijheatmasstransfer.2015.10.019.
- [125] Fluent Inc, 'Introduction to Modeling Multiphase Flows'. <https://www.afs.enea.it/fluent/Public/Fluent-Doc/PDF/chp18.pdf> (accessed Jun. 08, 2020).
- [126] W.-Y. Li, H. Liao, G. Douchy, and C. Coddet, 'Optimal design of a cold spray nozzle by numerical analysis of particle velocity and experimental validation with 316L stainless steel powder', *Mater. Des.*, vol. 28, no. 7, pp. 2129–2137, Jan. 2007, doi: 10.1016/j.matdes.2006.05.016.
- [127] B. Sasanapuri, M. Kumar, and S. Wirogo, 'Simulation of flow through Supersonic Cruise Nozzle: A validation study', p. 28.
- [128] J. Pattison, S. Celotto, A. Khan, and W. O'Neill, 'Standoff distance and bow shock phenomena in the Cold Spray process', *Surf. Coat. Technol.*, vol. 202, no. 8, pp. 1443–1454, Jan. 2008, doi: 10.1016/j.surfcoat.2007.06.065.
- [129] S. V. Klinkov, V. F. Kosarev, and N. S. Ryashin, 'Comparison of experiments and computations for cold gas spraying through a mask. Part 2', *Thermophys. Aeromechanics*, vol. 24, no. 2, pp. 213–224, Mar. 2017, doi: 10.1134/S0869864317020068.
- [130] K. Binder, J. Gottschalk, M. Kollenda, F. Gärtner, and T. Klassen, 'Influence of Impact Angle and Gas Temperature on Mechanical Properties of Titanium Cold Spray Deposits', *J. Therm. Spray Technol.*, vol. 20, no. 1, pp. 234–242, Jan. 2011, doi: 10/cbfbp3.

---

# Appendix A

---

## Maximum deflection calculation:

Vertical particle velocity - 400 m/s

Particle radius - 20  $\mu\text{m}$

Particle Area facing pressure differential =  $4\pi \times 10^{-10} \text{ m}^2$

Particle density - 8960  $\text{kg/m}^3$

Particle mass = volume x density =  $(32\pi \times 10^{-15})/3 \times 8960 = 3.0 \times 10^{-10} \text{ kg}$

Maximum pressure gradient =  $2.5 \times 10^8 \text{ Pa/m}$

Maximum pressure diff across particle =  $2.5 \times 10^8 \times 40 \times 10^{-6} = 1 \times 10^4 \text{ Pa}$

Force on particle = pressure change across particle x Area =  $1 \times 10^4 \times 4\pi \times 10^{-10} = 1.26 \times 10^{-5} \text{ N}$

Acceleration =  $F/m = 4.19 \times 10^4 \text{ m/s}^2$

High pressure zone length =  $3 \times 10^{-3} \text{ m}$

Time in pressure zone = high pressure zone length/particle velocity =  $7.5 \times 10^{-6} \text{ s}$

Horizontal velocity on leaving high pressure zone =  $at = 0.314 \text{ m/s}$

Max deflection =  $vt = 0.314 \times (20 \times 10^{-3}/400) = \mathbf{16 \mu\text{m}}$